The 'Electric' Pascal: Absolute and Dynamic Calibration Techniques

Brandon J. Dillon

Thesis submitted to the Faculty of the
Virginia Polytechnic Institute and State University
in partial fulfillment of the requirements for the degree of

Master of Science
in
Mechanical Engineering

Clinton Dancey, Co-Chair
Panayiotis Diplas, Co-Chair
Mark Paul

12 September 2013
Blacksburg, Virginia

Keywords: Dynamic Pressure Calibration, Metrology, Automatic Control

THE 'ELECTRIC' PASCAL: ABSOLUTE AND DYNAMIC CALIBRATION TECHNIQUES

B. J. DILLON

Abstract. This article describes a pressure generation technique that has been applied to the task of calibrating hydraulic pressure transducers. The technique combines principles given by the Lorentz Force and Faraday's Law of Induction to generate a hydrostatic pressure within a cavity. The time history of this pressure is given by the device without reliance on a reference transducer or knowledge of: the local gravity; thermodynamic properties of the working fluid; or acceleration of the cavity. In this way, the Pascal can be defined by reference only to the standards of the Amp, the Volt, the Meter, and – in the case of time varying pressure – the Second. Using this technique, a prototype device has been developed using commonly available tooling and can generate pressures in the range of 0.1 to 600 Pa with relative errors of 1.5%.

Date: October 28, 2013.
Key words and phrases. Dynamic Pressure Calibration, Metrology, Automatic Control.

Contents

List of Figures

List of Tables

1. Introduction

The last thing one knows when writing a book is what to put first.

–Blaise Pascal, *Penses*

The practical calibration of absolute and dynamic pressure transducers has historically relied on a comparison between the transducer and other calibrated artifacts. This calibration method determines a difference between what is transduced (an *a posteriori* value) and what should be transduced (an *a priori* value). The difference between the two values (a calibration factor) is noted and applied to the subsequent operation of the calibrated transducer. In this way, through a chain of comparisons between the primary standard and the object in use, a pressure transducer obtains its properties of accuracy and traceability.

This calibration methodology of forming a comparison chain presents several issues to the practitioner, whose primary concern is not typically one of metrology. First, the attempt to calibrate any object merely transfers the burden of calibration to another object. A question about the accuracy of one transducer (e.g. a microphone) promptly begs the same accuracy question of the transducer used to calibrate it (e.g. a pistonphone).

Secondly, the comparison chain that is formed from transducer to artifact ultimately ends in the principles of thermodynamics for pressure calibration. This subject, however, is far removed from the experience of most practitioners versed in practical pressure measurement, and even further removed from direct comparison to the *SI* base unit standards.

In an effort to overcome these issues and develop an 'in-house' calibration method owing its accuracy solely to a comparison with base unit standards, a new technique for generating and encoding hydrostatic pressure has been developed. The technique allows a Pascal to be defined by sensitive comparison to the standards of the Amp, the Volt, the Meter, and the Second. The key to this technique is the construction of a device that is able to compare these standards in composite form – synthesized using first principles of classical physics – to the transduction of pressure phenomena.

2. The 'Electric' Pascal

This proposal is the first time [1] that a pressure standard can be specified entirely on base units that enjoy an 'electric' definition. Here, and in the title of the paper, the term electric is used in its colloquial form as found in the metrology community to refer to units which are defined by universal physical constants as was first done with the Ampere in 1946.

2.1. **Universal Physical Constants.**

The kilogram is the only remaining SI unit which is not defined by universal physical constant. At the time of the publication of this document, the kilogram, internationally, is defined by the platinum-iridium International Prototype Kilogram (IPK) and housed at the *Bureau International des Poids et Mesures* in Sévres, France.

In the United States, NIST has custody of the K4 and K20 prototype kilograms which were produced along side of the IPK in 1884. Paradoxically the K20 artifact forms the legal standard for the kilogram in the United States but because it is not *the* primary reference standard, it is *always* in error. Any US-legal kilogram, other than K20, contains at least two errors – the error between the IPK and the K20 and the error between the K20 and the kilogram in question.

For this reason, and others such as the unexplainable mass divergence issue among kilogram prototypes, in 2005 the Comit International des Poids et Mesures recommended that the kilogram be defined in terms of universal physical constants. This move would bring its definition in-line philosophically with the other six base units in the SI system (the Meter, the Second, the Ampere, the Kelvin, the Mole, and the Candela) – all of which are currently defined using universal physical constants. In 2011, the CIPM preliminarily agreed that the Planck constant would form the foundation of this definition, however, the final decision was tabled until 2014.

Under the new definition, the Kilogram would be calibrated against the Planck constant. To perform this calibration, a device would be constructed to perform the comparison between physical artifact and physical constant. Error becomes a function solely of craftsmanship – how well a comparison device is made. And while all physical standards would then contain error, the benefit of this redefinition is the error can be bounded as a level of uncertainty provided by the comparison device.

Any physical kilogram – measured anytime, anywhere – could in theory be in error by only one step. The cumulative error which presently exists in any secondary standard that is "several steps down the comparison chain" can be eliminated. The primary standard exists throughout time and space as an unvarying constant which is accessible to anyone with the knowledge to construct the comparison device.

The motivation of this paper is to provide similar knowledge, in the form of a mathematical proof, to the community concerned with pressure measurement. The broad concept of the device described in this paper is to provide a method of sensitive comparison between the Pascal and the standards of the Amp, the Volt, the Meter, and – in the case of time varying pressure – the Second.

3. State of the Art

There shall be but one Measure throughout the Realm

– Magna Carta, 1225 A.D

The Pascal is a derived unit in the *Le Systéme international d'unités* (The SI System). The unit is formed from the ratio of the units for force and area (e.g. $\frac{N}{m^2}$ or $\frac{kg}{m \cdot s^2}$). While this ratio may give a formulation for the derived unit from base units, it gives little insight into the 'construction' of a Pascal.

3.1. **Primary Reference Standards.** Historically, two devices are used to generate time invariant pressures – the dead weight piston and the manometer [11]. In the case of the dead weight piston, weights are applied to a piston acting on an enclosed fluid. The effect that motivates the fluid to escape from its enclosure and keeps the piston buoyed-up is called pressure. As the definition of a Pascal would suggest, this effect can be quantified by dividing the force applied by the weights by the area of the piston over which it is applied. The construction of such a device focuses on the faithful (and repeatable) comparison of the force provided by the weights and the pressure provided at the output of the device. For example, because the piston expresses the force of the weights to a slightly larger area than the simple face-area of the piston due to fluid viscosity, user of a dead weight piston device would need to focus on precisely deducing the effective area of the piston. In the case of the manometer, the body force of the fluid contained in the manometer can be equated to a value of pressure. This process requires invoking another concept like Archimedes' principle when thinking about pressure effects present at the manometer's fluid interfaces. However, the basic concept of a force being applied across an area still applies. The craftsman of a manometer device may be focused on accurately determining the difference in fluid height between columns. Devices in vogue accomplish this by using capacitance sensing technology, ultrasonic interferometry, or, much more rarely, laser interferometry.

The choice of device depends on the pressure range that is under investigation. The use of dead weight pistons is common in high pressure applications, while manometers are typically used to calibrate low pressure devices.

In the case of the time varying Pascal, NIST defines the dynamic Pascal using a diatomic gas shock tube device.[2] In such a device, a single chamber is divided in two by a thin membrane – typically a metal foil. Both cavities are purged of air using Helium. One cavity is pressurized while the other is evacuated. The bursting of the membrane causes a shock wave to form inside of the chamber which propagates away from the area previously occupied by the foil membrane. The shock wave interact with the transducers that are being calibrated by sweeping perpendicularly over the face of the transducer, or by stagnating in a directional normal to the face of the transducer. Knowledge of the magnitude of the pressure change and the period over which it changes becomes a function of thermodynamic shock theory, or laser spectroscopy measurement. NIST prefers the use of the laser spectroscopy method.

3.2. **Secondary Reference Standards.** The document "A Guide for the Dynamic Calibration of Pressure Transducers" contains an excellent review of the state of pressure calibration methodology.[1] The document is produced and maintained by three committees at the Instrumentation, Systems, and Automation Society located in Research Triangle Park, North Carolina. These committees – totaling 46 people – represent a cross-section of industry, academia, and national laboratories.

Seventy-seven peer-reviewed articles, books, white papers, and symposium lectures covering a publication time span of over fifty years are cited in the document. The Guide covers calibration methods, techniques, theory, and data processing. And while direct reference to many of the citations may be necessary for a serious research inquiry, the Guide is able to articulate the core of these topics to a reader with an engineering or scientific background.

Readers who may wish to have a deeper appreciation of the very human struggle for accuracy and precision in measurement and its role in the creation of modern science and society are referred to the book *Foundations of Mechanical Accuracy* by Wayne R. Moore.[7] While, this book does not directly cover the topic of pressure measurement, it is a singular work that deserves to be read by any student of the modern sciences. The book begins by detailing the four first principles of the mechanical arts – Geometry, Standards of Length, Dividing the Circle, and Roundness – and extends that knowledge, step-by-step, to the construction of the instrumentation that is helping answer the largest unsolved problems of empirical science.

4. The Technique

> ... the architect in his work ought to be practiced in all accomplishments. Yet reason, in view of the scope of matters, does not permit us, as need demands, to have a complete, but only a moderate knowledge of the various subjects involved. Hence I beg your Highness and other readers of these volumes to pardon any explanation that too little agrees with the rules of literary art. For it is not as a lofty thinker, nor as an eloquent speaker, nor as a scholar practiced in the best methods of literary criticism, but as an architect who has a mere tinge of these things, that I have striven to write the present treatise. But in respect to the meaning of my craft and the principles which it involves, I hope and undertake to expound them with assured authority, not only to persons engaged in building, but also to the learned world.
>
> –Vitruvius, *De Architectura*

It is known that a highly accurate force can be produced using a well-built and property calibrated linear motor.[5] [10] Contemporary work on Watt Balance devices used in a possible redefinition of the Kilogram have produced force values with uncertainties less than one part per 10^8.[8] Calibration of these linear motors is achieved by utilizing two principles of the Lorentz Force: a) linear motors produce force in a fixed ratio to their applied electrical current, and b) linear motors produce resisting electromotive force in a fixed ratio to the velocity of their voice coils. The fact that these two ratios are the same value (the Bl number) allows the linear motor of the Watt Balance to be calibrated. Moving the voice coil at a fixed, known velocity gives rise to a voltage at the terminals of the linear motor. When the Bl number is deduced from this calibration step, it can be used to generate a specified force by applying current to the linear motor.

One can imagine that a practitioner wishing to generate a hydrostatic pressure could couple such a linear motor to a cavity of fluid, contained under a piston. By applying an electrical current to the linear motor, a load would be applied to the piston and subsequently applied to the fluid in the form of pressure (Figure 1). After a sufficient time, transient effects associated with the application of the test load would tend towards zero and a constant hydrostatic pressure would exist in the cavity. Before this time, though, acceleration and frictional effects produced by the compliance of the cavity, working fluid, and seals would tend to distort the relationship between the applied current and the cavity's hydrostatic pressure.

Dynamic pressure calibration devices have historically taken steps to increase rigidity to a point that dynamic compliance effects, such as these, can be removed from the analysis of the device. While such compliance effects can never be completely eliminated, they are not beyond quantitative description.

Performing a dynamic analysis of the piston gives an equation of motion which describes the time-dependent movement of the piston with respect to momentum imparted to it. In the case of the piston depicted in Figure 1, this momentum change is a function of only the forces generated by the linear motor, the friction of the piston, and the pressure acting on the face of the piston. Because the movement of the piston is bounded by the momentum imparted to it, it follows that the motion of the piston can act as a sensitive balance between the momentum added to it by the voice coil, and subtracted from it by the friction of the piston and the deflection of the cavity under pressure. That is to say, if there is no movement of the piston, all of the force generated by the voice coil will be realized as a pressure in the cavity. However, if there is

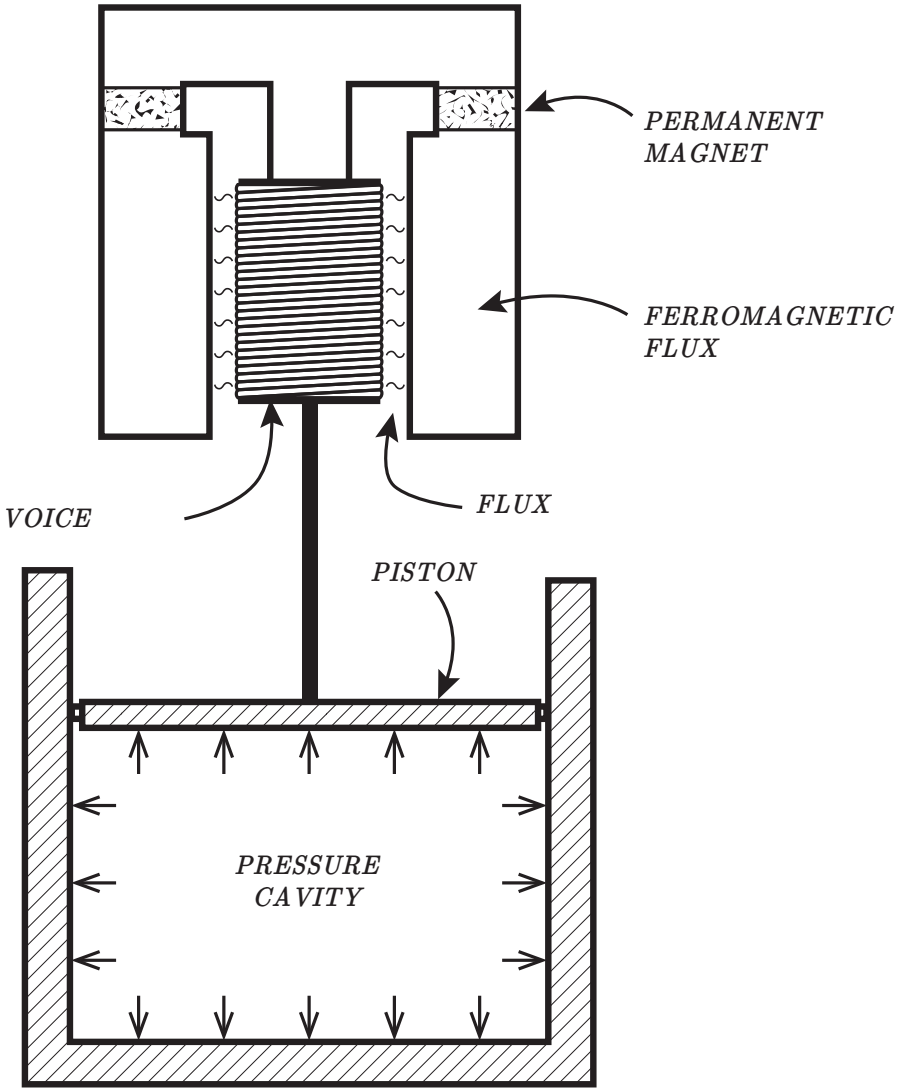

FIGURE 1. Schematic of Cavity, Piston, and Voice Coil

motion, the momentum stored or dissipated by the movement of the piston is quantifiable – leaving only the unknown and unquantifiable compliance of the cavity.

Because the velocity and applied force of the voice coil are accessible as terms in the electrical circuit of the voice coil (e.g. current and voltage), the momentum applied to, stored in, and dissipated from the piston can be quantified. The remaining term, applied pressure, is simply the difference between the momentum that has been applied and the the momentum that can be accounted for by the motion of the piston. In this way, the dynamics of the voice coil and piston have the effect of linking the dynamics of the cavity with the

dynamics of the electrical circuit. Therefore the hydrostatic cavity pressure can be deduced from observation of the electrical circuit alone.

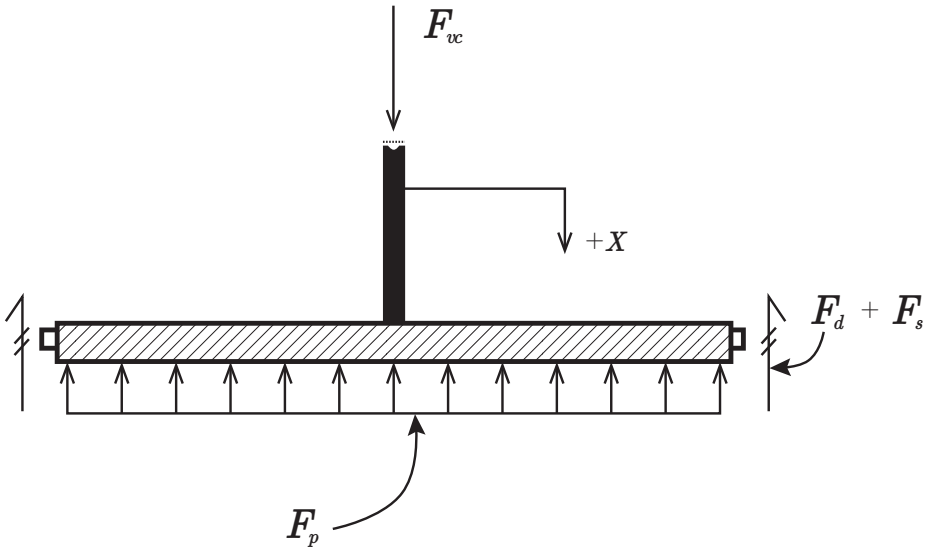

FIGURE 2. The Piston as a Force-Supported Free Body

4.1. **The Math.** Analysis of the piston is performed by conceptualizing it as a force-supported free body as shown in Figure 2. Taking the piston to have a mass, a set of externally applied forces, and a linear resistance to displacement and velocity, application of Newton's Second Law yields an equation of motion (Equation 4.1). The terms of this equation along with their modeled values are described in Table 1.

$$\sum F_x = m\ddot{x} = \mathbf{F}_s(t) + \mathbf{F}_d(t) + \mathbf{F}_p(t) + \mathbf{F}_{vc}(t) \tag{4.1}$$

TABLE 1. Description of Terms in the Equation of Motion

Term	Value	Description
$\mathbf{F}_s(t)$	$-kx(t)$	Spring force applied in proportion to the piston's displacement
$\mathbf{F}_d(t)$	$-c\dot{x}(t)$	Damping force applied in proportion to the piston's velocity
$\mathbf{F}_p(t)$	$-A \cdot P(t)$	Force generated by the hydrostatic pressure acting on the piston
$\mathbf{F}_{vc}(t)$	$Bl \cdot i(t)$	Force applied by the voice coil in proportion to electrical current

Substitution of these terms into Equation 4.1 gives the traditional form of a single-degree-of-freedom mechanical system that is being excited by an externally applied force:

$$m\ddot{x} + c\dot{x} + kx = Bl \cdot i(t) - A \cdot P(t) \tag{4.2}$$

Problems of these type are typically solved by finding a unique $x(t)$ which completes the equation for a given excitation force. In this case, however, the force generated by the hydrostatic pressure of the cavity is also unknown. This lack of information prevents the formation of a unique solution.

Fortunately, information about the motion of the piston (*e.g.* x, $\dot{x}$, and $\ddot{x}$) is available as a function of the linear motor's electrical circuit. Faraday's Law of Induction provides this link by requiring the back-emf of the linear motor to be proportional the voice coil's instantaneous velocity. The mathematical consequence of this law provides the equations listed in Table 2.

TABLE 2. Application of Faraday's Law of Induction to the Voice Coil

Term	Value	Description
$\ddot{x}(t)$	$= \frac{d}{dt}[\frac{e(t)}{Bl}]$	Piston's acceleration is proportional to the change in back-emf
$\dot{x}(t)$	$= \frac{e(t)}{Bl}$	Piston's velocity is proportional to the back-emf
$x(t)$	$= \int_0^t \frac{e(\lambda)}{Bl} d\lambda$	Piston's position is proportional to the sum of the back-emf

Combination of Equation 4.2 with the equations in Table 2 yields an equation that relates the voice coil's back-emf ($e(t)$), current, and pressure:

$$m\frac{\dot{e}(t)}{Bl} + c\frac{e(t)}{Bl} + k\int_0^t \frac{e(\lambda)}{Bl} d\lambda = Bl \cdot i(t) - A \cdot P(t) \tag{4.3}$$

Because the back-emf in this equation is only one source of electrical potential in the linear motor's circuit, one further equation is required to completely solve for the cavity's pressure in terms of terminal voltage and current. A schematic of the voice coil's electrical circuit is depicted in Figure 3. Application of Kirchhoff's Voltage Law to this circuit yields an equation that sums the resistive, inductive, and back-emf potentials of the circuit and relates it to the measurable terminal voltage (Equation 4.4).

$$V(t) = L\frac{di(t)}{dt} + R \cdot i(t) + e(t) \tag{4.4}$$

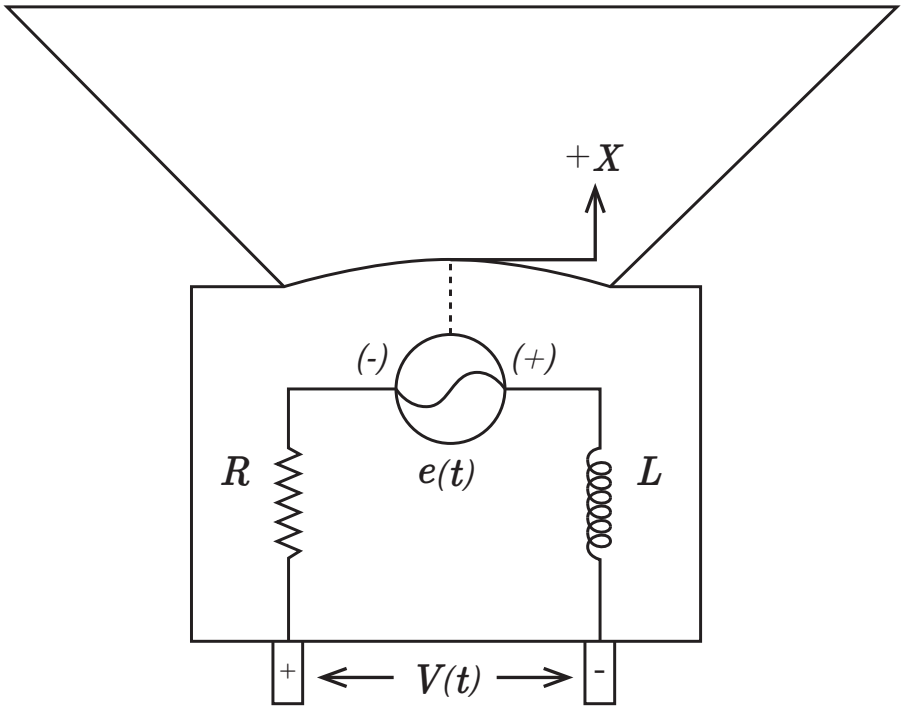

FIGURE 3. Circuit Schematic of Voice Coil

Solving this equation for $e(t)$ and substituting it into Equation 4.3 gives the equation for the hydrostatic cavity pressure in terms of the linear motor terminal voltage and current:

$$\begin{aligned} P(t) = & \frac{Bl}{A} \cdot i(t) \\ & - \frac{m}{BlA} \cdot \frac{d}{dt}[V(t) - L\frac{di(t)}{dt} - R \cdot i(t)] \\ & - \frac{c}{BlA} \cdot [V(t) - L\frac{di(t)}{dt} - R \cdot i(t)] \\ & - \frac{k}{BlA} \cdot \int_0^t [V(\hat{t}) - L\frac{di(\hat{t})}{d\hat{t}} - R \cdot i(\hat{t})]d\hat{t} \end{aligned}$$

4.2. **Interpretation.** A careful observer, having a background in the mathematics of integral transforms, will note that the previous equation can be constructed as a convolution operation. Cultivation of this view point will permit the practical use of the equation and provide a deeper understanding to the characterization

process. Rearranging the pressure equation will aid in the understanding of the steps that will be taken subsequently:

$$\begin{aligned} P(t) = \frac{1}{BlA} \cdot & \quad [(Bl)^2 \cdot i(t)] \\ + \frac{m}{BlA} \cdot & \frac{d}{dt}\,[L\frac{di(t)}{dt} + R \cdot i(t)] \quad - \quad \frac{m}{BlA} \cdot \frac{d}{dt}\,[V(t)] \\ + \frac{c}{BlA} \cdot & \quad [L\frac{di(t)}{dt} + R \cdot i(t)] \quad - \quad \frac{c}{BlA} \cdot \quad [V(t)] \\ + \frac{k}{BlA} \cdot & \int_0^t [L\frac{di(\hat{t})}{d\hat{t}} + R \cdot i(\hat{t})]\, d\hat{t} \quad - \quad \frac{k}{BlA} \cdot \int_0^t [V(\hat{t})]\, d\hat{t} \end{aligned}$$

Here it can be seen that the system is being modeled by a function that operates on the trending ($\frac{d}{dt}$), the instantaneous, and the running-sum ($\int_0^t d\hat{t}$) of circuit voltage and current. The mathematical notions of these terms can be converted to an expression of convolved kernels without loss of generality (see Appendix B.

It is important to note that the Dirac Delta ($\delta(t)$), its derivatives, and anti-derivatives can be thought of as place-holders for calculus operations that undergo convolution. In this way, the previous equation can be written in a much simpler form as:

$$\begin{aligned} P(t) = & \frac{1}{BlA} \cdot [(Bl)^2 \cdot i(t)] \\ & + \frac{1}{BlA} \cdot [m \cdot \delta'(t) + c \cdot \delta(t) + k \cdot H(t)] * \left[[L\frac{di(t)}{dt} + R \cdot i(t)] - [V(t)] \right] \end{aligned}$$

This place-holding technique can be further applied to the current terms found on the right hand side of the convolution operator. Now, the dynamics of the pressure cavity system are represented by two kernels – $[m\delta'(t) + c\delta(t) + kH(t)]$ and $[L\delta'(t) + R\delta(t)]$ – while the absolute pressure value is captured in the $\frac{1}{BlA}$ and $(Bl)^2$ terms.

It is interesting to note that the current term on the right hand side of the first convolution operator under goes two convolutions, leaving:

$$\begin{aligned} P(t) = & \frac{1}{BlA} \cdot [(Bl)^2 \cdot i(t)] \\ & + \frac{1}{BlA} \cdot [m \cdot \delta'(t) + c \cdot \delta(t) + k \cdot H(t)] * [(L \cdot \delta'(t) + R \cdot \delta(t)) * i(t) - V(t)] \end{aligned}$$

This dual operation represents the voltage generated by current induced by the movement of the pressure cavity's piston. In this way, the mechanical compliance of the pressure cavity and any spurious pressure fluctuations (e.g. erroneous vibration) are automatically accounted for in $P(t)$.

While this new form of the pressure equation can be compactly written and intuitively understood, its practical application is limited. Because the unit impulse ($\delta(t)$) and unit double ($\delta'(t)$) lack mathematical support in the time domain, their practical application can only be an approximation. However, these distributions gain various levels of mathematical support when represented in other domains.

Because of its simple support for the unit impulse and doublet, its admittance of the convolution theorem, and its ease of evaluation by those familiar with digital signal processing, the remainder of this paper will be presented in the Laplace Domain. For those unfamiliar with these techniques, excellent guides can be found in books by Smith and Bracewell. [4] [9]

Transforming the pressure equation into the Laplace Domain gives:

$$\hat{P}(s) = \frac{1}{BlA} \cdot \left[(Bl)^2 \cdot \hat{I}(s) + [ms + c + \frac{k}{s}] \cdot \left[[sL + R] \cdot \hat{I}(s) - \hat{V}(s) \right] \right] \tag{4.5}$$

5. The Encoding Equations

The Laplace Domain representation of the cavity's pressure, given in the preceding section, contains the $[ms + c + k/s]$ and $[sL + R]$ kernels. It should be noted that these kernels have units of force-over-velocity and voltage-over-current. In this way, they can be recognized as the complex impedances of the mechanical and electrical systems. These impedances appear here in a form traditional to their subject matter, as it aids the understanding of the mathematics, but it is important to note that these impedances can take any form that is admissible in the chosen mathematical domain. To underscore this abstraction, these impedance kernels will now be represented by $\mathbb{Z}(s)_{elec}$ for the $[sL + R]$ kernel and $\mathbb{Z}(s)_{mech}$ for the $[ms + c + \frac{k}{s}]$ In this case, the pressure equation takes the following form:

$$\hat{P}(s) = \frac{Bl}{A} \cdot \frac{\mathbb{Z}(s)_{mech}}{(Bl)^2} \left[\left(\mathbb{Z}(s)_{elec} + \frac{(Bl)^2}{\mathbb{Z}(s)_{mech}} \right) \cdot \hat{I}(s) - \hat{V}(s) \right] \tag{5.1}$$

This equation is called an encoding equation. It allows a device that would typically only *generate* an aperiodic pressure to also *transduce* the value of that pressure. In this way, this equation takes the place of an encoding transducer that would otherwise be required to evaluate the pressure in such a cavity. This step is important because it allows a pressure transducer to be calibrated, not by relying on an unbroken chain of calibrated artifacts, but through relation to fundamental physical constants. Furthermore, it allows the creation of known pressures, not though a feed-back control loop, but rather, causally. The problem may be best expressed by the publication "A Guide for the Dynamic Calibration of Pressure Transducers" [1]:

> The dynamic calibration of a pressure transducer could ideally be accomplished by sensing known inputs from a periodic pressure generator at known frequencies and amplitudes if such a device existed. *-(ISA37.16.01)*

This causal link has been missing from the world of dynamic pressure calibration standards and will allow laboratories to create their own low-cost calibration devices.

Other information about the state of the cavity's working fluid can also be deduced using this encoding process. For example, the volume velocity of the piston (e.g. the volume compliance of the pressure cavity) can be encoded using Equation 5.2.

$$\hat{Q}(s) = \frac{A}{Bl} \left[\hat{V}(s) - \mathbb{Z}(s)_{elec} \cdot \hat{I}(s) \right] \tag{5.2}$$

The derivation for this equation can be found in Appendix B. In short, the velocity of the voice coil can be encoded by subtracting two voltages. The first is the voltage that *should be* generated by the coil's electrical impedance and the second is the voltage that it is actually being developed. This quantity is divided by the Bl number to arrive at units of velocity. Multiplying the voice coil's velocity by the effective area of the piston (A) yields the piston's volume velocity.

5.1. **System Characterization.** In the last section, the Encoding Equations for the cavity's pressure and volume compliance (5.1 and 5.2) were presented. These equations prescribe a method to deduce the cavity pressure and volume velocity generated by the system's oscillating piston. However, in order to apply this method, three coefficients which describe the dynamics of the electrical and mechanical systems must be quantified: $\mathbb{Z}(s)_{elec}$, $\frac{(Bl)^2}{\mathbb{Z}(s)_{mech}}$, and $\frac{Bl}{A}$. These characterization coefficients are found by performing three *in-situ* electrical interrogations of the piston-motor system which isolate the behavior of one sub-system from another. This isolation is mathematically represented by setting one term in the Encoding Equations to zero and solving for the resulting ratio. Each equation formed by setting a new term to zero further restricts the solution space to a point which uniquely represents the piston.

There are four terms in two encoding equations which may be zeroed in the experimental setup – voltage $\hat{V}(s)$, current $\hat{I}(s)$, pressure $\hat{P}(s)$, and volume velocity $\hat{Q}(s)$. Current may easily be nulled by opening the terminals of the linear motor. Measuring the electrical potential of the motor's terminals would provide insight into $\mathbb{Z}(s)_{elec}$ and $\mathbb{Z}(s)_{mech}$. However, this method would require a known time-varying pressure which could interrogate a wide range of the complex s-plane. In other words, another physical device would be required to calibrate this device. Similar characterization schemes can be imagined for the nullification of the voltage term, which yields an equally disadvantageous result.

Zeroing the pressure and volume velocity terms, however, leaves two equations which simply compare voltage to current. Choosing this relationship is important because the standards for voltage and current enjoy a much higher level of experimental repeatability, a lower uncertainty of theoretical accuracy, and a wider distribution of high-quality secondary standards than those of time-varying pressure or time-varying volume. The mathematical steps of these processes are provided in Tables 3 and 4.

TABLE 3. Solving for $\mathbb{Z}(s)_{elec}$

$$\hat{Q}(s) = 0$$

$$\begin{array}{rcl} \cancelto{0}{\hat{Q}(s)} & = & \frac{A}{Bl}\left[\hat{V}(s) - \mathbb{Z}(s)_{elec} \cdot \hat{I}(s)\right] \\ 0 & = & \frac{A}{Bl}\left[\hat{V}(s) - \mathbb{Z}(s)_{elec} \cdot \hat{I}(s)\right] \\ 0 & = & \hat{V}(s) - \mathbb{Z}(s)_{elec} \cdot \hat{I}(s) \\ \hat{V}(s) & = & \mathbb{Z}(s)_{elec} \cdot \hat{I}(s) \end{array}$$

$$\boxed{\mathbb{Z}(s)_{elec} = \left.\frac{\hat{V}(s)}{\hat{I}(s)}\right|_{Q=0}}$$

TABLE 4. Solving for $\mathbb{Z}(s)_{mech}$

$$\hat{P}(s) = 0$$

$$\begin{aligned}
\cancel{\hat{P}(s)}^{0} &= \tfrac{\mathbb{Z}(s)_{mech}}{BL\cdot A}\left[\left(\mathbb{Z}(s)_{elec} + \tfrac{(Bl)^2}{\mathbb{Z}(s)_{mech}}\right)\cdot \hat{I}(s) - \hat{V}(s)\right] \\
0 &= \tfrac{\mathbb{Z}(s)_{mech}}{BL\cdot A}\left[\left(\mathbb{Z}(s)_{elec} + \tfrac{(Bl)^2}{\mathbb{Z}(s)_{mech}}\right)\cdot \hat{I}(s) - \hat{V}(s)\right] \\
0 &= \left(\mathbb{Z}(s)_{elec} + \tfrac{(Bl)^2}{\mathbb{Z}(s)_{mech}}\right)\cdot \hat{I}(s) - \hat{V}(s) \\
\hat{V}(s) &= \left(\mathbb{Z}(s)_{elec} + \tfrac{(Bl)^2}{\mathbb{Z}(s)_{mech}}\right)\cdot \hat{I}(s) \\
\left.\tfrac{\hat{V}(s)}{\hat{I}(s)}\right|_{P=0} &= \mathbb{Z}(s)_{elec} + \tfrac{(Bl)^2}{\mathbb{Z}(s)_{mech}}
\end{aligned}$$

$$\boxed{\frac{(Bl)^2}{\mathbb{Z}(s)_{mech}} = \left.\frac{\hat{V}(s)}{\hat{I}(s)}\right|_{P=0} - \left.\frac{\hat{V}(s)}{\hat{I}(s)}\right|_{Q=0}}$$

While the first two characterization coefficients ($\mathbb{Z}(s)_{elec}$, $\frac{(Bl)^2}{\mathbb{Z}(s)_{mech}}$) capture the dynamic characteristics of the motor-piston assembly, the third characterization coefficient ($\frac{Bl}{A}$) captures the ability of the system to produce a gauge pressure by 'fixing' the dynamics of system to a known level. Intuition may suggest that a manometer or dead-weight piston device could be used to generate a known static pressure. Formally, this would be solving for $\hat{P}(s)$ in the limit of $s \to 0$. However, tracking elevation changes of the free surfaces of the working fluids and pistons in this experimental configuration poses a serious threat to the accuracy of the true gauge pressures applied across the motor-piston assembly. Furthermore, this characterization process requires accurate knowledge of the local gravity field and densities of the working fluids which ultimately requires the use of a mass standard, and thereby a physical artifact, into the calibration chain.

Direct reference to a mass standard can be removed from this characterization process through analysis of the volume velocity equation. If the circuit of the linear motor is opened such that a charge cannot flow (e.g. $\hat{I}(s) = 0$), $\hat{Q}(s)$ is reduced to

$$\hat{Q}(s) = \frac{A}{Bl}\cdot \hat{V}(s)$$

Solutions to this equation can be developed in a few ways. First, because $\frac{Bl}{A}$ is not a function of s, the equation can be multiplied by $\frac{1}{s}$. This factoring process can be interpreted physically as relating the time integrations of the volume velocity of the piston and the open-circuit voltage of the linear motor:

$$\int_0^t Q(\tau)d\tau = \frac{A}{Bl}\cdot \int_0^t V(\tau)d\tau$$

Assuming the time history of the volume velocity of the piston can be thought of as beginning and ending at zero with the integration being path independent, the time integral on the left can be replaced by a simple difference in volumes:

$$\Delta \mathbf{V} = \frac{A}{Bl} \cdot \int_0^t V(\tau) d\tau \tag{5.3}$$

or

$$\boxed{\frac{Bl}{A} = \frac{1}{\Delta \mathbf{V}} \int_0^t V(\tau) d\tau}$$

This change in volume ($\Delta \mathbf{V}$) can be measured in several ways. For example, prototypes of the device described in the next section have used drawn-brass tubes, pipette nozzles, and quartz gauge tubes and an incompressible working fluid (e.g. water) to measure the volume change of the test cavity as the piston was activated. Specifically, the energy of the fluid falling in the gauge tube was used to move the piston while the circuit of the linear motor was held open. The time-summation of the open circuit voltage when compared to the displacement of the falling fluid gave $\frac{Bl}{A}$.

The generality of the mathematics that describe $\hat{Q}(s)$ allows for a wide range of creative methods to measure the change in the cavity's volume. These methods, however, are limited practically by the assumption of incompressablity of the working fluid and the cavity. A method is needed that can deduce a volume change without relying on inferences provided by the movement of fluid-fluid or fluid-solid interfaces. That is, the volume change of the cavity must be detectable in such a way that the pressure that is used to motivate the volume change does not change the volume of the working fluid. For more information on this method and a proposal for future work, see Appendix A.

6. The Device

6.1. **Construction Techniques.** A prototype device has been constructed that makes use of the technique described above. It consists of two standard 8 inch diameter ANSI B36 steam pipes (Figures I.1 to I.1), flanged at each end, and separated by a commercial loudspeaker driver. Each steam pipe section is constructed from an ASTM A53 carbon steel with a nominal wall thickness of $\frac{3}{8}in$ which provides a high degree of mechanical and electromagnetic isolation from the outside environment. The flanged pipe sections are approximately $15in$ in length. This gives the system a total internal volume of around 1500 cubic inches.

The loudspeaker driver was a M8a type manufactured by Swans Speaker Systems, Inc. It provided a low-cost means of creating a columnated piston-motor assembly. The driver's cone, which acted as the piston's working surface, was of an aluminum-magnesium composition. The cone was surrounded by a neoprene rubber spring which connected the cone to the driver's die-cast aluminum chassis and completed the seal between the two steam pipe cavities.

The driver was mounted on a hot-worked, paramagnetic, 304 stainless steel plate with a nominal thickness of $\frac{5}{16}in$ (Figure I.1). This plate was inserted between the flanges of the two steam pipes and secured with eight $\frac{3}{4}in$ grade 5 hex bolts torqued to 150 in-lb. The interfaces between the driver, the plate, and the surrounding pipe flanges were sealed using Dow-Corning 976V vacuum grease.

The M8a driver was specially modified (machining steps shown in Figures I.2 to I.2) to accept a 5mm inductive proximity probe that was manufactured by Bently Nevada, Inc. This probe was used as a "sanity check" to confirm the position and velocity of the loudspeaker's voice coil and cone. The probe was positioned co-axially with the speaker driver (Figures I.2 to I.2) and aimed at an alloy steel 'cup-shaped' target that was affixed through the inside-rear-center of the driver cone (Figures I.2 and I.2). The mechanical bond between the cone and the target was provided by two 6061-T4 aluminum nuts which were machined to match the profile of the driver cone and tightened together with threads machined into the outside diameter of the alloy target. Details on the calibration of this probe can be found in the Appendix.

All wiring was performed using single conductor, PTFE insulated, 18awg wire which was tightly twisted to avoid loop induction and was further isolated from the surrounding environment by being directed through steel conduit. Copper-copper pressure-welded crimp connections were used where construction constraints allowed – otherwise, connections were formed using a silver bearing solder. The voltage being developed by the voice coil was measured using a 4-wire kelvin circuit while the current being passed through the coil was measured using a custom-made 0.08mm Manganin wire-wound resistor shunt that was placed in thermal contact with a 5lb aluminum heat sink via a ISO-150 oil bath.

All experiments were conducted in the basement of an EM-remote facility. The only devices in the building that were powered during the tests were the data acquisition computer and power amplifiers. The measurement equipment was separated from the control station via an aluminized fabric screen. The construction techniques and experimental precautions provided an average noise floor of -161.56dB (0-20kHz) or about 0.03% of the dynamic range of the data acqusition system.

The testing facility provided limited control of the ambient temperature conditions; however, all tests were conducted in the range of 67.5 - 68.5F with a inter-test air temperature variation of less than $\frac{1}{2}^{\circ}F$.

6.2. **Characterization Tests.** Because the characterization and operation of the experimental system relies almost entirely on electrical measurements, a great deal of time was devoted to the generation of high quality signals. The current and voltage measurements were made via a common-mode rejecting op-amp circuit linked to a PCI-DAS6402/16 series data acquisition card made by Measurement Computing, Inc. The gain of the op-amp network was incrementally adjustable to use most of the 16 bit dynamic range of the DAS64. The card was operated at a sampling rate of 100kHz with no anti-aliasing pre-filter. However, a low-pass filter was used on the output of the amplifier to insure no current of an aliasing frequency entered the test chamber.

6.2.1. *Dynamics.* The dynamic characterization of the M8a driver was performed using a band-limited random number sequence in the frequency range of 0Hz to 250Hz. Mechanical jamming (*e.g.* $\hat{Q}(s) = 0$) of the driver's cone was provided by a 0.25in brass (alloy 360) rod that was inserted into the pressure cavity and threaded into the back of proximity probe target at the center of the driver's cone and voice coil. The other end of the rod was clamped by a specially designed jack-screw mechanism which allowed the voice coil to be positioned at its "free hanging" location. After the position was located, and verified using the inductive proximeter probe, the jack-screw mechanism was clamped.

The vacuum tests (*e.g.* $\hat{P}(s) = 0$) were performed by pumping down the pressure cavity with the use of an Edwards RV8 rotary vane pump. Absolute pressures of approximately $28Pa$ were achievable through considerable effort. It is assumed that surface contamination of the pressure vessel or driver system was the limiting factor from achieving lower pressures.

6.2.2. *Pressure-Voltage Ratio.* The volume velocity equation was used to derive a value for the pressure-voltage ratio (*e.g.* $\frac{Bl}{A}$). As discussed in the Encoding Equations section, a summation of voltage appearing on the voice coil's open circuit can be used to find this ratio. In this characterization phase, the pressure chamber was filled with water. Rigid copper tubing was used to connect the test chamber cavity to a $\frac{1}{2}in$ O.D. quartz gauge tube. This quartz tube was positioned vertically and could be moved up and down by approximately $18in$.

During the test, the free standing fluid level in the tube was aligned with a graduated etching on the tube. This level served as a 'zero' for a conductive probe that could be lowered into the quartz tube. When the probe made contact with the water's surface, an electrical circuit was closed and an indicator light was illuminated. This point served as the starting height of the column of water. When the zeroing process was completed, a valve between the quartz tube and the pressure chamber was closed and the quartz tube assembly was raised. Upon the triggering of the data acquisition system this valve was opened and the fluid in the quartz tube was allowed to fall; in the process displacing the cone of the loudspeaker. This displacement caused the voice coil to be moved though the magnetic field of the loudspeaker. The voltage that was generated as a function of the movement was recorded using the data acquisition system.

When the fluid level stopped moving, the conductance probe was lowered into the quartz tube in increments of $1.000in$. The total change in water column height was determined by adding the number of increments the probe was lowered and measuring the relative final probe position using a L.S. Starrett 319-3654 dial indicator. Knowledge of the total volume displaced though time and the time history of the voice coil voltage allowed the $\frac{Bl}{A}$ ratio to be calculated.

6.3. **Accuracy Tests.** Several tests of accuracy were conducted to verify the encoding technique. In these tests, the gauge pressure between the two pressure cavities of the prototype device was directed through two $30in$ lengths of 304 stainless steel braid enclosed $\frac{1}{8}in$ ID PTFE tubing to a differential diaphragm-style pressure transducer manufactured by Celsco, Inc. This pressure transducer was statically calibrated using a Model MM-3 null-reading micromanometer manufactured by the Flow Corporation. This micromanometer uses a $3in$ L.S. Starrett micrometer head to raise and lower one half of a u-tube style manometer. The null point is marked by eye using a 10 power magnifying lens. A null height reading is taken before and after pressure is applied. The difference in height of these null points, as measured by the micrometer head ($\Delta Z = 0.0001in$) gives the pressure head of the applied pressure. A value for the local gravity field ($g = 9.79718\frac{m}{s^2}$) was obtained using NOAA's US National Geodetic Survey database.

The accuracy tests were conducted using signals that imparted minimum amount of power to the voice coil. This step was specified due to concerns over the dependence of the voice coil's electrical resistance on temperature. It was found during preliminary testing the change in resistance caused by the operational heating of the voice coil caused serious stability problems for the mathematical technique. In line with these concerns (detailed in Appendix C), three signal types were chosen: 1) the impulse, 2) the pulse and, 3) the sinusoid.

The impulse test was performed to demonstrate the maximum differential pressure generation capability of the prototype device. The pulse test (two step functions back-to-back – starting and ending at zero) was performed to demonstrate the device's accuracy at generating and maintaining a static gauge pressure. And finally, the sinusoidal tests were performed to demonstrate the device's accuracy at generating a time-varying gauge pressure.

7. Results

7.1. **The Model.** As discussed in the Encoding Equations Section (Sec. 5), the kernels $\mathbb{Z}(s)_{elec}$ and $\mathbb{Z}(s)_{mech}$, in general, contain an arbitrary number of terms. The number and nature of these terms are a function of the physical device that is being modeled. In the case of the experiment that has been conducted for this paper, the form of these kernels can be found in Table 5.

Table 5. Kernel Models of the M8a Loudspeaker

Kernel	Model	Description
$\mathbb{Z}(s)_{elec}$	$[sL + R + \lvert s\rvert R_h]$	Kernel describing the electrical system
$\mathbb{Z}(s)_{mech}$	$[ms + c + k/s]$	Kernel describing the mechanical system

The chosen kernels have, for the most part, remained unchanged compared to those that were presented in the development of the theory. In practice, however, a small but significant amount of current was impeded in proportion with the real and positive value of the current's frequency. The author assumes this effect is a function of the voice coil inductively heating the loudspeaker's magnetic circuit material. To this end, the extra $|s|R_h$ term has been added to the electrical kernel to account for this impedance.

7.2. **Characterization Parameters.** Knowledge of three terms is required to fully solve the encoding equations (Section 5). Of these three terms ($\frac{(Bl)^2}{\mathbb{Z}(s)_{mech}}$, $\mathbb{Z}(s)_{elec}$, and $\frac{Bl}{A}$), two are of a dynamic nature in that their values change as a function of time (t) or the s parameter, and one is a static multiplier in either domain.

7.2.1. *Dynamic Characterization.* The dynamic characterization coefficients that were used to evaluate the experiments reported later in this paper are found in Table 6. Coefficients of complex terms are reported with respect to frequency $[\frac{1}{sec}]$ not radians. The characterization experiments were repeated one time per day over a period of ten days. The standard deviations of the values that were measured over these ten days are also reported. Details on the methods used to induce these parameters can be found in Appendix H.

Table 6. Kernel Coefficients of the M8a Loudspeaker

Parameter	Value	Standard Deviation	Std. Dev. Percent	Units
R	6.256881	$2.439x10^{-2}$	0.387%	Ω
R_h	$2.941878x10^{-3}$	$2.164x10^{-5}$	0.734%	H
L	$9.796739x10^{-3}$	$5.517x10^{-6}$	0.056%	H
$k/(Bl)^2$	5.229925	$7.750x10^{-2}$	1.482%	$\frac{N}{T-m^2}$
$c/(Bl)^2$	$1.929801x10^{-2}$	$5.158x10^{-4}$	2.673%	$\frac{N-s}{T-m^2}$
$m/(Bl)^2$	$3.465614x10^{-3}$	$3.821x10^{-5}$	1.110%	$\frac{N-s^2}{T-m^2}$

The parameters for the mechanical kernel are presented in the form in which they were measured. Because the dynamics of the mechanical system are studied through the 'lens' of the voice coil's electromotive feedback (*e.g.* $e(t) = Bl \cdot \dot{x}(t)$), the parameters are inseparable from the Bl number without a further test. Furthermore, the values are also in the form that is required by the $\frac{(Bl)^2}{\mathbb{Z}(s)_{mech}}$ term.

When the values listed in Table 6 are combined with the kernel models listed in Table 5 they form an idealized representation of the *in situ* loudspeaker driver. This representation accounts for 98.79% of the energy that was imparted into the device during the characterization test. The remainder of this energy (1.207%) is assumed lost to non-linear effects.

7.2.2. *Pressure-Voltage Ratio Characterization.* The static characterization phase allows the $\frac{Bl}{A}$ ratio to be determined. This ratio is required to 'translate' the dynamics of the mechanical and electrical systems of the loudspeaker, as measured in units of voltage, to units of pressure. In the case of the experiments reported in this paper, the $\frac{Bl}{A}$ ratio was determined by displacing the cone of the loudspeaker using a known volume of water. This volume of water was measured using a quartz gauge tube. The tube had inner diameter of $0.3139 - 0.0003in$ as check fitted by a set of "workshop" grade (B) gauge pins. The change in fluid height during a static characterization test in the quartz tube was nominally $8.90in$. This allowed the conductive probe to be moved down into the quartz tube by eight increments ($8.000in$) and the remaining $0.900in$ (nom.) to be measured by the Starrett 319-3654 dial indicator.

Ten tests which measured this ratio were performed over ten days in a similar fashion to the tests performed to characterize the dynamic kernels of the M8a driver. Details can be found in Table 7.

TABLE 7. Pressure-Voltage Ratio of the M8a Loudspeaker

Parameter	Value	Standard Deviation	Std. Dev. Percent	Units
$\frac{Bl}{A}$	$3.234132x10^2$	4.318	1.391%	$\frac{C}{m^3}$

7.3. **Device Accuracy.** The accuracy of the prototype device, utilizing the M8a loudspeaker driver, was evaluated. Three sets of tests were performed that each evaluated a different criteria of the device.

7.3.1. *Maximum Pressure.* Accurately assessing the maximum achievable differential pressure the system could generate was a daunting task. In short, the generation of high pressures requires the use of high electrical currents. However, these high electrical currents cause power to be resistively dissipated by the voice coil, which had the consequence of raising its temperature. As specified in Appendix C, the voice coil's temperature required stringent control which forced this test to use a minimum amount of power. With this condition in mind, an impulse was used to evaluate this criteria.

The impulse, during its application, instantaneously used nearly three Watts of power. However, its duration was short enough to allow the average power dissipation value to fall below the testing threshold. The time history of this test can be found in Figure 4. The green line in the figure shows the pressure that was measured by the Celsco gauge pressure transducer, while the blue line shows the pressure that was inferred

from the Encoding Equations. The peak-to-peak applied pressure in this test was $630.58Pa$ or approximately $150dB$.

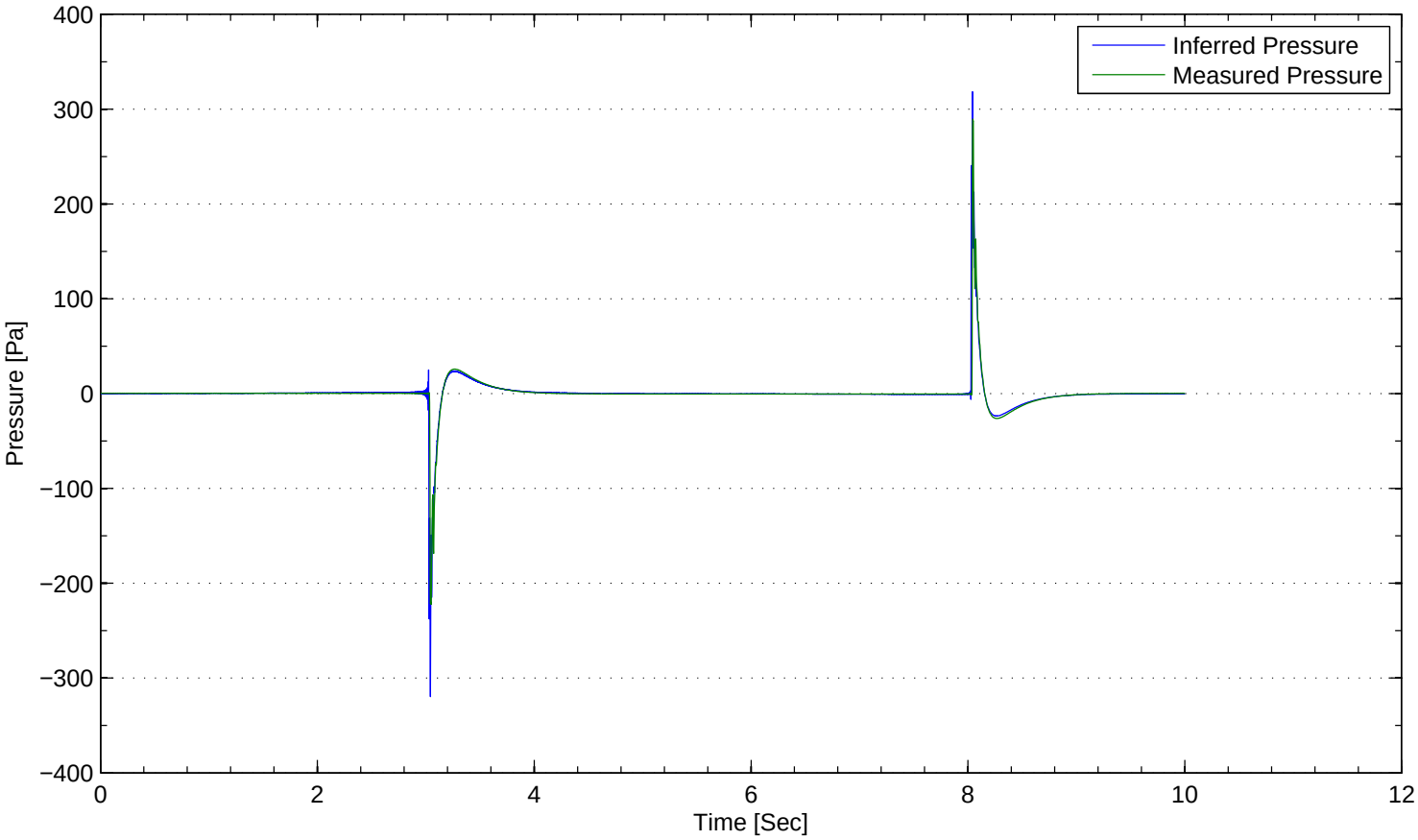

FIGURE 4. Maximum Differential Pressure Test

Closer inspection of the impulse reveals several qualitative points about the operation of the device as a system. First, there is a lag time between the initiation of the pressure event and the detection of the event at the differential pressure transducer. Some lag is to be expected as the pressure wave takes time to propagate between the loudspeaker cone and the reference transducer. The Encoding Equations only yield the pressure incident on the face of loudspeaker's cone – not what is occurring in the chamber uniformly. The lag time measured between the inferred and measured pressures was $9ms$ (Figure 5). This is contrasted to the lag time between the electrical initiation of the impulse and the detection of the pressure wave at the transducer of $8ms$.

Secondly, there is a discrepancy between the pressure peaks found in the inferred pressure time history and the measured pressure time history (Figures 5 & 6). This effect has a characteristic period of $12ms$, and because it is found to decay in both the time history of the inferred pressure and the electrical current signal

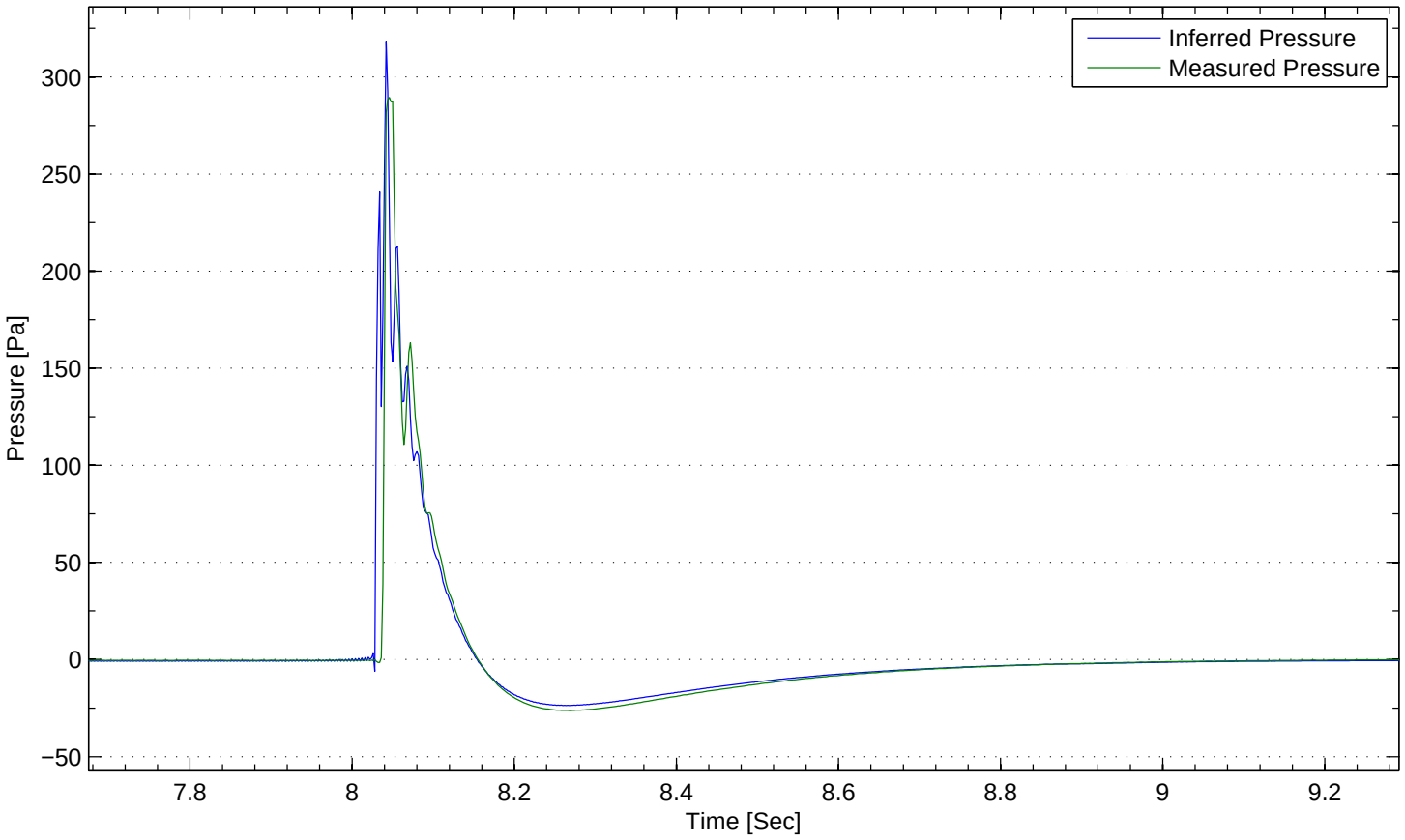

FIGURE 5. Time Histories of the Impulse Test

it is assumed that this effect is a coupling of the dynamics of the air found in the cavity and the loudspeaker. It is also assumed that the lack of a 'sharp' point on the first peak of the measured time history is a function of the compressibility of the air in the chamber and the low-pass filtering effect the connection tubes would impart. Issues of amplitude accuracy will be addressed in the next section.

7.3.2. *Static Gauge Pressure.* In the static gauge pressure tests, the prototype was directed to generate a pulse of pressure. The maximum pressure of this pulse was held for a few seconds to remove dyanmic characteristics of the pressure cavity or led tubes.

Two tests were performed. The first generated a pressure of $2.4Pa$ (nom.) and the second generated a pressure of $16.7Pa$ (nom.). These pressures reflect the accurate working range of the prototype device as it was built. Higher pressures would require a more power. This would heat the voice coil, change its resistance, and distort the output of the Encoding Equations. For more information on this limitation, see Appendix C.

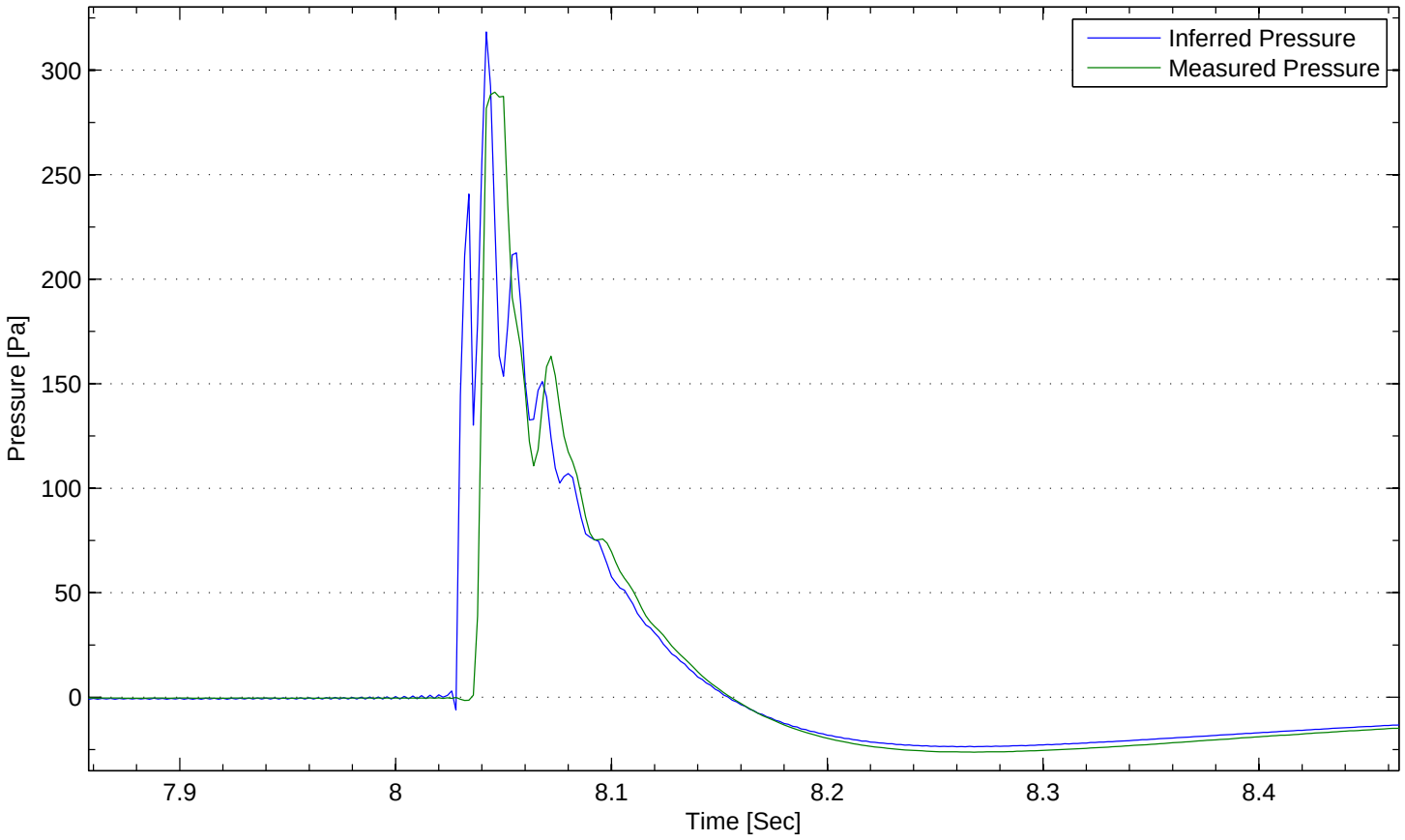

FIGURE 6. Qualitative Inspection of the Impulse Test

The time histories of these two pulse tests can be found in Figures 7 and 8. The pulses were generated using an analog bench power power supply. The various small steps and ringing behavior was caused by the operation of the power supply.

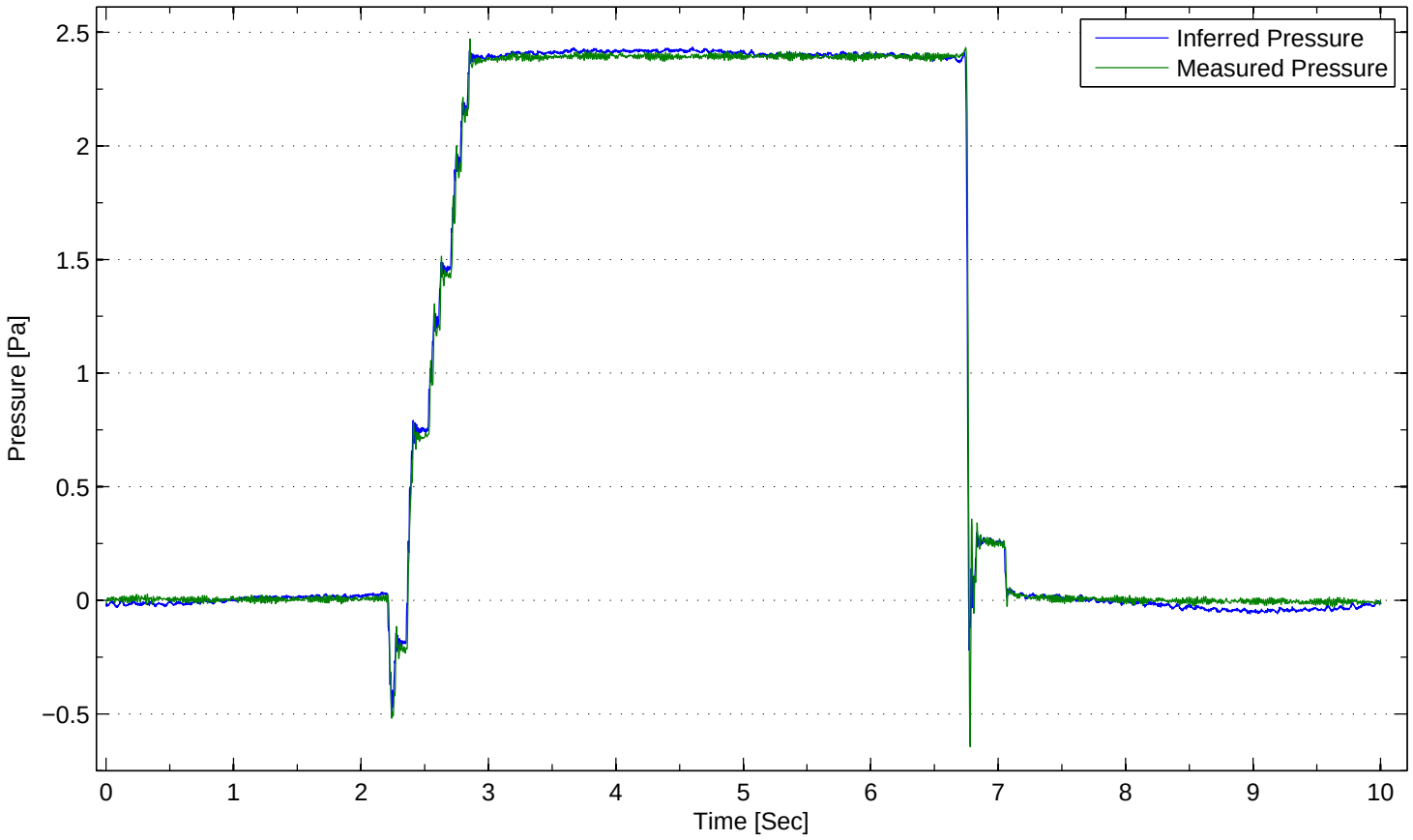

FIGURE 7. Time History of the Static Gage Pressure Test - 2.4 Pa

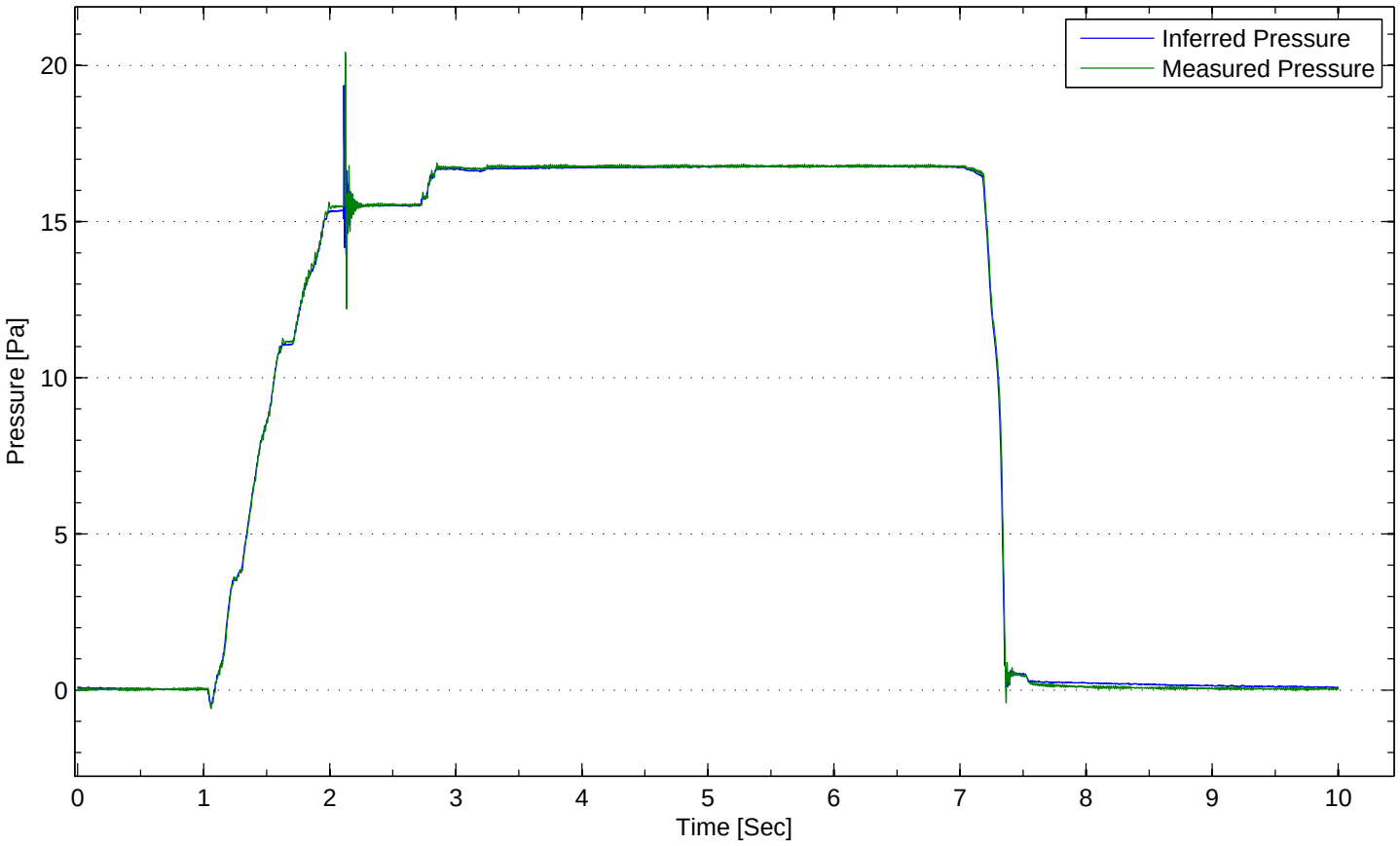

FIGURE 8. Time History of the Static Gage Pressure Test - 16.7 Pa

The averages of pressure over the last 0.25 seconds of the pressure pulse are given in Table 8.

TABLE 8. Results from Pressure Pulse Tests

Inferred Amplitude	Measured Amplitude	Std. Dev. of Difference	Std. Dev. Percent
$2.3907Pa$	$2.3913Pa$	$1.71x10^{-2}$	0.714%
$16.7547Pa$	$16.5225Pa$	$2.76x10^{-2}$	0.165%

Over- and under-shoot signal processing artifacts of the encoding equations are well controlled during the pressure transitions (Figures 9 and 10). These figures show the same $12ms$ period ringing phenomia found in the impulse tests. Again, these observations are assumed to be the product of real pressures acting on the loudspeaker and differ from a Gibbs Phenomia in that the ringing does not appear with pressure transitions to zero (Figures 11 and 12).

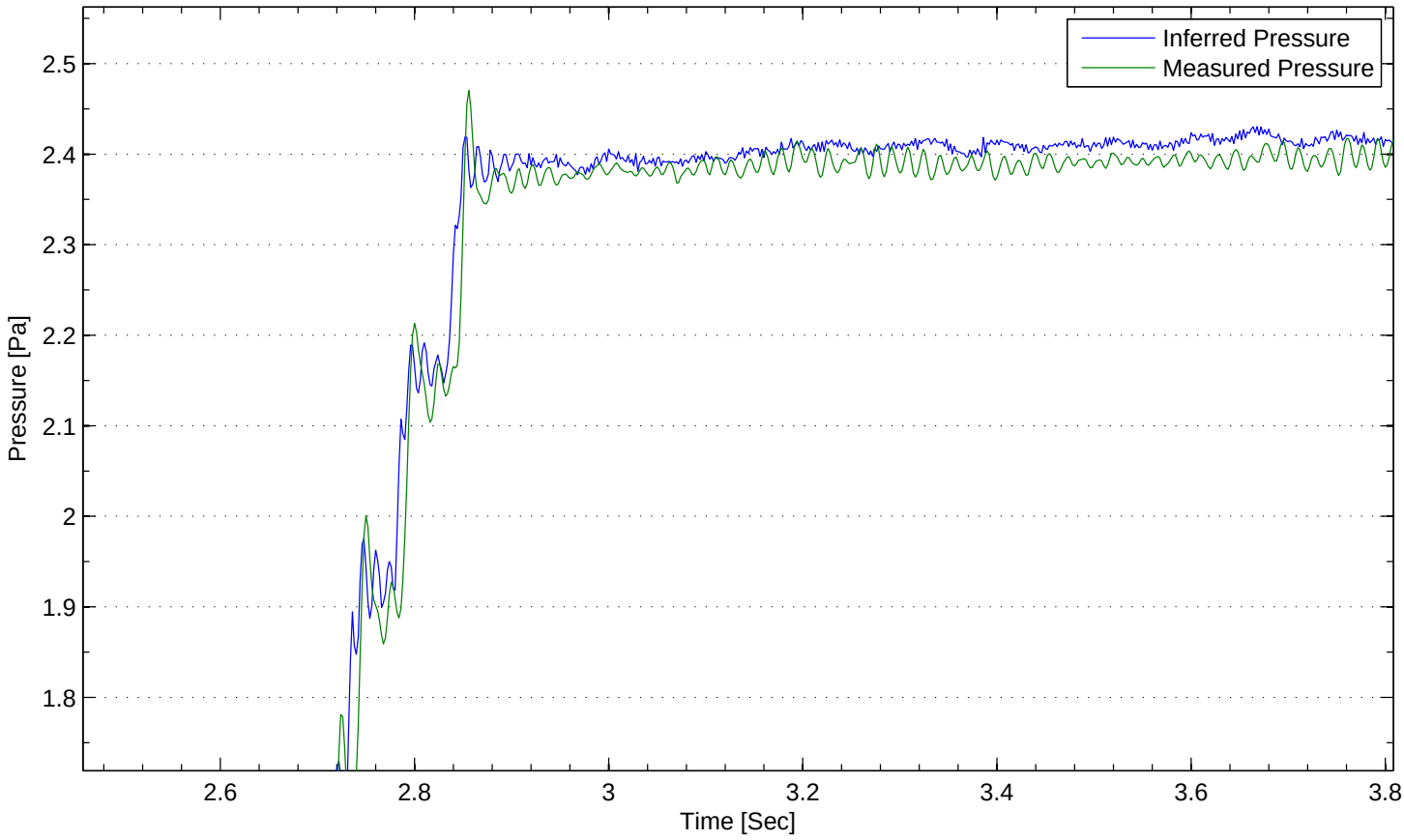

FIGURE 9. Overshoot of the Static Gage Pressure Test - 2.4 Pa

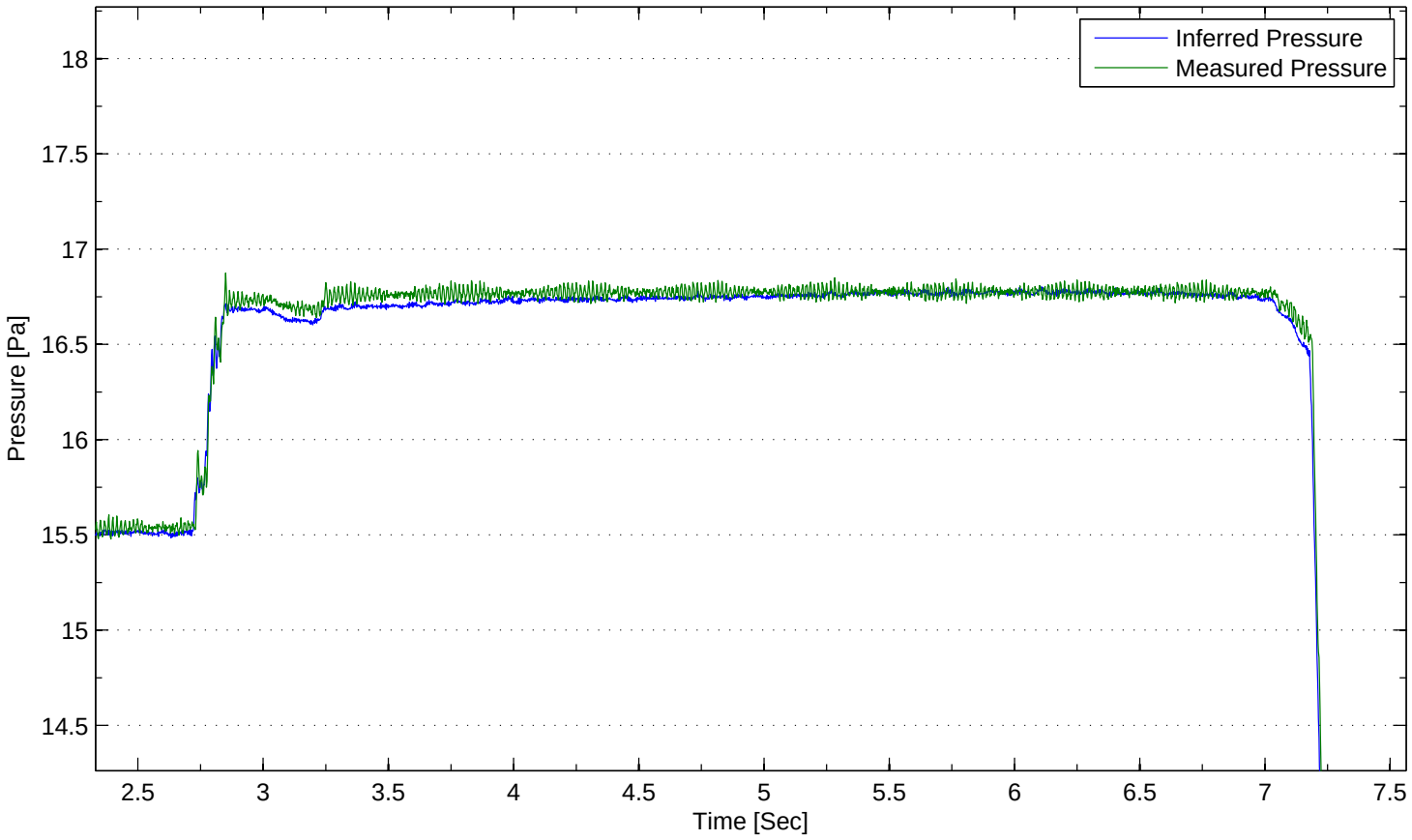

FIGURE 10. Overshoot of the Static Gage Pressure Test - 16.7 Pa

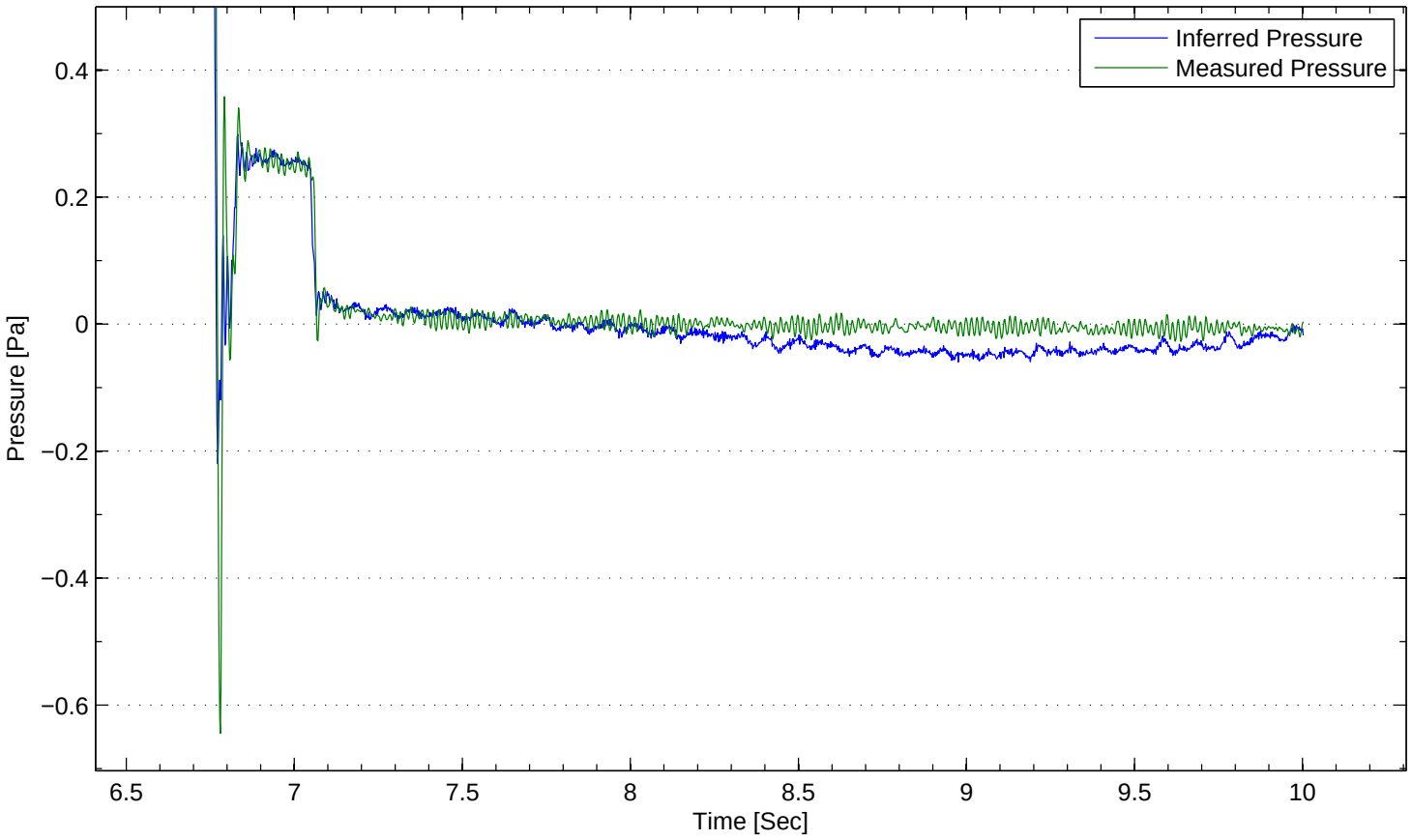

FIGURE 11. Undershoot of the Static Gage Pressure Test - 2.4 Pa

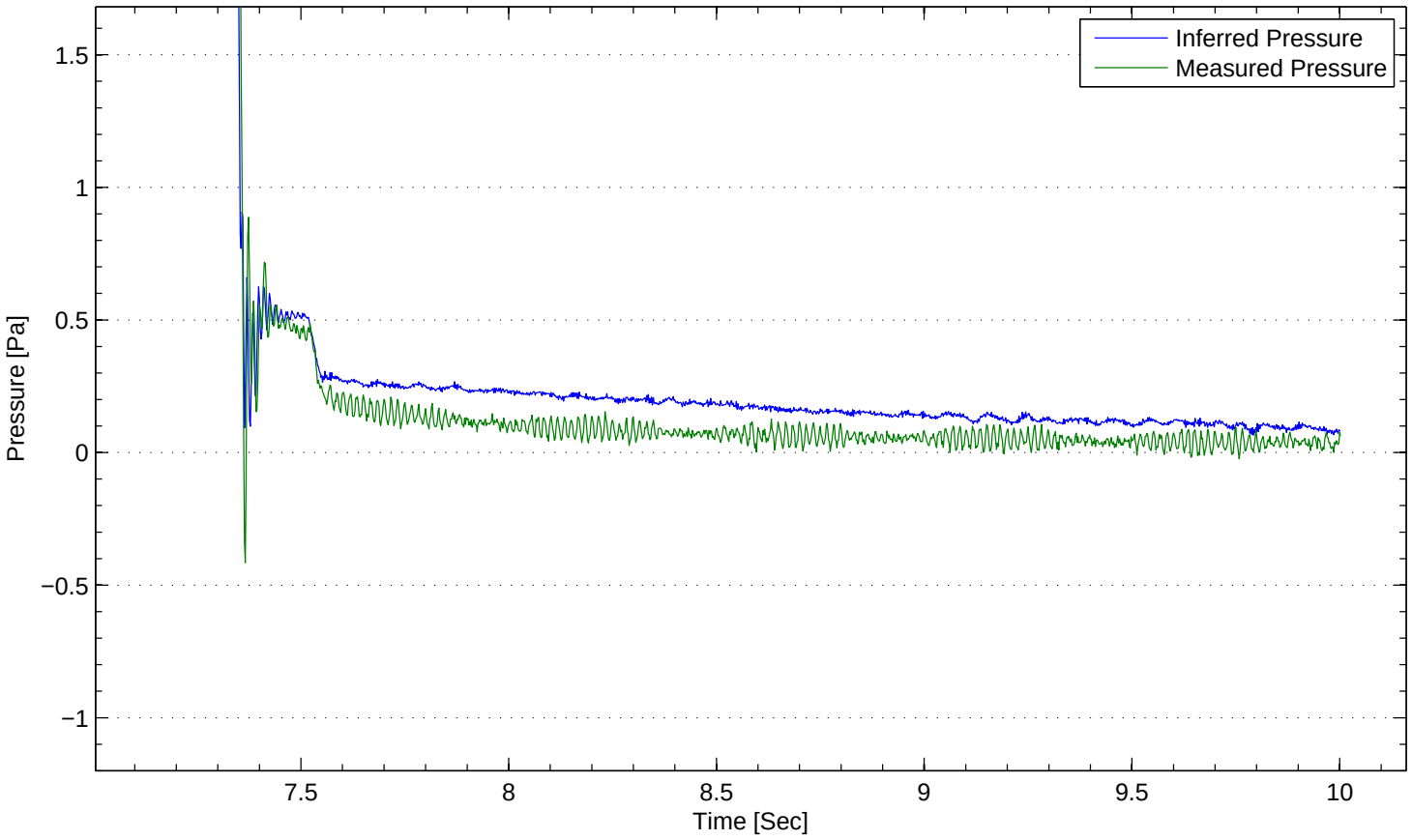

FIGURE 12. Undershoot of the Static Gage Pressure Test - 16.7 Pa

Figures 11 and 12 also show the drift caused by the slight change in resistance of the voice coil during the pulse. The departure of the inferred pressure is a result of integration drift due to the difference in the measured voltage and expected voltage of the loudspeaker system. At the start of the pulse (Figures 13 and 14), it can be seen that this drift process is not active. The average difference in pressures at this time was less than $0.02Pa$ in both cases. However, after current is applied to the voice coil, its resistance increases. This causes a integration drift to occur during the test time period which causes the inferred pressure to be in error by $0.04Pa$ in the case of the low pressure test and $0.2Pa$ in the case of the high pressure test. These values reflect a 1.67% and 1.20% error when compared to the nominally applied pressure.

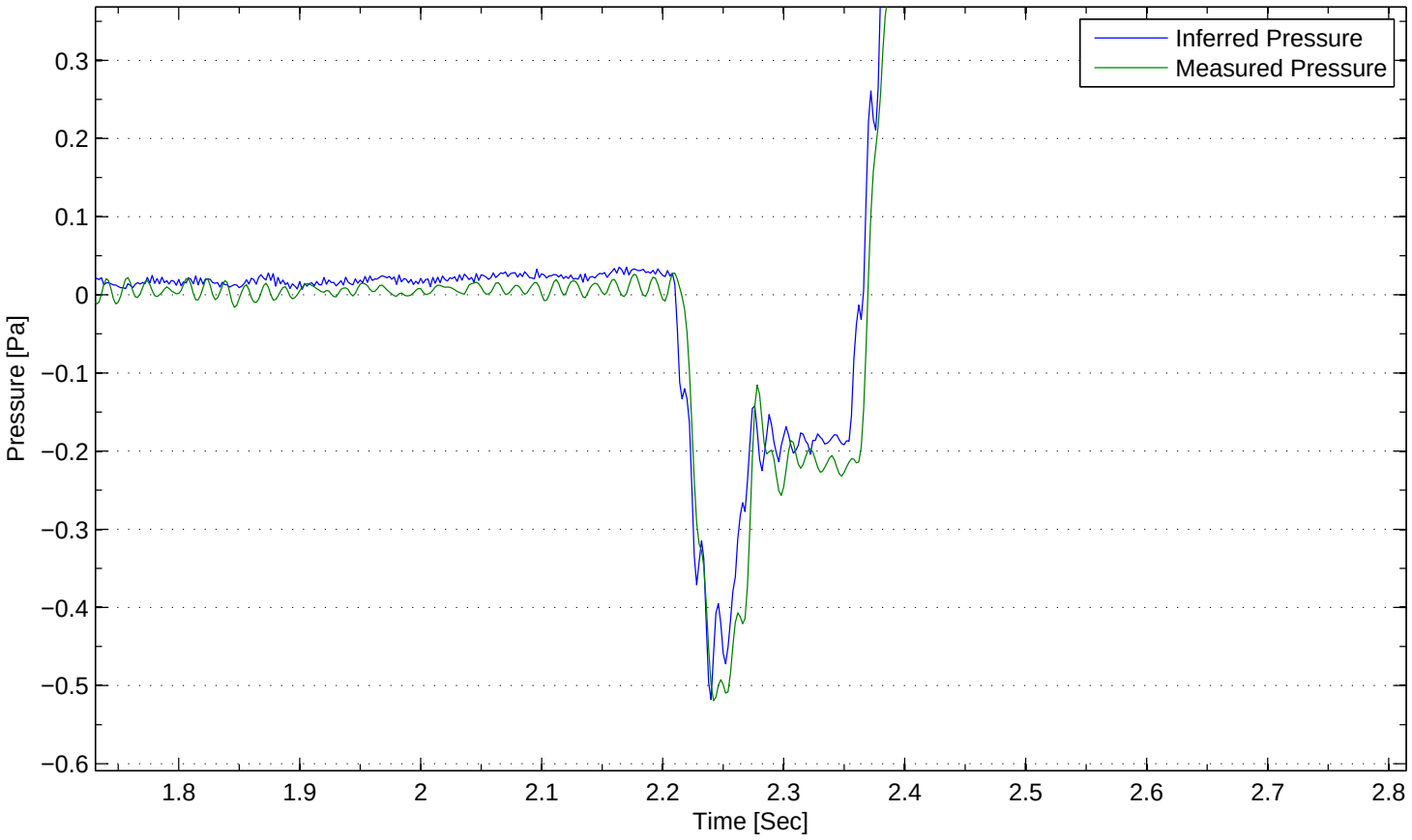

FIGURE 13. Pulse Start of the Static Gage Pressure Test - 2.4 Pa

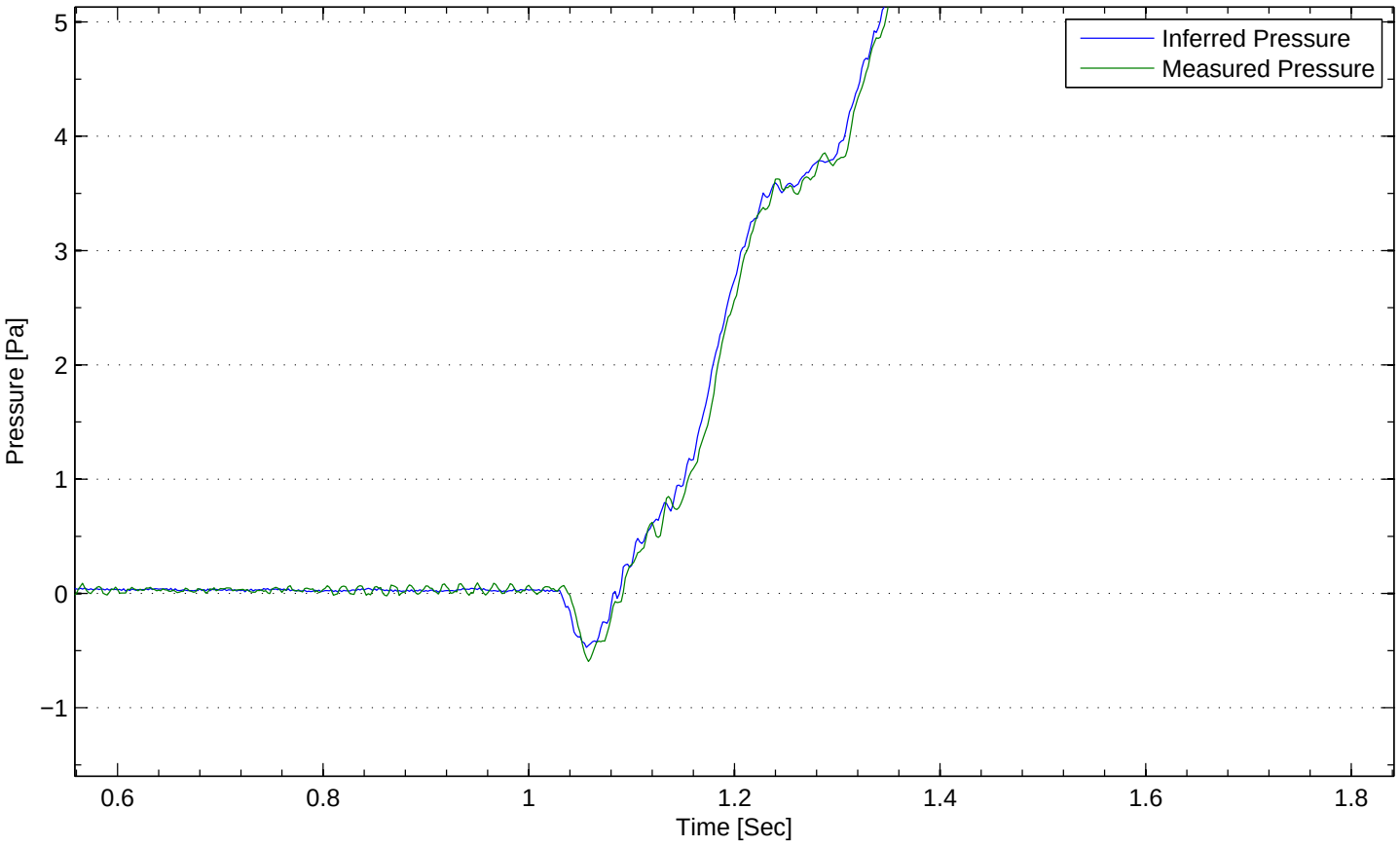

FIGURE 14. Pulse Start of the Static Gage Pressure Test - 16.7 Pa

7.3.3. *Dynamic Gauge Pressure.* Five tests were performed to evaluate the accuracy of the device at generating and reporting time varying gauge pressures. These tests evaluated dynamic pressures at frequencies below $10Hz$. This frequency limit was found to be the onset of modal behavior of the pressure cavity in other experiments. That is the pressure response of the cavity became dominated by a number (> 1) of degrees of freedom and would no longer act as single compressive body above $10Hz$ (see Appendix G).

TABLE 9. Sine Tests Amplitude Comparison

Frequency	Inferred Amplitude	Measured Amplitude	Difference	Percent Difference
$0.5Hz$	$1.2407Pa$	$1.2712Pa$	$-0.0305Pa$	-2.45%
$1.0Hz$	$2.3907Pa$	$2.3913Pa$	$-0.0161Pa$	-0.20%
$2.5Hz$	$9.1203Pa$	$9.2537Pa$	$-0.1334Pa$	-1.46%
$5.0Hz$	$10.1072Pa$	$10.0874Pa$	$0.0198Pa$	0.195%
$10Hz$	$9.8452Pa$	$9.7142Pa$	$0.1310Pa$	1.330%

The amplitude values reported in Table 9 were calculated via a Discrete Fourier Transform centered on the frequency in question. Four of the five frequencies tested showed an discrepancy in amplitude of less than 1.5%. The 2.45% discrepancy for the $0.5Hz$ test is most likely in error as a function of the pole that exists in the mechanical impedance kernel at $s = 0$. A further discussion on this type of error can be found in Appendix C.

The phase lag between the inferred and measured sinusoids were also calculated. The results can be found in Table 10. Results from the impulse test experiments suggest the nominal propagation time of the pressure wave between loudspeaker and reference transducer was 8 to $9ms$. This delay agrees with three of the five sinusoid tests. It is assumed that the odd lag behavior of the $0.5Hz$ and $1.0Hz$ tests was also in error as a function of the mechanical impedance pole at $s = 0$.

TABLE 10. Sine Tests Phase Comparison

Frequency	Phase Difference	Phase Delay
$0.5Hz$	$0.435°$	$2.417ms$
$1.0Hz$	$10.76°$	$29.912ms$
$2.5Hz$	$8.20°$	$9.120ms$
$5.0Hz$	$22.57°$	$12.542ms$
$10Hz$	$48.18°$	$13.383ms$

Time histories of the $1.0Hz$ and $2.5Hz$ tests are shown in Figures 15 and 16

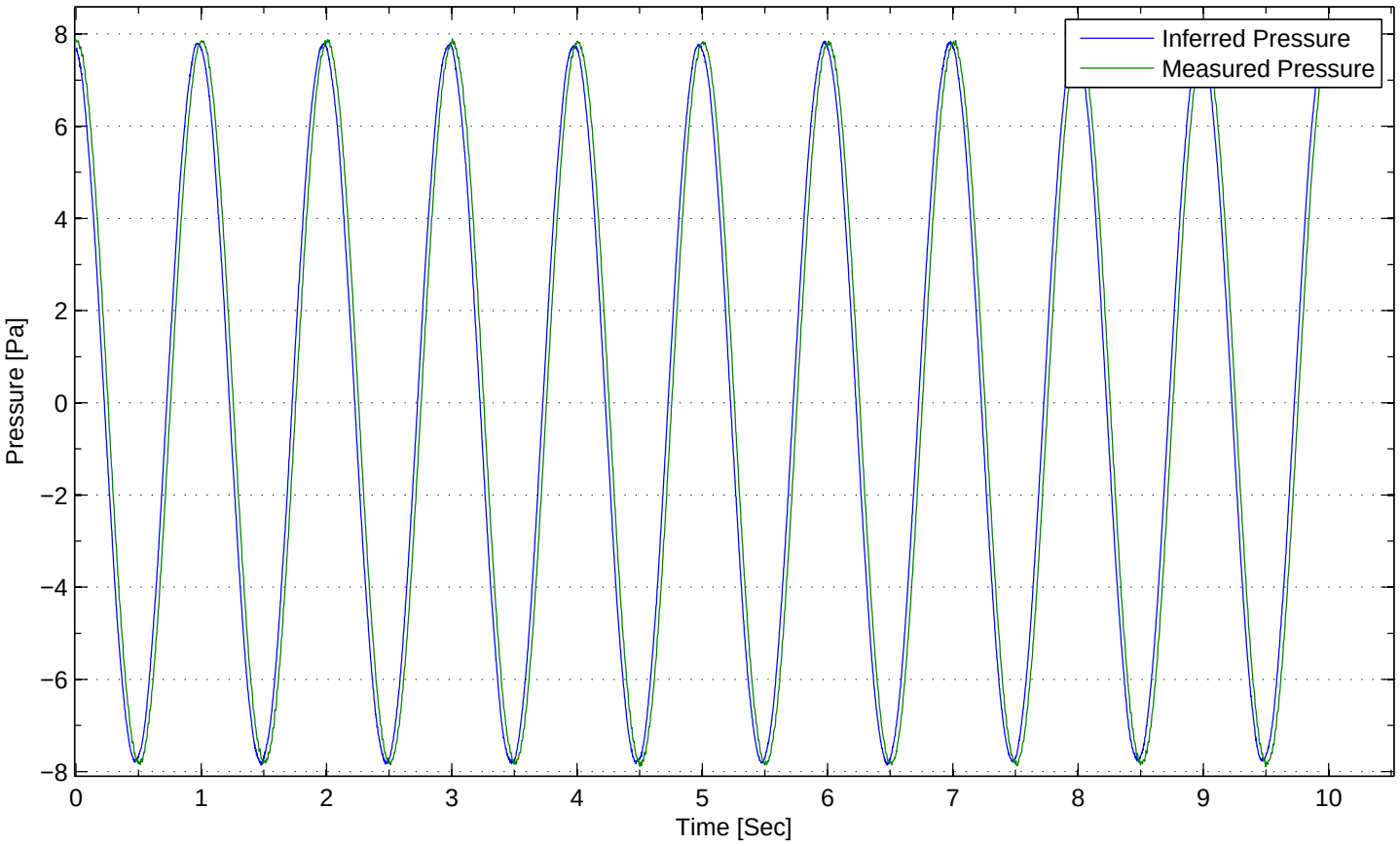

FIGURE 15. Time Histories of the $1.0Hz$ Test

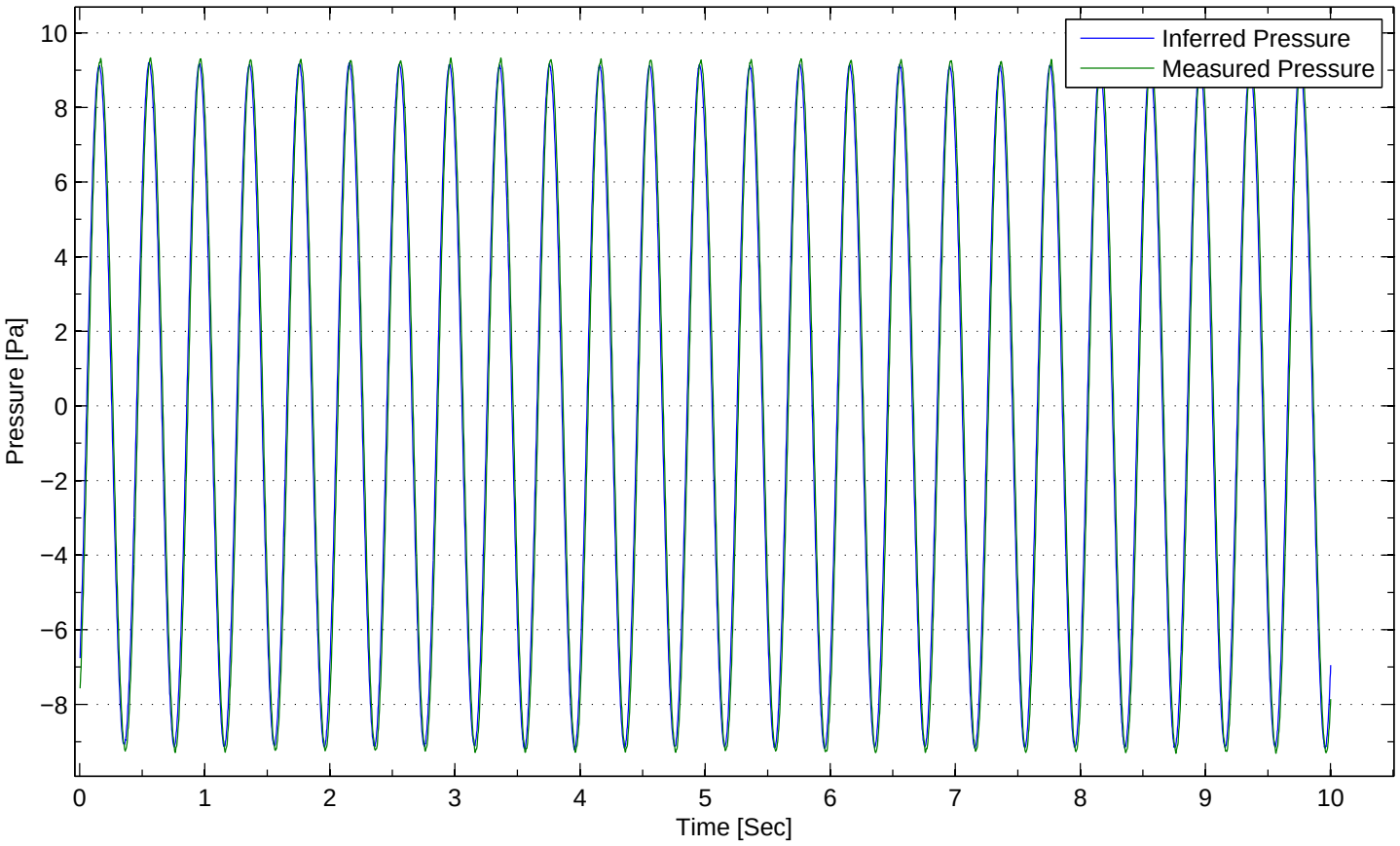

FIGURE 16. Time Histories of the $2.5Hz$ Test

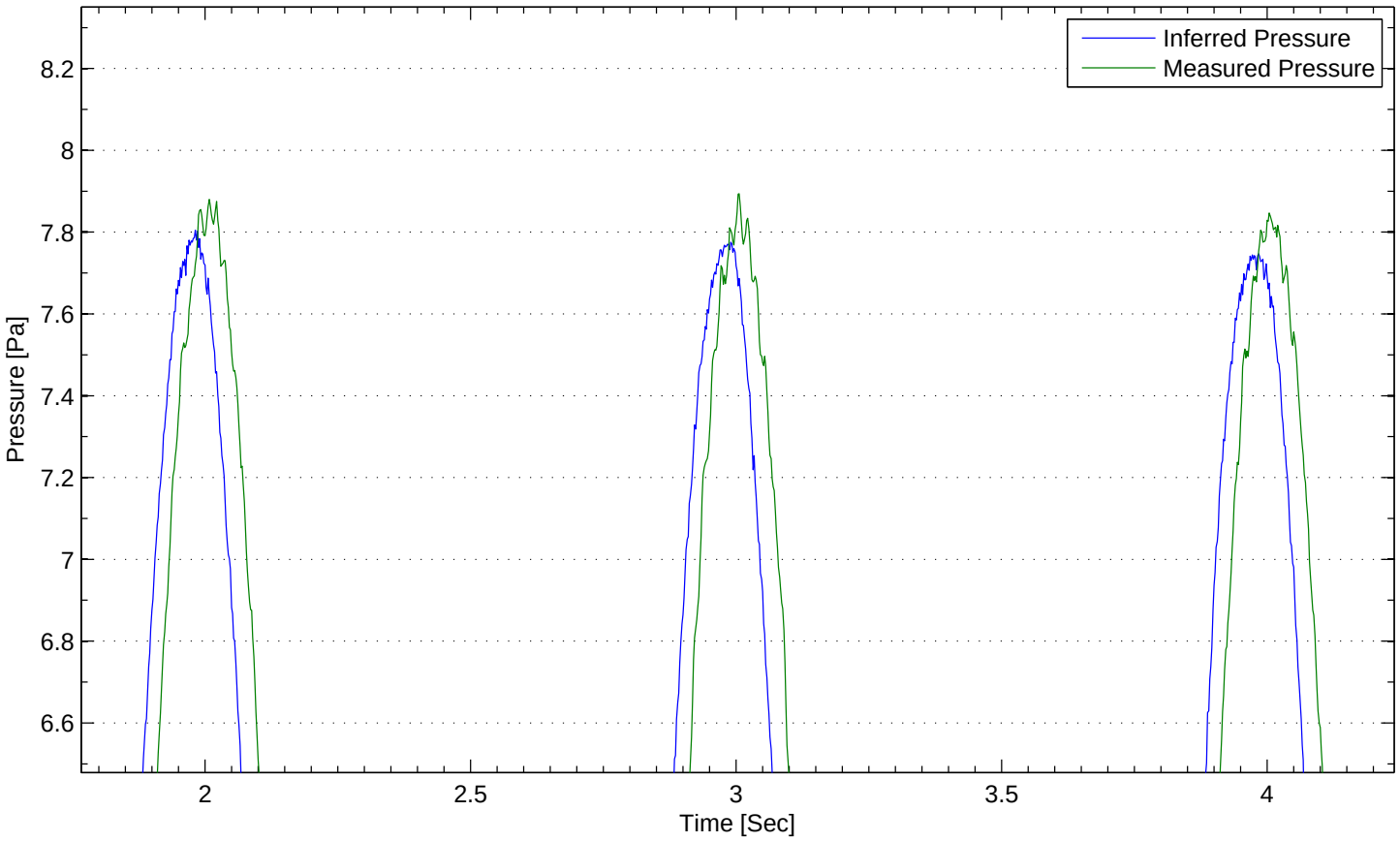

FIGURE 17. Sinusoid Peaks of the $1.0Hz$ Test

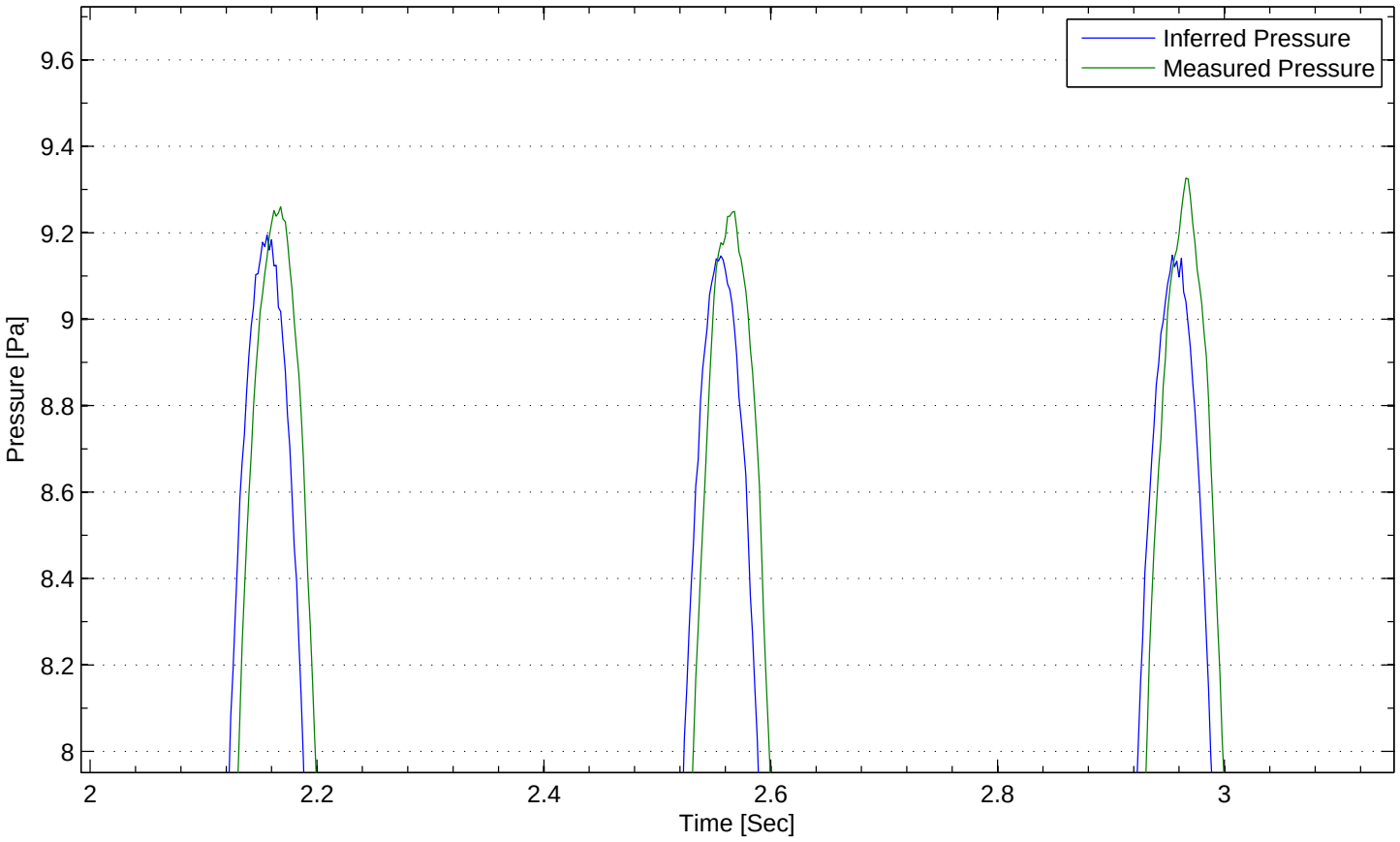

FIGURE 18. Sinusoid Peaks of the $2.5Hz$ Test

8. Conclusion

A technique has been developed that can both generate and accurately transduce hydrostatic pressures. A prototype device has been constructed which achieved a relative accuracy approaching 1%. This accuracy is provided solely by the device and without reliance on a reference transducer or knowledge of: the local gravity; thermodynamic properties of the working fluid; or acceleration of the cavity. In this way, a pressure standard was defined by reference only to the standards of the Amp, the Volt, the Meter, and – in the case of time varying pressure – the Second.

8.1. **Impact.** The implementation of this technique represents the first time that a reference standard can be defined without the use of another pressure standard (e.g. a primary pressure standard) or the implicit use of a mass standard. In this way, a unit of pressure can now be defined by comparison to universal physical constants – making it, colloquially, an "electric unit". The mathematical formulation of this statement and a proposal for a prototype device to extend the idea with future work can be found in Appendix A.

Secondly, the concept of using an actuator as its own encoding device may represent a new area of study in the discipline of control theory. Whereas the concept of an automatic control device typically assumes the use of a separate error signal in its theory of operation, now that signal can be provided by observing the driving signal of the device. Furthermore, it is conceptually feasible to develop a type of electrical control network that performs its operations not based on the impedance of the device under control (as is the case with all contemporary control networks and power amplifiers) but rather on the instantaneous difference between two impedances – the device under control and an idealized model of the device under control. This concept is merely a restatement of what was performed 'off-line' in the experiments detailed in this paper. Work currently under way is extending these experiments to include 'on-line' or real time results.

8.2. **Accuracy.** The accuracy of the prototype device described in this paper is only slightly lower than accuracies provided by commercial secondary reference standards. Material properties of the low-cost loudspeaker used in this experiment was the primary impediment to achieving higher accuracies (See Appendix C). With further study, the accuracy of the technique should approach an order of accuracy comparable to the 'electric' reference standards used in the device's construction (e.g. better than 1 part in 100,000). Work currently under way is attempting to extend the accuracy of the device by using specialized voice coil windings and signal processing techniques to interrogate the instantaneous resistance of the voice coil.

9. Bibliography

References

[1] *A Guide for the Dynamic Calibration of Pressure Transducers*. Instrumentation, Systems, and Automation Society, Research Triangle Park, NC, 2002.

[2] V.E. Bean. Dynamic pressure metrology. *Metrologia*, 30(6), 1994.

[3] D.A. Bies and C.H. Hansen. *Engineering Noise Control: Theory and Practice*. Spon Press, New York, 2003.

[4] Ronald N. Bracewell. *The Fourier Transform and Its Applications*. McGraw-Hill, New York, 1965.

[5] G. Geneves and et al. The bnm watt balance project. *IEE Transactions on Instrumentation and Measurement*, 54(2), 2005.

[6] T. Kobata and et al. Measurement of the volume of weights using an acoustic volumeter and the reliability of such measurement. *Metrologia*, 41, 2004.

[7] Wayne R. Moore. *Foundations of Mechanical Accuracy*. The Moore Special Tool Company, Inc., Bridgeport, Connecticut, 1970.

[8] A. Picard and et al. The bipm watt balance. *IEE Transactions on Instrumentation and Measurement*, 56(2), 2007.

[9] Steven W. Smith. *The Scientist and Engineer's Guide to Digital Signal Processing*. California Technical Pub., New York, 1998.

[10] R.L. Steiner and et al. The nist watt balance: progress toward monitoring the kilogram. *IEE Transactions on Instrumentation and Measurement*, 46(2), 1997.

[11] C.R. Tilford and A.P. Miiller. Development of a low differential-pressure standard. Presented at the 1997 NCSL Workshop and Symposium, 1997.

Appendix A. The Flux Balance

Physical interpretation of the right hand side of Equation 5.3 can guide the search for a volume change detection method that does not rely on a changing pressure. A similar term to the right hand side of this equation appears in Faraday's Law of Induction and is related to the magnetic flux (ϕ_m) through a surface.

$$\begin{aligned}
\nabla \times E &= -\frac{dB}{dt} \\
\iint_S \nabla \times E \ dA &= -\iint_S \frac{dB}{dt} \ dA \\
\oint_{dS} E \cdot dl &= -\frac{d}{dt} \iint_S B \ dA \\
V(t)\Big|_l &= -\frac{d}{dt} \ \phi_m(t)\Big|_A \\
\int_0^t V(\tau)\Big|_l \, d\tau &= \phi_m(t)\Big|_A
\end{aligned}$$

Above, Stoke's Theorem has been applied to the differential form of Fraday's Law. Integrating with respect to time yields an expression that relates the time-summation of voltage appearing on a loop of wire and the magnetic flux contained by that loop.

The expression may at first appear a unconventional. It is simply the application of the same law used to derive Equation 5.3. In Equation 5.3 the change in magnetic flux through a loop of wire is provided by the relative movement of the linear motor's voice coil and the magnetic field appearing in the motor's permanently magnetized flux gap. It is important to note that this voltage is proportional to: 1) the voice coil's speed ($\dot{x}(t)$), 2) the magnetic field strength (B), and 3) the number of wire loop turns per unit distance (l).

However, the combination of these terms can also been seen as a rate of change of a volume quantity. In Equation 5.3, the quantity is the magnetic field strength (B) – otherwise known as magnetic flux density – while in the most recently developed equation, the quantity is seen as the rate of change of a volume quantity that produces a magnetic field.

This volume quantity is also known as a magnetic dipole moment and has units of magnetic field strength times a moment arm. It can be conceptualized as the per-area strength of an ordinary bar magnet times the length of this bar magnet. In other words, connecting two identical bar magnetics face-to-face will increase the magnetic field strength appearing at the exposed faces.

This fact can be understood at the elementary school level by noting that two magnetics, when placed end-to-end, will pick up heavier objects than a single magnetic. However, it is important to note that the field strength appearing at the exposed face of the newly-created magnet is the volume summation of the magnetic flux density of each part of the magnet positioned in-line with a vector representing the length and direction of the macroscopic magnet. Formally, this becomes:

$$\nabla \times B = \mu_0 M$$
$$\iint_S \nabla \times B \ dA = \mu_0 \iint_S M \ dA$$
$$\oint_{dS} B \cdot dl = \mu_0 \iint_S M \ dA$$

This equation is otherwise known as Ampre's Law for magnetized materials, where l is a loop and S is a manifold that both define the cross-sectional area of the bar magnetic.

While the magnetization of ferromagnetic materials is one way to generate a magnetic dipole (M), another way is to move electrical current around a loop. When this occurs, a magnetic field is created inside of the loop that is proportional to the current density contained by that loop. This is the effect that gives rise to the magnetization of a common hardware nail when wrapped with a coil of wire. If the nail and the bar magnetic are viewed similarly, it can be said that the magnetic flux density of each longitudinal slice of the nail is proportional to the total current contained in a small longitudinal slice of the coil. In this slice of the coil, equal amounts of electrical charge are being moved in opposing directions while being separated by a moment arm – the diameter of the nail. The same magnetic field could be created by negatively charging the outside of the nail and then spinning it around its longitudinal axis in the same direction the current was flowing.

It follows that if the nail were postivelly charged, it would need to be spun in the opposite direction to produce the same magnetic field. By extension, if two nails were oppositely charged – one positive and one negative – the same magnetic field would appear between them if they were moved in a sweeping motion while separated by a distance. This magnetic field would be inversely proportional to their separation distance and proportional to their speed and total charge.

One may now imagine that the charged nails, while in close proximity, would tend to polarize the air between them. Atomic or molecular charge separation would tend to become aligned with the plane defining the separation between the nails. The movement of only the air then would generate a magnetic field in the direction normal to the plane defining the separation between the nails and the movement direction of the air in proportion to the average speed of the total volume of air being moved. Formally this is

$$\nabla \times B = \mu_0 \left[\nabla \times (P \times u)\right] \tag{A.1}$$

Of course, the movement of air polarized by any charge comparable to that produced by the archetypal '6V lantern battery' commonly used in such nail-coil experiments would be practicably undetectable. However, if the charge-separation gap is narrowed, the electrical potential between the polarizing conductors is increased, and a dielectric working fluid with a higher electric permittivity is used, sensitivities of 0.05 $\frac{Vs}{m^3}$ per turn can be achieved by a properly positioned wire loop.

If, as in the above example, the nails are elongated to produce the top and bottom plates of a fluid duct and a pair of Helmholtz coils are positioned to produce the side-walls of the duct, a practical measurement device can be produced. In this configuration, the projection of the cross sectional area of the coils and charge plates into the duct form a volume boundary working fluid. The normal vectors of the plates and coils produce a single imaginary surface inside of the flowing fluid. When the charge plates are energized and the fluid is moving, a magnetic field will be produced that is proportional to the volume transport speed across this imaginary surface. The change in this magnetic field is related to the time-rate change of volume transport across the imaginary surface, and can be detected by the production of voltage in the Helmholtz coil pair. Formally this is,

$$
\begin{aligned}
\nabla \times B &= \mu_0 \left[\nabla \times (P \times u)\right] \\
\iint \nabla \times B \; dxdz &= \mu_0 \iint \left[\nabla \times (P \times u)\right] dxdz \\
\oint B \cdot d\vec{l} &= \mu_0 \oint \left(\vec{P} \times \vec{u}\right) dl \\
\oint B \cdot d\vec{l} &= \mu_0 \int_{y_0}^{y_1} \left(\vec{P} \times \vec{u}\right) \cdot d\vec{y} \\
\oint B \cdot d\vec{l} &= \mu_0 \int_{y_0}^{y_1} \left(|P|\hat{P} \times \vec{u}\right) \cdot d\vec{y} \\
\oint B \cdot d\vec{l} &= \mu_0 |P| \int_{y_0}^{y_1} \left(\hat{P} \times \vec{u}\right) \cdot d\vec{y} \\
\oint B \cdot d\vec{l} &= \mu_0 |P| \int_{y_0}^{y_1} \left(\hat{P} \times \vec{u}\right) \cdot \hat{y} dy \\
\oint B \cdot d\vec{l} &= \mu_0 |P| \int_{y_0}^{y_1} \vec{u} \cdot \left(\hat{y} \times \hat{P}\right) dy \\
\oint B \cdot d\vec{l} &= \mu_0 |P| \int_{y_0}^{y_1} \vec{u} \cdot \hat{A} \; dy \\
\oint B \cdot d\vec{l} &= \mu_0 |P| \bar{\vec{u}} \cdot \hat{A} \; y \\
\int_{y_0}^{y_1} \vec{B} \; dy &= \mu_0 |P| \bar{\vec{u}} \cdot \hat{A} \; y \\
\vec{B} y &= \mu_0 |P| \bar{\vec{u}} \cdot \hat{A} \; y \\
\vec{B} &= \mu_0 |P| \left(\bar{\vec{u}} \cdot \hat{A}\right)
\end{aligned}
$$

Here, $\hat{A}$ is the unit vector that defines the volume measurement plane inside of the duct. It is formed from the cross product of the unit vectors that define the polarization field ($\hat{P}$) and the magnetic field ($\hat{l}$). The absolute value of the magnetic flux density ($|B|$) is proportional to the volume rate of the fluid passing through that its field line. This magnetic flux density can be collected and summed giving the total volume

flux rate occurring in the downstream direction inside of the measurement volume. This can be seen by applying Fraday's Law of Induction to the Helmholtz coil pair.

$$
\begin{aligned}
\nabla \times E &= -\frac{dB}{dt} \\
\iint_{hc} \nabla \times E \ dxdz &= -\iint_{hc} \frac{dB}{dt} \ dxdz \\
\oint_{hc} E \cdot dl &= -\frac{d}{dt} \iint_{hc} B \ dxdz \\
\oint_{hc} E \cdot dl &= -\frac{d}{dt} \iint_{hc} \mu_0 |P| \left(\bar{\vec{u}} \cdot \hat{A} \right) \ dxdz \\
\oint_{hc} E \cdot dl &= -\mu_0 |P| \iint_{hc} \frac{d}{dt} \left(\bar{\vec{u}} \cdot \hat{A} \right) \ dxdz \\
\oint_{hc} E \cdot dl &= -\mu_0 |P| \frac{d}{dt} \overline{\left(\vec{u} \cdot \hat{A} \right)} xz \\
\frac{V_{hc}}{n} &= -\mu_0 |P| \frac{d}{dt} \overline{\left(\vec{u} \cdot \hat{A} \right)} xz
\end{aligned}
$$

Here,the over-bar represents the spatial average of $\vec{u} \cdot \hat{A}$ on a per-volume basis, V_{hc} is the voltage appearing on the terminals of the Helmholtz coil pair, and n is the number of loops in those coils. Rearranging this equation to solve for the full volume flux quantity gives:

$$
\frac{d}{dt} \overline{\left(\vec{u} \cdot \hat{A} \right)} = \frac{-V_{hc}}{n \mu_0 |P| xz} \tag{A.2}
$$

The polarization field strength is assumed to be uniform throughout the measurement volume. In this case, $|P|$ is related the electric field between the charged plates and the electric permittivity of the dielectric fluid as

$$
|P| = \kappa \epsilon_0 |E|
$$

Where κ is a dimensionless number giving the relative permitivity of the dielectric, ϵ_0 is the electric permittivity of free space, and E is the electric field. Because the electric field created by the charged plates is irrotational ($\nabla \times E = 0$) during the operation of the flux balance, the field is simply given by the gradient of the voltage potential ($E = -\nabla V_p$). In other words, the electric field strength is the measured voltage between the plates (V_p) divided by the distance between the plates (z):

$$|P| = \kappa\epsilon_0|E|$$
$$|P| = \kappa\epsilon_0\frac{V_p}{z}$$

Plugging this back into Equation A.2 yields:

$$\frac{d}{dt}\overline{\left(\vec{u}\cdot\hat{A}\right)} = \frac{-V_{hc}(t)}{nV_p}\frac{1}{\mu_0\kappa\epsilon_0}\frac{1}{x} \tag{A.3}$$

Here the quantity $\mu_0\epsilon_0$ can be recognized as the inverse of the square of the speed of light (c):

$$\frac{d}{dt}\overline{\left(\vec{u}\cdot\hat{A}\right)} = \frac{-V_{hc}(t)}{nV_p}\frac{c^2}{\kappa}\frac{1}{x} \tag{A.4}$$

Now it can be seen that the $\frac{Bl}{A}$ term from the previous section can be defined as the ratio of two time integrals of voltage:

$$\frac{Bl}{A} = V_p\frac{xn\kappa}{c^2}\left[\frac{\int_0^t V_{vc}(\tau)d\tau}{\int_0^t V_{hc}(\tau)d\tau}\right] \tag{A.5}$$

Appendix B. Mathematical Derivation

The following section is an almost word-for-word transcription of laboratory notes dated between 19 August 2011 and 17 October 2012. These notes are included in this thesis to aid in the understanding of the mathematics which are described in the main section.

B.1. **The Speaker.** Under the assumption of treating the speaker diaphragm as a solid, rigid member, the diaphragm can be analyzed using a free body diagram method.

The forces applied to the diaphragm during its dynamic excitation are as follows:

Table 11. Application of Faraday's Law of Induction to the Voice Coil

Equation	Description
$F_e(t) = Bl \cdot I(t)$	Voice Coil, Magnetic
$F_s(t) = -k \cdot x(t)$	Surround and Spider Compliance (spring rate)
$F_d(t) = -c \cdot \dot{x}(t)$	Surround and Spider Damping (damping rate)
$F_w(t) = -A \cdot P(t)$	Force Developed by Hydrostatic Pressure

where $I(t)$ is the current though the voice coil measured in amps, $P(t)$ is the pressure inside of the test cavity, A is the effective area of the speaker diaphragm, and Bl is the Force Ratio of the voice coil.

B.2. **Dynamics.** The summation of dynamic forces applied to the speaker diaphragm is expressed as:

$$\begin{aligned} \sum F = m\ddot{x} &= F_e(t) + F_s(t) + F_d(t) + F_w(t) \\ m\ddot{x} &= Bl \cdot I(t) - kx(t) - c\dot{x}(t) - A \cdot P(t) \\ m\ddot{x} + c\dot{x} + kx &= Bl \cdot I(t) - A \cdot P(t) \end{aligned}$$

In this case, we are interested in inferring two fluid parameters from inside the box: Pressure and Volume Velocity.

In the case of pressure, we can solve the above equation with the addition of the relationship:

$$e(t) = Bl \cdot \dot{x}(t)$$

where $e(t)$ is the back EMF from the voice coil on the electrical side.

In the case of volume velocity, we can solve the above equation with the addition of the relationship:

$$Q(t) = A \cdot \dot{x}(t)$$

where $Q(t)$ is the volume velocity of the fluid moving in or out of a control volume around the speaker.

B.3. **Pressure Solution.** Using the relation $e(t) = Bl \cdot \dot{x}(t)$ we can solve the above dynamic equation for pressure in terms of voltage and current. When we have this equation, we can relate the back EMF developed by the movement of the speaker coil to the voltage developed at the speaker's lugs, and finally to the input of the complete electrical circuit.

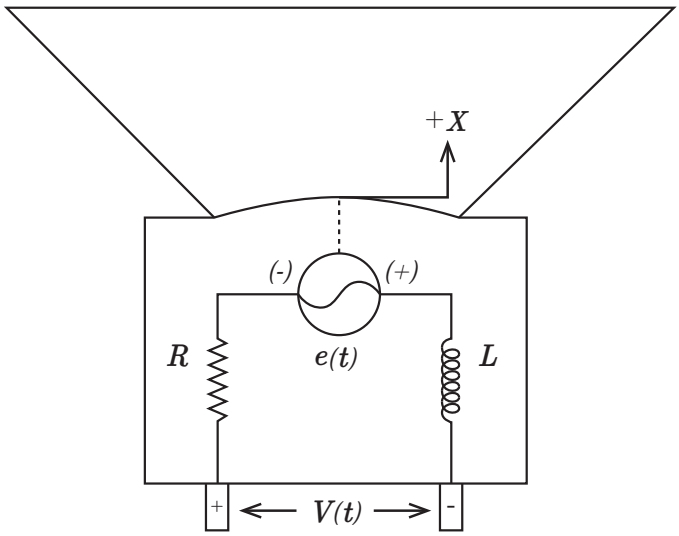

FIGURE 19. Speaker's Electrical Circuit

B.3.1. *Internal Back-EMF.* The back EMF is the voltage measured at the speaker electrical terminal lugs minus the voltage developed by the speaker's electrical system's complex impedance:

$$V(t) = e(t) + I(t) \cdot \mathbb{Z}$$

where $V(t)$ is the voltage measured at the speaker lugs and $\mathbb{Z}$ is the complex impedance of the speaker's electrical system.

Rewriting the governing dynamic equation in terms of velocity yields:

$$m\dot{v} + cv + k\int_0^t v(\lambda)d\lambda = Bl \cdot I(t) - A \cdot P(t)$$
$$m \cdot \frac{\dot{e}(t)}{Bl} + c \cdot \frac{e(t)}{Bl} + k\int_0^t \frac{e(\lambda)}{Bl}d\lambda = Bl \cdot I(t) - A \cdot P(t)$$
$$\frac{1}{Bl}\left[m \cdot \dot{e}(t) + c \cdot e(t) + k\int_0^t e(\lambda)d\lambda\right] = Bl \cdot I(t) - A \cdot P(t)$$

Which is Laplace Transformed as:

$$\frac{1}{Bl}[m \cdot \dot{e}(t) + c \cdot e(t) + k\int_0^t e(\lambda)d\lambda] = Bl \cdot I(t) - A \cdot P(t)$$
$$\frac{1}{Bl}[ms\hat{E}(s) - me_0 + c\hat{E}(s) + \frac{k}{s}\hat{E}(s)] = Bl \cdot \hat{I}(s) - A \cdot \hat{P}(s)$$

Where e_0 is assumed to be 0 as the speaker will not be moving during the start of the test :

$$\frac{1}{Bl}[ms\hat{E}(s) + c\hat{E}(s) + \frac{k}{s}\hat{E}(s)] = Bl \cdot \hat{I}(s) - A \cdot \hat{P}(s)$$
$$\frac{1}{Bl}[ms + c + \frac{k}{s}] \cdot \hat{E}(s) = Bl \cdot \hat{I}(s) - A \cdot \hat{P}(s)$$
$$\frac{1}{Bl}[ms + c + \frac{k}{s}] \cdot \hat{E}(s) - Bl \cdot \hat{I}(s) = -A \cdot \hat{P}(s)$$

B.3.2. *Speaker Lug Voltage.* Equating the back emf of voice coil's movement to the voltage developed at the speaker's terminal lugs:

$$V_{lug}(t) = L \cdot \frac{di(t)}{dt} + R \cdot i(t) + \frac{1}{C} \cdot \int_0^t i(\lambda)d\lambda + e(t)$$
$$e(t) = V_{lug}(t) - L \cdot \frac{di(t)}{dt} - R \cdot i(t) - \frac{1}{C} \cdot \int_0^t i(\lambda)d\lambda$$

which transforms as:

$$e(t) = V_{lug}(t) - L \cdot \frac{di(t)}{dt} - R \cdot i(t) - \frac{1}{C} \cdot \int_0^\lambda i(\lambda)d\lambda$$
$$\hat{E}(s) = \hat{V}_{lug}(s) - [sL \cdot \hat{I}(s) - Li_0 + R \cdot \hat{I}(s) + \frac{1}{sC} \cdot \hat{I}(s)]$$

Where i_0 is assumed to be 0 as the test will start at $t = 0$:

$$\hat{E}(s) = \hat{V}_{lug}(s) - [sL \cdot \hat{I}(s) + R \cdot \hat{I}(s) + \frac{1}{sC} \cdot \hat{I}(s)]$$
$$\hat{E}(s) = \hat{V}_{lug}(s) - [sL + R + \frac{1}{sC}] \cdot \hat{I}(s)$$

Substitution into the above equation yields:

$$\frac{1}{Bl \cdot A}[ms + c + \frac{k}{s}] \cdot \hat{E}(s) - \frac{Bl}{A} \cdot \hat{I}(s) = -\hat{P}(s)$$
$$\frac{1}{Bl \cdot A}([ms + c + \frac{k}{s}] \cdot [\hat{V}_{lug}(s) - [sL + R + \frac{1}{sC}] \cdot \hat{I}(s)]) - \frac{Bl}{A} \cdot \hat{I}(s) = -\hat{P}(s)$$
$$\frac{1}{Bl \cdot A}([ms + c + \frac{k}{s}] \cdot \hat{V}_{lug}(s) - [ms + c + \frac{k}{s}] \cdot [sL + R + \frac{1}{sC}] \cdot \hat{I}(s)) - \frac{Bl}{A} \cdot \hat{I}(s) = -\hat{P}(s)$$
$$\frac{1}{Bl \cdot A}([ms + c + \frac{k}{s}] \cdot \hat{V}_{lug}(s) - [(ms + c + \frac{k}{s}) \cdot (sL + R + \frac{1}{sC}) + (Bl)^2] \cdot \hat{I}(s)) = -\hat{P}(s)$$

Letting...

$$\mathbb{Z}(s)_{mech} = [ms + c + \frac{k}{s}]$$
$$\mathbb{Z}(s)_{elec} = [sL + R + \frac{1}{sC}]$$

we now have:

$$\frac{1}{Bl \cdot A}\left[\mathbb{Z}(s)_{mech} \cdot \hat{V}_{lug}(s) - \left[\mathbb{Z}(s)_{mech} \cdot \mathbb{Z}(s)_{elec} + (Bl)^2\right] \cdot \hat{I}(s)\right] = -\hat{P}(s)$$

B.3.3. *Terminal Circuit.* A 1 Ohm resistor is placed in-line with the speaker terminal lugs to measure the current. In order to "zero-out" $\hat{V}_{lug}(s)$ in the equation above, and still have an accurate current measurement, the impedance of this resistor must be incorporated. The voltage measured between the the speaker's terminal lug and acounting for the 1 Ohm shunt resistor:

$$V(t) = L \cdot \frac{di(t)}{dt} + R \cdot i(t) + \frac{1}{C} \cdot \int_0^t i(\lambda)d\lambda + R_{sh} \cdot i(t) + e(t)$$
$$e(t) = V(t) - L \cdot \frac{di(t)}{dt} - R \cdot i(t) - \frac{1}{C} \cdot \int_0^t i(\lambda)d\lambda - R_{sh} \cdot i(t)$$

which transforms as:

$$e(t) = V(t) - L \cdot \frac{di(t)}{dt} - R \cdot i(t) - \frac{1}{C} \cdot \int_0^{\lambda} i(\lambda) d\lambda - R_{sh} \cdot i(t)$$
$$\hat{E}(s) = \hat{V}(s) - [sL \cdot \hat{I}(s) - Li_0 + R \cdot \hat{I}(s) + \frac{1}{sC} \cdot \hat{I}(s) + R_{sh} \cdot \hat{I}(s)]$$

Where i_0 is assumed to be 0 as the test will start at $t = 0$:

$$\hat{E}(s) = \hat{V}(s) - [sL \cdot \hat{I}(s) + R \cdot \hat{I}(s) + \frac{1}{sC} \cdot \hat{I}(s) + R_{sh} \cdot \hat{I}(s)]$$
$$\hat{E}(s) = \hat{V}(s) - [sL + R + \frac{1}{sC}] \cdot \hat{I}(s) - R_{sh} \cdot \hat{I}(s)$$
$$\hat{E}(s) = \hat{V}(s) - \mathbb{Z}(s)_{elec} \cdot \hat{I}(s) - R_{sh} \cdot \hat{I}(s)$$

Substitution into the mechanical system yields:

$$\frac{1}{Bl \cdot A} \left[\mathbb{Z}(s)_{mech} \cdot \hat{E}(s) - (Bl)^2 \cdot \hat{I}(s) \right] = -\hat{P}(s)$$
$$\frac{1}{Bl \cdot A} \left[\mathbb{Z}(s)_{mech} \cdot \left[\hat{V}(s) - \mathbb{Z}(s)_{elec} \cdot \hat{I}(s) - R_{sh} \cdot \hat{I}(s) \right] - (Bl)^2 \cdot \hat{I}(s) \right] = -\hat{P}(s)$$
$$\frac{1}{Bl \cdot A} \left[\mathbb{Z}(s)_{mech} \cdot \hat{V}(s) - \mathbb{Z}(s)_{mech} \cdot \mathbb{Z}(s)_{elec} \cdot \hat{I}(s) - \mathbb{Z}(s)_{mech} \cdot R_{sh} \cdot \hat{I}(s) - (Bl)^2 \cdot \hat{I}(s) \right] = -\hat{P}(s)$$
$$\frac{1}{Bl \cdot A} \left[\mathbb{Z}(s)_{mech} \cdot \hat{V}(s) - \left[\mathbb{Z}(s)_{mech} \cdot \mathbb{Z}(s)_{elec} + \mathbb{Z}(s)_{mech} \cdot R_{sh} + (Bl)^2 \right] \cdot \hat{I}(s) \right] = -\hat{P}(s)$$

Distributing the $\frac{1}{Bl \cdot A}$ term yields two unknown quantities:

$$\frac{1}{Bl \cdot A} \left[\mathbb{Z}(s)_{mech} \cdot \hat{V}(s) - \left[\mathbb{Z}(s)_{mech} \cdot \mathbb{Z}(s)_{elec} + \mathbb{Z}(s)_{mech} \cdot R_{sh} + (Bl)^2 \right] \cdot \hat{I}(s) \right] = -\hat{P}(s)$$
$$\left[\frac{1}{Bl \cdot A} \cdot \mathbb{Z}(s)_{mech} \right] \cdot \hat{V}(s) - \left[\frac{1}{Bl \cdot A} \cdot \left(\mathbb{Z}(s)_{mech} \cdot \mathbb{Z}(s)_{elec} + \mathbb{Z}(s)_{mech} \cdot R_{sh} + (Bl)^2 \right) \right] \cdot \hat{I}(s) = -\hat{P}(s)$$
$$[\beta_v(s)] \cdot \hat{V}(s) - [\beta_c(s)] \cdot \hat{I}(s) = -\hat{P}(s)$$

or...

$$\hat{P}(s) = [\beta_c(s)] \cdot \hat{I}(s) - [\beta_v(s)] \cdot \hat{V}(s)$$

where

$$\beta_v(s) = \frac{1}{Bl \cdot A} \cdot \mathbb{Z}(s)_{mech}$$
$$\beta_c(s) = \frac{1}{Bl \cdot A} \cdot \left(\mathbb{Z}(s)_{mech} \cdot \mathbb{Z}(s)_{elec} + \mathbb{Z}(s)_{mech} \cdot R_{sh} + (Bl)^2\right)$$

B.4. **Volume Velocity Solution.** Using the relation $Q(t) = A \cdot \dot{x}(t)$ we can solve the governing dynamic equation for volume velocity in terms of pressure and current. When we have this equation, we can use the above pressure-to-terminal voltage relation to equate the volume velocity of the speaker to the input of the full electrical circuit.

B.4.1. *Volume Velocity.* Rewriting the governing dynamic equation in terms of velocity yields:

$$m\dot{v} + cv + k\int_0^t v(\lambda)d\lambda = Bl \cdot I(t) - A \cdot P(t)$$

Which is Laplace Transformed as:

$$m \cdot \dot{v}(t) + c \cdot v(t) + k\int_0^t v(\lambda)d\lambda = Bl \cdot I(t) - A \cdot P(t)$$
$$ms\hat{v}(s) - mv_0 + c\hat{v}(s) + \frac{k}{s}\hat{v}(s) = Bl \cdot \hat{I}(s) - A \cdot \hat{P}(s)$$

Where v_0 is assumed to be 0 as the speaker will not be moving during the start of the test :

$$ms\hat{v}(s) + c\hat{v}(s) + \frac{k}{s}\hat{v}(s)] = Bl \cdot \hat{I}(s) - A \cdot \hat{P}(s)$$
$$[ms + c + \frac{k}{s}] \cdot \hat{v}(s) = Bl \cdot \hat{I}(s) - A \cdot \hat{P}(s)$$

Applying the relation $Q(t) = A \cdot \dot{x}(t)$, or $v(t) = \frac{Q(t)}{A}$ yields:

$$[ms + c + \frac{k}{s}] \cdot \hat{v}(s) = Bl \cdot \hat{I}(s) - A \cdot \hat{P}(s)$$
$$[ms + c + \frac{k}{s}] \cdot \frac{\hat{Q}(s)}{A} = Bl \cdot \hat{I}(s) - A \cdot \hat{P}(s)$$
$$[ms + c + \frac{k}{s}] \cdot \hat{Q}(s) = Bl \cdot A \cdot \hat{I}(s) - A^2 \cdot \hat{P}(s)$$

or...

$$[\mathbb{Z}(s)_{mech}] \cdot \hat{Q}(s) = Bl \cdot A \cdot \hat{I}(s) - A^2 \cdot \hat{P}(s)$$

B.4.2. *Relating Pressure to Voltage and Current.* Applying the above developed equation for internal pressure in terms of the calibration box's circuit parameters (terminal voltage and circuit current)

$$\hat{P}(s) = \left[\frac{1}{Bl \cdot A} \cdot \left(\mathbb{Z}(s)_{mech} \cdot \mathbb{Z}(s)_{elec} + \mathbb{Z}(s)_{mech} \cdot R_{sh} + (Bl)^2\right)\right] \cdot \hat{I}(s) - \left[\frac{1}{Bl \cdot A} \cdot \mathbb{Z}(s)_{mech}\right] \cdot \hat{V}(s)$$

yields:

$$[\mathbb{Z}(s)_{mech}] \cdot \hat{Q}(s) = Bl \cdot A \cdot \hat{I}(s) - \left[\frac{A^2}{Bl \cdot A} \cdot \left(\mathbb{Z}(s)_{mech} \cdot \mathbb{Z}(s)_{elec} + \mathbb{Z}(s)_{mech} \cdot R_{sh} + (Bl)^2\right)\right] \cdot \hat{I}(s) ...$$
$$... + \left[\frac{A^2}{Bl \cdot A} \cdot \mathbb{Z}(s)_{mech}\right] \cdot \hat{V}(s)$$
$$[\mathbb{Z}(s)_{mech}] \cdot \hat{Q}(s) = \frac{A}{Bl} \cdot (Bl)^2 \cdot \hat{I}(s) - \left[\frac{A}{Bl} \cdot \left(\mathbb{Z}(s)_{mech} \cdot \mathbb{Z}(s)_{elec} + \mathbb{Z}(s)_{mech} \cdot R_{sh} + (Bl)^2\right)\right] \cdot \hat{I}(s) ...$$
$$... + \left[\frac{A}{Bl} \cdot \mathbb{Z}(s)_{mech}\right] \cdot \hat{V}(s)$$
$$[\mathbb{Z}(s)_{mech}] \cdot \hat{Q}(s) = -\left[\frac{A}{Bl} \cdot (\mathbb{Z}(s)_{mech} \cdot \mathbb{Z}(s)_{elec} + \mathbb{Z}(s)_{mech} \cdot R_{sh})\right] \cdot \hat{I}(s) + \left[\frac{A}{Bl} \cdot \mathbb{Z}(s)_{mech}\right] \cdot \hat{V}(s)$$
$$[\mathbb{Z}(s)_{mech}] \cdot \hat{Q}(s) = \left[\frac{A}{Bl} \cdot \mathbb{Z}(s)_{mech}\right] \cdot \hat{V}(s) - \left[\frac{A}{Bl} \cdot (\mathbb{Z}(s)_{mech} \cdot \mathbb{Z}(s)_{elec} + \mathbb{Z}(s)_{mech} \cdot R_{sh})\right] \cdot \hat{I}(s)$$

or...

$$\hat{Q}(s) = \left[\frac{A}{Bl}\right] \cdot \hat{V}(s) - \left[\frac{A}{Bl} \cdot (\mathbb{Z}(s)_{elec} + R_{sh})\right] \cdot \hat{I}(s)$$
$$\hat{Q}(s) = [\xi_v(s)] \cdot \hat{V}(s) - [\xi_c(s)] \cdot \hat{I}(s)$$

where

$$\xi_v(s) = \frac{A}{Bl}$$
$$\xi_c(s) = \frac{A}{Bl} \cdot (\mathbb{Z}(s)_{elec} + \cdot R_{sh})$$

B.5. **Calibration.** The governing equations of the speaker system are

$$\hat{P}(s) = [\beta_c(s)] \cdot \hat{I}(s) - [\beta_v(s)] \cdot \hat{V}(s)$$
$$\hat{Q}(s) = [\xi_v(s)] \cdot \hat{V}(s) - [\xi_c(s)] \cdot \hat{I}(s)$$

Rearranging the pressure equation yields a clue as to how to calibrate the system:

$$\hat{P}(s) = [\beta_c(s)] \cdot \hat{I}(s) - [\beta_v(s)] \cdot \hat{V}(s)$$
$$\hat{P}(s) = \left[\frac{1}{Bl \cdot A} \cdot \left(\mathbb{Z}(s)_{mech} \cdot \mathbb{Z}(s)_{elec} + \mathbb{Z}(s)_{mech} \cdot R_{sh} + (Bl)^2\right)\right] \cdot \hat{I}(s) - \left[\frac{1}{Bl \cdot A} \cdot \mathbb{Z}(s)_{mech}\right] \cdot \hat{V}(s)$$
$$\hat{P}(s) = \left[\frac{1}{Bl \cdot A} \cdot \left(\mathbb{Z}(s)_{mech} \cdot (\mathbb{Z}(s)_{elec} + R_{sh}) + (Bl)^2\right)\right] \cdot \hat{I}(s) - \left[\frac{1}{Bl \cdot A} \cdot \mathbb{Z}(s)_{mech}\right] \cdot \hat{V}(s)$$
$$\hat{P}(s) = \left[\frac{\mathbb{Z}(s)_{mech}}{Bl \cdot A} \cdot \left((\mathbb{Z}(s)_{elec} + R_{sh}) + \frac{(Bl)^2}{\mathbb{Z}(s)_{mech}}\right)\right] \cdot \hat{I}(s) - \left[\frac{\mathbb{Z}(s)_{mech}}{Bl \cdot A}\right] \cdot \hat{V}(s)$$
$$\hat{P}(s) = \frac{\mathbb{Z}(s)_{mech}}{Bl \cdot A}\left[\left((\mathbb{Z}(s)_{elec} + R_{sh}) + \frac{(Bl)^2}{\mathbb{Z}(s)_{mech}}\right) \cdot \hat{I}(s) - \hat{V}(s)\right]$$
$$\hat{P}(s) = \frac{Bl}{A} \cdot \frac{\mathbb{Z}(s)_{mech}}{(Bl)^2}\left[\left((\mathbb{Z}(s)_{elec} + R_{sh}) + \frac{(Bl)^2}{\mathbb{Z}(s)_{mech}}\right) \cdot \hat{I}(s) - \hat{V}(s)\right]$$

The rearrangement reveals three unknown quantities:

$$\mathbb{Z}(s)_{elec} + R_{sh}$$

$$\frac{(Bl)^2}{\mathbb{Z}(s)_{mech}}$$

$$\frac{Bl}{A}$$

These unknown quantities can be found by performing three simple tests...

B.5.1. *Volume Velocity Calibration.* The volume velocity calibration step could be performed if the speaker cone was held motionless such that Q(s) = 0.

Of course something as delicate as a speaker cone or voice coil cannot be 'clamped' in a traditional method. The closest thing might be to glue a threaded fastener to the speaker cone, in line with the voice coil, and use a threaded insert as a brace. Since the gluing method might be complicated, a close alternative can be accomplished by placing a rigid brace on one side of the cone and forward loading the cone's voice coil into the brace such that the cone never departs contact from the brace. That is I(t) = I0 + Isig(t), such that Isig(t) is greater than I0 for all time.

The math looks like...

$$\begin{aligned}
\hat{Q}(s) &= \left[\frac{A}{Bl}\right] \cdot \hat{V}(s) - \left[\frac{A}{Bl} \cdot (\mathbb{Z}(s)_{elec} + R_{sh})\right] \cdot \hat{I}(s) \\
0 &= \left[\frac{A}{Bl}\right] \cdot \hat{V}(s) - \left[\frac{A}{Bl} \cdot (\mathbb{Z}(s)_{elec} + R_{sh})\right] \cdot \hat{I}(s) \\
\left[\frac{A}{Bl}\right] \cdot \hat{V}(s) &= \left[\frac{A}{Bl} \cdot (\mathbb{Z}(s)_{elec} + R_{sh})\right] \cdot \hat{I}(s) \\
\hat{V}(s) &= (\mathbb{Z}(s)_{elec} + R_{sh}) \cdot \hat{I}(s) \\
\frac{\hat{V}(s)}{\hat{I}(s)} &= \mathbb{Z}(s)_{elec} + R_{sh}
\end{aligned}$$

B.5.2. *Mechanical System Calibration.* Assuming the dynamic pressure acting on the speaker diaphragm can be forced to zero by placing the speaker in a vacuum, the function

$$\frac{(Bl)^2}{\mathbb{Z}(s)_{mech}}$$

can be found by setting

$$\hat{P}(s) = 0$$

This results in the following evaluation:

$$\begin{aligned}
\hat{P}(s) &= [\beta_c(s)] \cdot \hat{I}(s) - [\beta_v(s)] \cdot \hat{V}(s) \\
0 &= [\beta_c(s)] \cdot \hat{I}(s) - [\beta_v(s)] \cdot \hat{V}(s) \\
[\beta_v(s)] \cdot \hat{V}(s) &= [\beta_c(s)] \cdot \hat{I}(s) \\
[\beta_v(s)] \cdot \hat{V}(s) &= [\beta_c(s)] \cdot \hat{I}(s)
\end{aligned}$$

$$\frac{\hat{V}(s)}{\hat{I}(s)} = \frac{\beta_c(s)}{\beta_v(s)}$$

This ratio can be reduced to:

$$\frac{\beta_c(s)}{\beta_v(s)} = R + R_{sh} + Ls + \frac{(Bl)^2}{ms + c + k/s}$$

Here, the quantity $R + R_{sh} + Ls$ can be recognized as $\mathbb{Z}(s)_{elec} + R_{sh}$. So...

$$\begin{aligned}
\frac{\beta_c(s)}{\beta_v(s)} &= R + R_{sh} + Ls + \frac{(Bl)^2}{ms + c + k/s} \\
\frac{(Bl)^2}{ms + c + k/s} &= \frac{\beta_c(s)}{\beta_v(s)} - R + R_{sh} + Ls \\
\frac{(Bl)^2}{ms + c + k/s} &= \frac{\beta_c(s)}{\beta_v(s)} - \frac{\xi_c(s)}{\xi_v(s)}
\end{aligned}$$

or...

$$\frac{(Bl)^2}{\mathbb{Z}(s)_{mech}} = \frac{\beta_c(s)}{\beta_v(s)} - \frac{\xi_c(s)}{\xi_v(s)}$$

B.5.3. *Voice Coil/Cone Calibration.* The last quanitiy to find is $\frac{Bl}{A}$. Finding this value requires the integration of the speaker's volume velocity under the application of a voltage designed to give a slow rise in displacement to a constant value (e.g. $v(t) = 1 - e^{-at}$, or slowly twisting a power supply's knob from $0 \rightarrow 5$ volts). The displaced volume, found by capturing the outflow of water from the box, is compared to the integrated volume velocity.

Analytically, this procedure could be performed in the s-domain by using the Final Value Theorem of the Laplace Transform. This would require dividing the equation by s (to sum the volume velocity to displaced

volume) and then then multiplying by s and taking the limit of the new function as $s \to 0$, per the Initial Value Theorem.

$$\hat{Q}(s) = [\xi_v(s)] \cdot \hat{V}(s) - [\xi_c(s)] \cdot \hat{I}(s) ... + \left[\frac{A}{Bl} \cdot L\right] \cdot i_0$$
$$\hat{Q}(s) = \left[\frac{A}{Bl}\right] \cdot \hat{V}(s) - \left[\frac{A}{Bl} \cdot (\mathbb{Z}(s)_{elec} + R_{sh})\right] \cdot \hat{I}(s) + \left[\frac{A}{Bl} \cdot L\right] \cdot i_0$$
$$\lim_{s\to 0} \hat{Q}(s) \left(\frac{s}{s}\right) = \left(\left[\frac{A}{Bl}\right] \cdot \hat{V}(s) - \left[\frac{A}{Bl} \cdot (\mathbb{Z}(s)_{elec} + R_{sh})\right] \cdot \hat{I}(s) + \left[\frac{A}{Bl} \cdot L\right] \cdot i_0\right) \left(\frac{s}{s}\right)$$
$$\lim_{s\to 0} \hat{Q}(s) = \left[\frac{A}{Bl}\right] \cdot \hat{V}(s) - \left[\frac{A}{Bl} \cdot (\mathbb{Z}(s)_{elec} + R_{sh})\right] \cdot \hat{I}(s) + \left[\frac{A}{Bl} \cdot L\right] \cdot i_0$$

But we have no way to easily express the values of either $\hat{V}(s)$ or $\hat{I}(s)$ in the s-domain. Therefore, it is easier to perform this analysis in the time domain...

$$\hat{Q}(s) = \left[\frac{A}{Bl}\right] \cdot \hat{V}(s) - \left[\frac{A}{Bl} \cdot (\mathbb{Z}(s)_{elec} + R_{sh})\right] \cdot \hat{I}(s) + \left[\frac{A}{Bl} \cdot L\right] \cdot i_0$$
$$Q(t) = \left[\frac{A}{Bl} \cdot \delta(t)\right] * V(t) - \left[\frac{A}{Bl} \cdot (L \cdot \delta'(t) + R \cdot \delta(t) + R_{sh} \cdot \delta(t))\right] * I(t) + \left[\frac{A}{Bl} \cdot L \cdot i_0\right] \cdot \delta(t)$$
$$Q(t) = \left[\frac{A}{Bl}\right] \cdot V(t) - \left[\frac{A}{Bl} \cdot \left(L \cdot \frac{d}{dt} I(t) + R \cdot I(t) + R_{sh} \cdot I(t)\right)\right] + \left[\frac{A}{Bl} \cdot L \cdot i_0\right] \cdot \delta(t)$$
$$Q(t) = \frac{A}{Bl} \cdot \left[V(t) - L \cdot \frac{d}{dt} I(t) - R \cdot I(t) - R_{sh} \cdot I(t)\right] + \frac{A}{Bl} \cdot [L \cdot i_0 \cdot \delta(t)]$$

Integrating...

$$Q(t) = \frac{A}{Bl} \cdot \left[V(t) - L \cdot \frac{d}{dt} I(t) - R \cdot I(t) - R_{sh} \cdot I(t)\right] + \frac{A}{Bl} \cdot [L \cdot i_0 \cdot \delta(t)]$$
$$\Delta V = \int_0^t Q(\tau) d\tau = \int_0^t \frac{A}{Bl} \cdot \left[V(t) - L \cdot \frac{d}{dt} I(t) - R \cdot I(t) - R_{sh} \cdot I(t)\right] d\tau + \int_0^t \frac{A}{Bl} \cdot [L \cdot i_0 \cdot \delta(\tau)] \, d\tau$$
$$\Delta V = \frac{A}{Bl} \cdot \left[\int_0^t V(\tau) d\tau - \int_0^t L \cdot \frac{d}{d\tau} I(\tau) d\tau - \int_0^t R \cdot I(\tau) d\tau - \int_0^t R_{sh} \cdot I(\tau) d\tau + \int_0^t L \cdot i_0 \cdot \delta(\tau) d\tau\right]$$
$$\Delta V = \frac{A}{Bl} \cdot \left[\int_0^t V(\tau) d\tau - L \cdot I(t) - L \cdot i_0 - \int_0^t R \cdot I(\tau) d\tau - \int_0^t R_{sh} \cdot I(\tau) d\tau + L \cdot i_0\right]$$
$$\Delta V = \frac{A}{Bl} \cdot \left[\int_0^t [V(\tau) - R \cdot I(\tau) - R_{sh} \cdot I(\tau)] \, d\tau - L \cdot I(t)\right]$$

This equation describes how to relate the final displaced volume to the current and voltage time histories recorded as the test was being performed. The first term on the RHS sums the difference between the voltage on the full circuit and the voltage that would be generated at any given time by the simple resistance of the circuit. This term gives the area under the voice coil's back-emf curve plus the area under the voltage curve generated by the voice coil's inductance. One can think about this quantity as the impulse-potential (sum of the motivating voltage) of the electrical circuit. This impulse-potential is "used up" in one of two ways: Either changing the volume displaced by the speaker's cone, or adding to the magnetic field of the voice coil. The magnetic potential of the voice coil is simply the inductance value of the coil times the instantaneous current. In this case, the instantaneous current is the current that is measured at the end of the test ($t \to \infty$).

The inductance L must be regressed from the $\mathbb{Z}(s)_{elec} + R_{sh}$ term. When plotted as a function of frequency, the slope of the curve gives $\frac{L}{2\pi}$.

Appendix C. Voice Coil Temperature Dependence

Controlling the resistance parameter of the voice coil became a paramount concern during the testing and use of the prototype device. Excursions of this parameter from its nominal value will cause large errors in the pressure inference process – most notably in the lower frequency band.

As noted in the theory of operation section (Section 4) the voltage that develops across the terminals of the voice coil is a function of two things: 1) the electrical impedance of current flowing through the voice coil; and 2) the velocity of the voice coil. The process of integrating to find the position of the voice coil, and subsequently the force applied by the spring-like mechanisms found in the loudspeaker, depends on accurately subtracting the voltage that *should be* developed by the nominal impedance of the voice coil from the *actual* voltage that is being developed. This step becomes less critical when the mechanical model does not include a spring mechanism. That is, if the piston was sealed by a purely frictional device (e.g. piston rings and oil vs. a spring-like rubber seal), knowledge of the position of the piston becomes unnecessary when determining the pressure incident inside of the cavity. However, because all loudspeakers use a spring-like seal, it is necessary to resolve the position, not just the velocity of the voice coil. During this integration process, small errors that do not sum to zero through time will propagate through the mathematical technique to yield disastrous errors in determining the pressure time history.

While excursions of the nominal real impedance parameter of the voice coil generate errors that propagate throughout the entire s-plane representation of the pressure's time history, the most notable errors occur in the limit of $s \to 0$. As seen in Figure 20, a pole exists in the mechanical impedance of the loud speaker at $s = 0$. If the s-plane representation of that error of the inferred velocity of the voice coil falls near $s = 0$, large errors will be generated in the time history of the inferred pressure. In other words, the pole at $s = 0$ in the mechanical impedance ultimately makes the technique unreliable at reporting pressures that remain invariant for long periods of time.

The first step in controlling this type of error is to control departures of the real resistance of the voice coil from its nominal value. In the case of the loudspeaker chosen for the prototype experiment, the voice coil is an extremely tightly wound loop of 32 awg copper wire with an length of about 22 meters. This configuration makes the coil's nominal resistance extremely temperature sensitive. The temperature coefficient of a voice coil removed from a second M8a was measured to be $2.521x10^{-3}\frac{\Omega}{^\circ F}$. This value makes the voice coil some four orders of magnitude more sensitive to temperature variations than the manganin shunt resistor used to measure the circuit's current.

Figure 21 is provided for reference. The temperature of the coil during this test was controlled using a peltier junction. The gap between $61F$ and $66F$ was a result of peltier junction inactivity in that range.

With this level of temperature sensitivity, control of the temperature of the voice coil during the experimental process became paramount. Great amounts of time and effort were used to insure the testing was completed with the voice coil operating in the ambient range of $67.5 - 68.5^\circ F$. The great problem of operating in this temperature range was thermal power expelled by the voice coil under operation. That is the total mass of the coil is less than $2g$ and its temperature responds very quickly to changes in dissipation power. To this

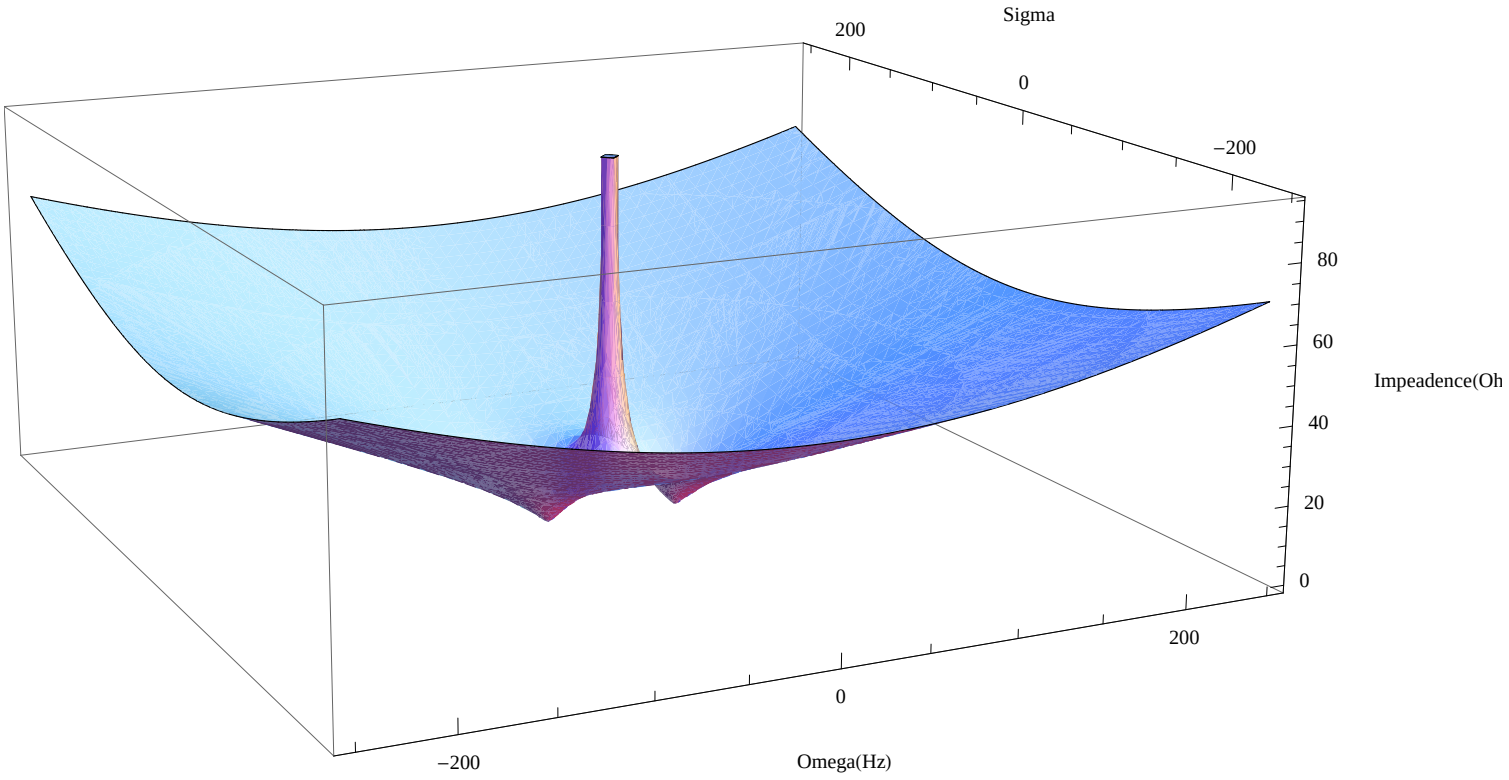

FIGURE 20. S-Domain Representation of the M8a's Mechanical Impedance

end, experiments were chosen where this power could be minimized. Through trial and error, it was found that the upper limit of the power that the voice coil was able to dissipate under isothermal conditions was $7.2x10^{-2}\frac{J}{s}$. The isothermal condition was considered to be valid if the resistance of the voice coil changed less than 0.01% during the test sequence, or about $\pm\frac{1}{4}^{\circ}F$.

The time history of a particularly poor choice of test signal is shown in Figure 22. In this test, the coil was energized with a nominal current of $10mA$ until a steady state was reached. At the start of the test, the current was reduced to near zero. Any current which is still flowing in the circuit (discussed in the next section) is now being impeded by the now slightly lower resistance provided by the voice coil's cooling. This effect causes an error to be produced in the inferred pressure in proportion to the square of time ($P(t)\ t^2$). In other words, the cooling generates a voltage discrepancy between what is measured and what should be measured. This voltage discrepancy is interpreted as the movement of the voice coil against the spring rate of the loudspeaker. After a short time, this voltage becomes almost constant and subsequently, the inferred velocity is constant. After this short time, the error takes on a linear relation with time ($P(t)\ t^1$).

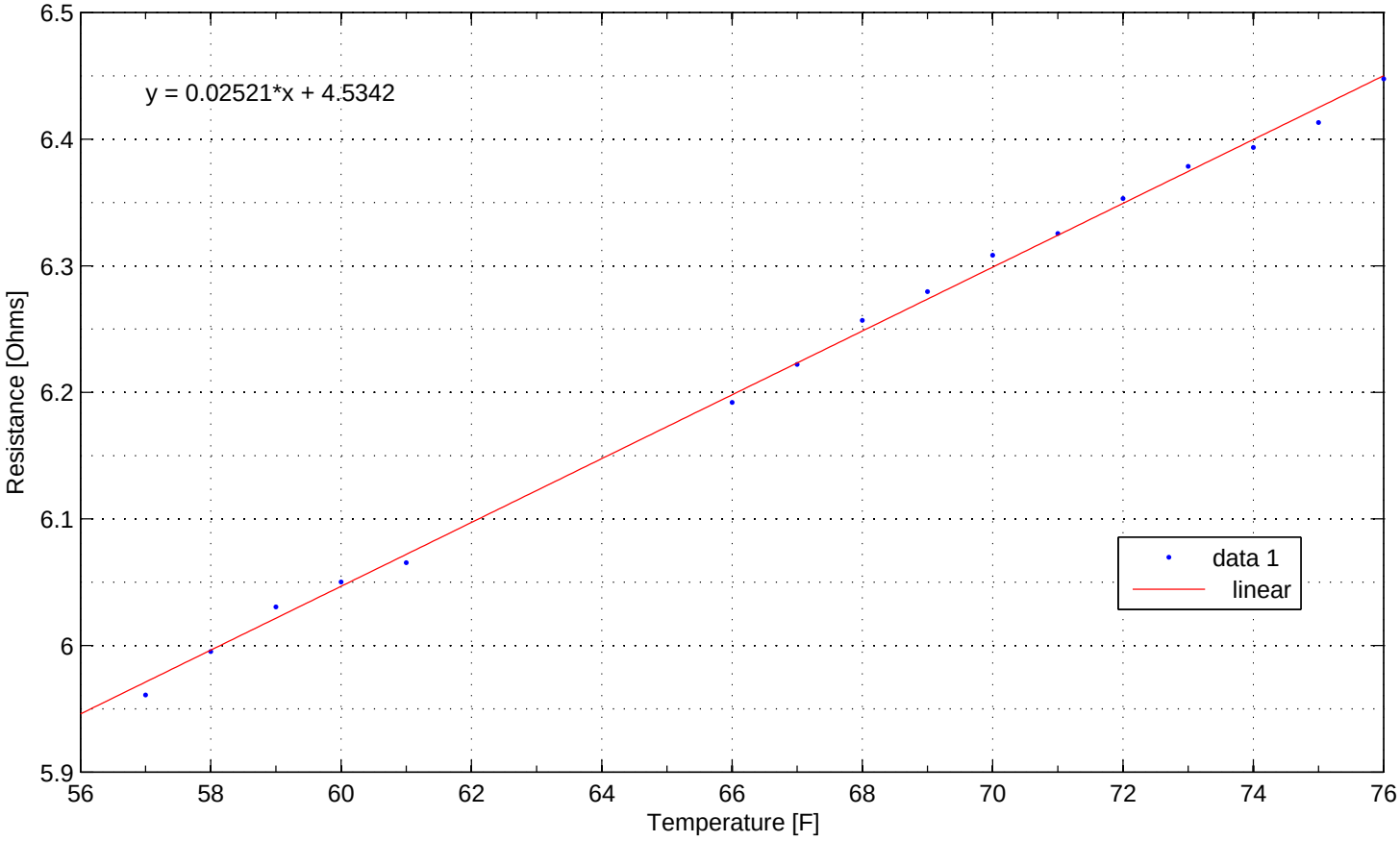

FIGURE 21. Temperature Dependence of the Voice Coil's Resistance

The second, less important step in controlling this type of resistance-related drift error is to control any extraneous DC current or large time-constant settling process that falls in the previously mentioned "danger zone" of $s = 0$. However, it is extremely difficult to construct a circuit of the type found in this prototype device that does not continually loop some amount of un-commanded current. Upon discovery of this source of error, an investigation revealed several sources of these types of electrical currents including ground loops between experimental devices, current leakage though solder flux tracks, and leakage current of the power amplifier's output stage. It took several weeks of investigation to track down these sources of un-commanded current. In the end, ground loop current was reduced to less than $4.1x10^{-6}A$ as measured by a pair of electrometers while the DC amplifier leakage was reduced to $9.7x10^{-4}A$.

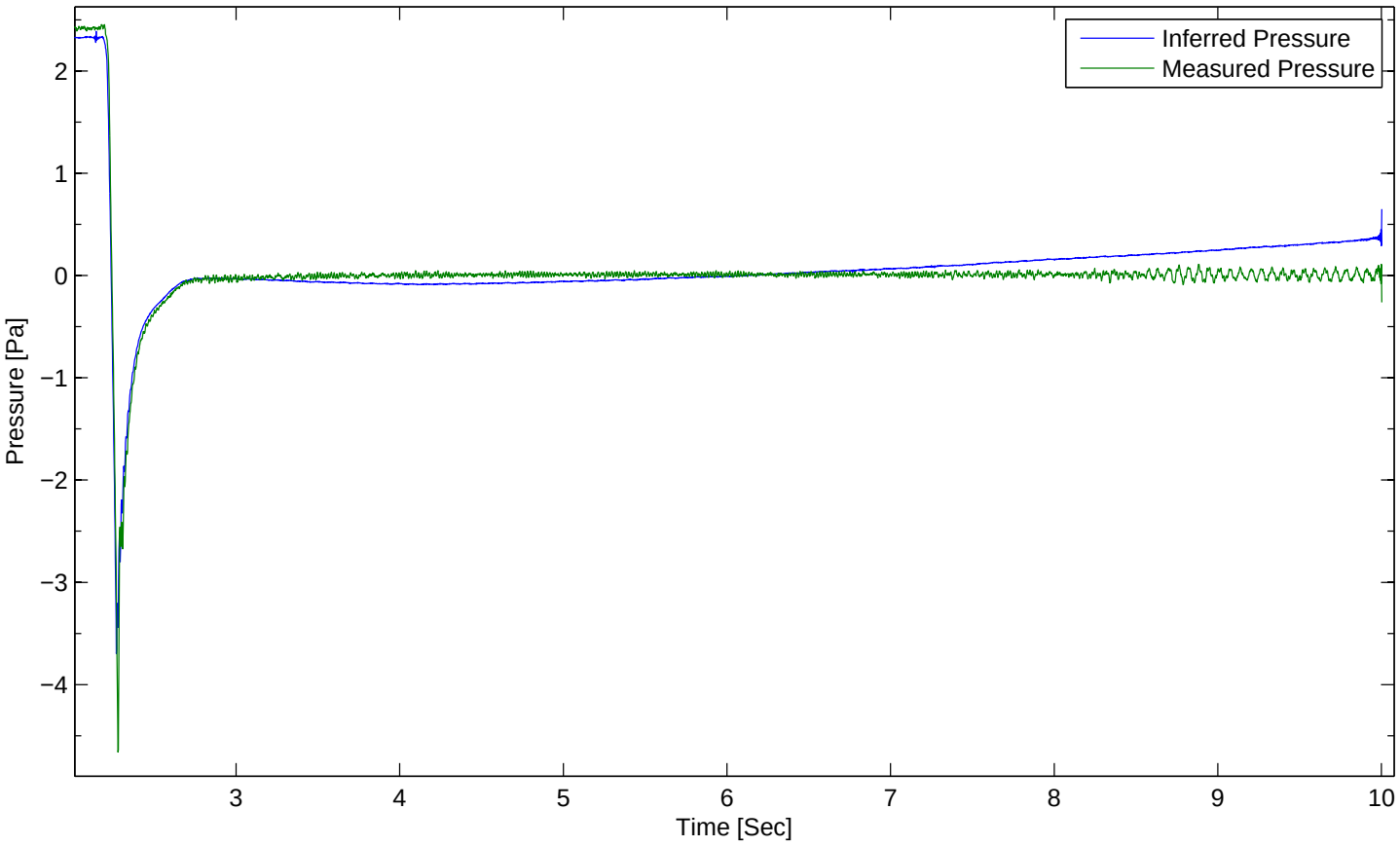

FIGURE 22. Pressure Drift Caused by Cooling of the Voice Coil

TABLE 12. Prototype Current Control

Current Type	Value
Ground Loop	$\leq 4.1x10^{-6}A$
Amplifier Leakage	$\leq 9.7x10^{-4}A$

APPENDIX D. CALIBRATION OF THE INDUCTIVE PROBE

An inductive probe was affixed to the loudspeaker to measure the displacement and velocity of the voice coil and loudspeaker cone. It gives critical information about the function and reaction of the loudspeaker during the development of the prototype device. The output of the probe's driving circuitry is a voltage that corresponds to the inductance measured by the probe. It is intended to function as a device that measures linear displacement. The inductance experienced by the probe is a function of its proximity to a ferromagnetic material. However, because this function is not linear and is highly dependent on the geometry of the ferromagnetic material, the probe must be calibrated *in situ*.

This calibration process was performed by attaching a Starrett 319-3654 dial indicator to the jack-screw mechanism that was used to jam the loudspeaker's movement during the characterization process. By moving the jack-screw in increments of $0.001in$, and recording the voltage output of the probe, a calibration equation relating position and voltage can be derived.

A plot of this data can be found in Figure 23. Included on this plot is a second order polynomial fit of the measured data. References to the measured position of the voice coil or speaker cone use this equation to yield the numerical result.

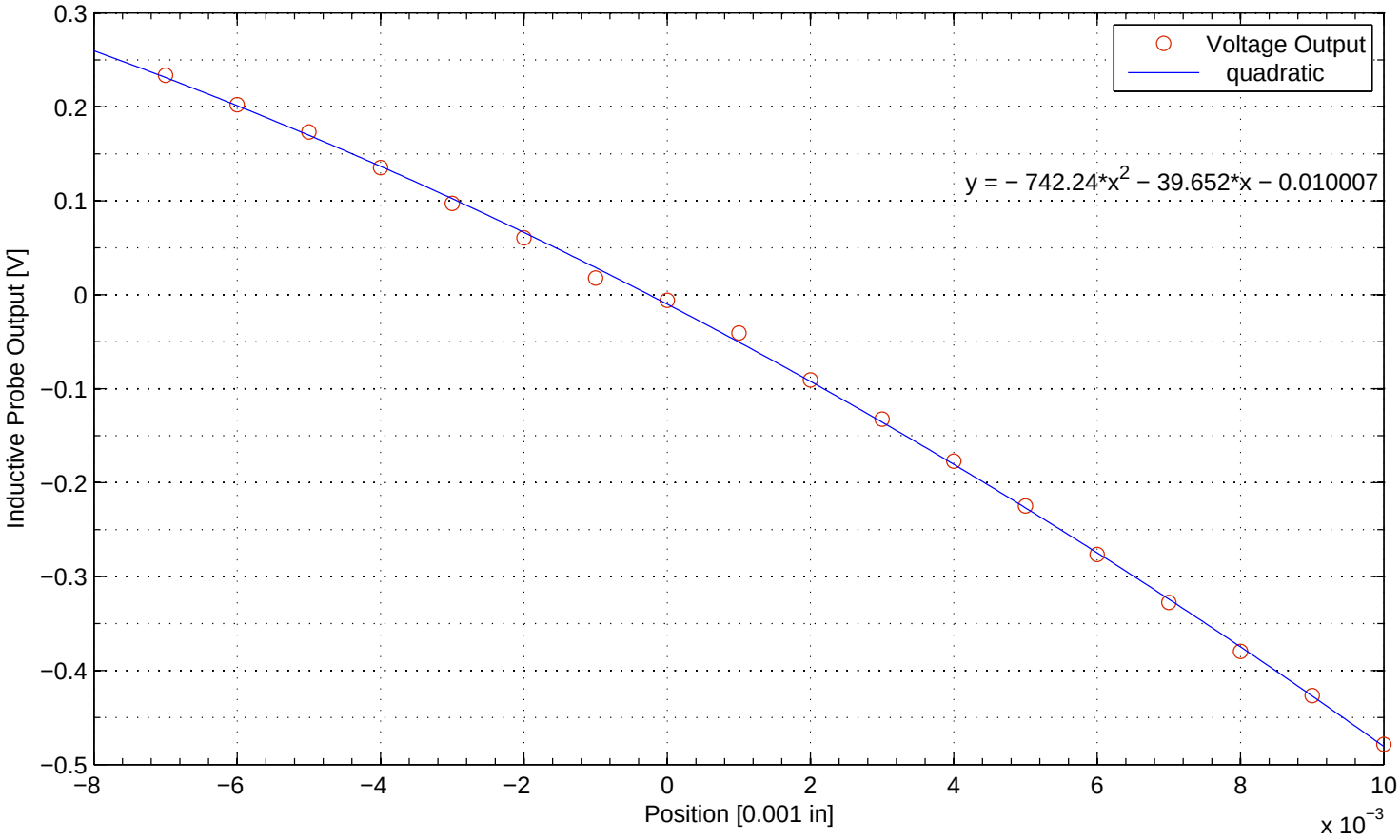

FIGURE 23. Quadratic Fit of Inductive Probe Calibration Data

Appendix E. Zero Pressure Assumption

Characterization of the mechanical kernel used to model the mechanical system of the M8a loudspeaker requires the cone and voice coil of the speaker to be moved with no external forces being applied. Practically, this means evacuating the air that typically surrounds the speaker's cone. For the experiments reported in this paper, the pressure chambers on both sides of the loudspeaker's cone were vacuum pumped down to $28Pa$. This small pressure is a result of air molecules that were unable to be evacuated during the pump-down process. The pressure reflects a reduction in the mass of the air found in the chamber by some four orders of magnitude (10^{-4}). This condition represents a *near* vacuum, but it is not a perfect vacuum. This section discusses the error that is associated with this assumption.

The pressure being generated by air remaining in cavities can be estimated using a procedure developed to estimate the radiation impedance of a loudspeaker mounted in an infinite baffle [3]:

$$\mathbb{Z}_R = \rho c \left[R_R(2ka) + jX_R(2ka) \right] \tag{E.1}$$

Using values of $\rho = 3.32x10^{-4}\,\frac{kg}{m^3}$, $c = 343.61\frac{m}{s}$, and, as provided in the cited work, $X_R = 0.05$ $R_R = 0.002$ at the worst case of $250Hz$, gives:

$$\mathbb{Z}_R = (2.27 + j56.9)x10^{-4}\frac{Pa}{m^3/sec} \tag{E.2}$$

The measured impedance of the mechanical system of the loudspeaker at $250Hz$ was $-0.0623 - j1.3449$ which means the non-zero pressure remaining inside of the test cavity generates an error in the range of 0.49% at the worst case of $250Hz$. This value approaches 0.005% at $25Hz$ and approaches 0 in the limt of $f \to 0Hz$

Appendix F. Jammed Voice Coil Movement

The use of the $\frac{1}{4}in$ brass rod to jam the movement of the voice coil during the characterization tests was investigated. The mathematics of forming the characterization terms of the encoding equations relies on the assumption that the voice coil is not permitted to move during a period when it is being excited by current flow in the voice coil. This may have been accomplished by "turning off" the magnetic field that the voice coil is exposed to in the flux gap of the loudspeaker, however when using permanent magnets, this is not possible. In this case, it was elected to jam the voice coil by attaching it to a brass rod (low inductance) and clamping the brass rod to the massive pressure cavity.

While the jamming of the voice coil dramatically lowers the level of audible noise during these characterization tests and is a striking suggestion that the voice coil is practically non-moving, the inductive probe was used to measure the movement. A special test was performed to measure this movement over a wide band of interrogation frequencies. A band-limited (0.1- 2000Hz) white noise sequence was used to measure the ability of the jamming method to keep the voice coil still. On average, the displacement of the cone while it was being jammed was less than $1.035x10^{-6}m$. The speed of this displacement was measured using the inductive probe, however the movement would also be fed-back into the electrical circuit appearing as a voltage. This voltage, or 'back-EMF', would be responsible for creating a false electrical impedance during the characterization calculations for $\mathbb{Z}(s)_{elec}$. That is, the movement of the cone would have appeared as if it were coming from the electrical circuit alone. The difference between the measured impedance and the impedance that *should have been* measured, if the velocity of the voice coil was actually zero, is an error. This error is generated by the physical constraints of the testing apparatus. If the brass jamming rod was more rigid or massive, was connected more tightly to the jamming screw, or if the voice coil itself deflected less under load, this error would be less.

This error can be estimated (using the inductive probe) but was not removed or compensated for in the results in any other section of this paper.

The absolute value of estimated impedance that was contributed to $\mathbb{Z}(s)_{elec}$ in error can be found in Figure 24. Most of this impedance appears as if it were an inductance in the electrical circuit and causes an overestimation of the actual inductance by 0.28%.

This phantom inductance creates an added impedance of about 0.0044% of the nominal resistance of the loudspeaker at $10Hz$. This means that the actual velocity of the voice coil during a test will be underestimated by a similar percentage due to the slight movement of the voice coil during the characterization phase.

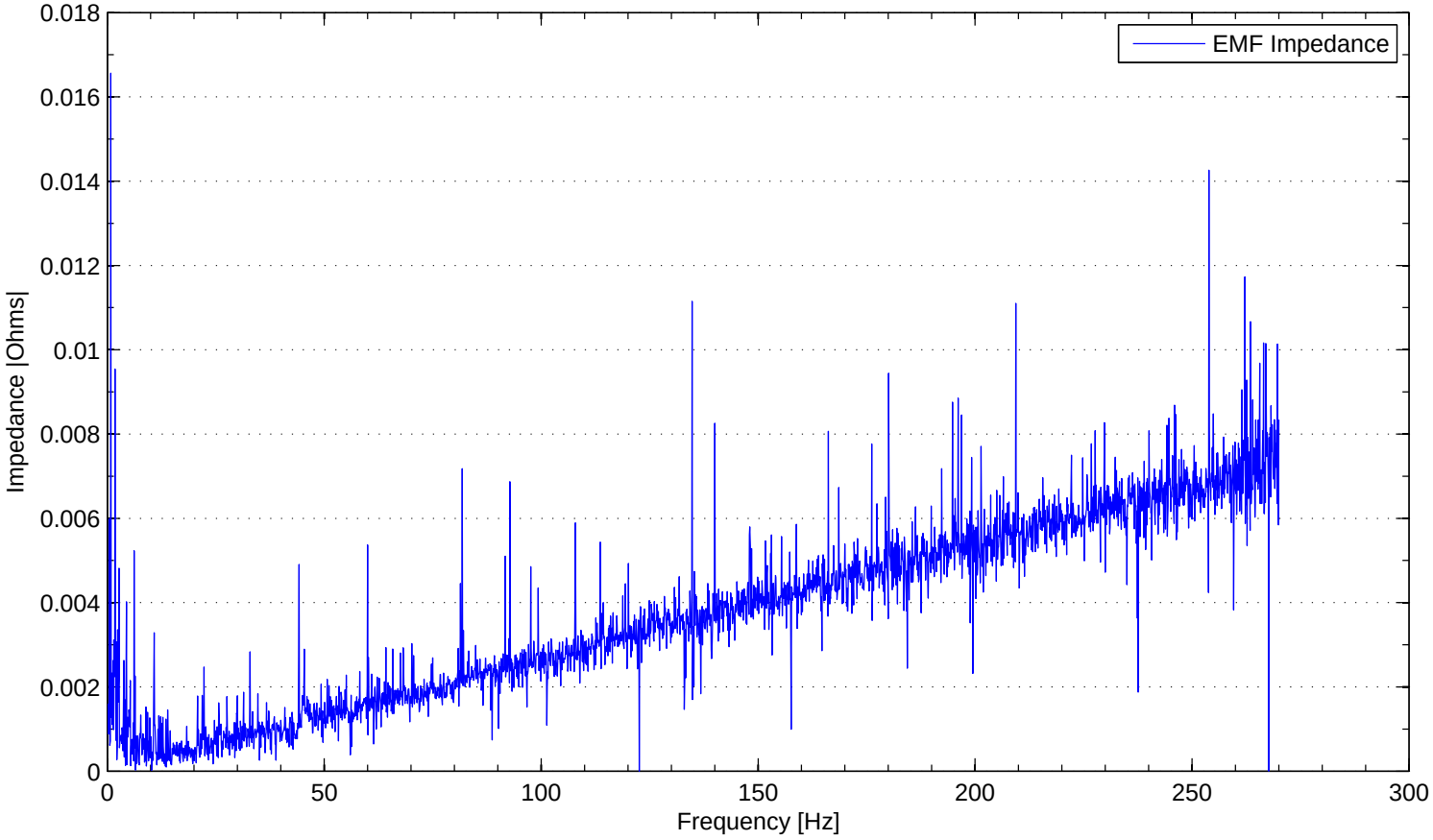

FIGURE 24. Estimated Impedance Error from Voice Coil Movement

APPENDIX G. PRESSURE-VOLTAGE RATIO - ALTERNATE TEST

As a comparison, a second type of test was conducted to derive the $\frac{Bl}{A}$ ratio. Borrowing from the principles used to construct National Metrology Institute of Japan's acoustic volumeter [6], this test calculated the ratio by comparing the compressibility of different volumes of gases.

In the case of NMIJ's volumeter, the ratio of acoustic pressure developed in two chambers separated by a loudspeaker driver is compared using microphones. The volume of both chambers is known. When an object of unknown volume is placed inside one of the chambers, the ratio of chamber pressure changes in proportion to the volume change.

Under the assumption of adiabatic compression, the state of the gas in the chambers is given by:

$$\frac{\partial P}{\partial V} = \gamma \frac{P_0}{V_0} \tag{G.1}$$

Because the volume change (∂V) and initial pressure (P_0) are the same for both chambers, a ratio between the change in pressure and the known and unknown volumes can be found.

In the case of the prototype that has been reported in Section 6, the ratio of the change in pressure over the change in volume of the pressure cavity can be written as:

$$\frac{\partial P}{\partial V} = \frac{(Bl)^2}{A^2} \cdot \frac{\mathbb{Z}(s)_{mech}}{(Bl)^2} \cdot \frac{\left[\left(\mathbb{Z}(s)_{elec} + \frac{(Bl)^2}{\mathbb{Z}(s)_{mech}}\right) \cdot \hat{I}(s) - \hat{V}(s)\right]}{\frac{1}{s}\left[\hat{V}(s) - \mathbb{Z}(s)_{elec} \cdot \hat{I}(s)\right]} \tag{G.2}$$

Or, when combined with Equation G.1:

$$\gamma \frac{P_0}{V_0} = \frac{(Bl)^2}{A^2} \cdot \frac{\mathbb{Z}(s)_{mech}}{(Bl)^2} \cdot \frac{\left[\left(\mathbb{Z}(s)_{elec} + \frac{(Bl)^2}{\mathbb{Z}(s)_{mech}}\right) \cdot \hat{I}(s) - \hat{V}(s)\right]}{\frac{1}{s}\left[\hat{V}(s) - \mathbb{Z}(s)_{elec} \cdot \hat{I}(s)\right]} \tag{G.3}$$

This equation can then be rearranged to solve for $\frac{(Bl)^2}{A^2}$:

$$\frac{(Bl)^2}{A^2} = \gamma \frac{P_0}{V_0} \cdot \frac{(Bl)^2}{\mathbb{Z}(s)_{mech}} \cdot \frac{\frac{1}{s}\left[\hat{V}(s) - \mathbb{Z}(s)_{elec} \cdot \hat{I}(s)\right]}{\left[\left(\mathbb{Z}(s)_{elec} + \frac{(Bl)^2}{\mathbb{Z}(s)_{mech}}\right) \cdot \hat{I}(s) - \hat{V}(s)\right]} \tag{G.4}$$

Because the exact volume of the pressure chambers for prototype reported in this paper were unknown, the method used by NMIJ's volumeter had to be modified slightly. An aluminum cylinder of well known dimensions was placed inside of the pressure chamber. The relative compressibility of the air contained in the pressure chamber was measured as $\gamma \frac{P_1}{V_1} \cdot \frac{A^2}{(Bl)^2}$. The aluminum cylinder was then removed from the chamber and the test was repeated; yielding another value for $\gamma \frac{P_0}{V_0} \cdot \frac{A^2}{(Bl)^2}$. Because $V_0 = V_1 + V_{cyl}$, $P_0 = P_1 = ATM$, and the value of V_{cyl} is known from length measurement, a solution for the Pressure-Voltage Ratio can be written as:

$$\frac{Bl}{A} = \frac{(Bl)^2}{\mathbb{Z}(s)_{mech}} \cdot \sqrt{\frac{V_{cyl}}{\gamma P_0}} \cdot \sqrt{\frac{\hat{I}_0(s)\hat{V}_1(s) - \hat{I}_1(s)\hat{V}_0(s)}{s\left[-\hat{V}_0(s) + \hat{I}_0(s)(\frac{(Bl)^2}{\mathbb{Z}(s)_{mech}} + \mathbb{Z}(s)_{elec})\right]\left[-\hat{V}_1(s) + \hat{I}_1(s)(\frac{(Bl)^2}{\mathbb{Z}(s)_{mech}} + \mathbb{Z}(s)_{elec})\right]}}$$

Where the subscripts 0 and 1 refer to the voltage and current measured during the empty-cavity and the cylinder-occupied tests, respectively.

This test was executed along side of the main characterization experiments during the ten-day testing period mentioned in the main document and offers a "sanity-check" of the primary method of determining the Pressure-Voltage Ratio. White noise in the range of 4 to 10 Hz was used to excite the loudspeaker driver. Results from these experiments can be found in Table 13.

TABLE 13. Pressure-Voltage Ratio of the M8a Loudspeaker (Alt. Test)

Parameter	Value	Standard Deviation	Std. Dev. Percent	Units
$\frac{Bl}{A}$	$3.2477501x10^2$	$1.053x10^1$	3.210%	$\frac{C}{m^3}$

The mean value obtained for $\frac{Bl}{A}$ by averaging these ten experiments compares favorably the value obtained from the change in volume tests reported in the main document. The difference between the two values amounts to a 1.323% error, if one is taken as the 'true' value. The high standard deviation is thought to be a function of variability in the physical configuration of the device between tests. Temperature differentials (due to handling), placement of the cylinder inside of the pressure cavity, atmospheric pressure changes, and changes in the inital volume of the cavity (e.g. vertical position of the loudspeaker's cone) were all factors that were not well controlled during these tests and are assumed to contribute to the high standard deviation.

Appendix H. Induction of Characterization Parameters

As discussed in Section 6, "Characterization Tests", the numeric parameters of the electrical and mechanical kernels are determined using a band limited random sequence interrogation technique (e.g. 'white noise'). Mathematically speaking, this white noise approximates a phase-randomized impulse function. This impulse function is used to excite the dynamics of the electrical and mechanical systems of the loudspeaker in an area of interest in the s-domain representation of the system's kernels. In turn, the measurement of this excitation can be used to solve for values of both $\mathbb{Z}(s)_{elec}$ and $\mathbb{Z}(s)_{mech}$ for discrete points in the s-domain. For example:

$$\mathbb{Z}(1+\hat{j}1)_{elec} = \frac{\hat{V}(1+\hat{j}1)}{\hat{I}(1+\hat{j}1)}\bigg|_{Q=0} = 0.7071 + j0.7071 \tag{H.1}$$

For more information on this process, readers are referred to books by Smith and Bracewell. [4] [9]

For the parameters reported in this paper (Tables 6 and 7), points along the real axis (*e.g.* $\sigma = 0$) of the s-domain were chosen for the characterization process. This step reduces signal processing requirements during the post processing step to a simple discrete Fourier analysis by taking a 'slice' out of the s-domain. Poles and zeros in this representation will most likely not extend exactly to '0' and '∞', but rather will appear as a 'muted' version of themselves. This is because the aforementioned slice at $\sigma = 0$ will cut near, but not directly at, the zeros and poles. Graphical examples of this slicing process are given in Figures 25, 26, and 27. Note how the s-domain slice and the Fourier representation mirror one another.

As noted in the previous paragraph, the location of zeros and poles of the impedance kernels are not directly accessible using the Fourier representation. Only a two dimensional projection of the pole or zero is available. Another way to think about this process is by asking the question: where must the zeros and poles be in the s-domain so that the $\sigma = 0$ slice looks the way it does? Mathematically, for the mechanical impedance kernel this is:

$$\begin{aligned}
\mathbb{Z}(s)_{mech} &= [ms + c + k/s] \\
\mathbb{Z}(\omega,\sigma)_{mech} &= m \cdot (\hat{j}\omega + \sigma) + c + \frac{k}{(\hat{j}\omega + \sigma)} \\
&\rightarrow \sigma = 0 \\
\mathbb{Z}(\omega,0)_{mech} &= m \cdot (\hat{j}\omega) + c + \frac{k}{(\hat{j}\omega)} \\
(\hat{j}\omega) \cdot \mathbb{Z}(\omega,0)_{mech} &= m \cdot (\hat{j}\omega)^2 + c \cdot (\hat{j}\omega) + k
\end{aligned}$$

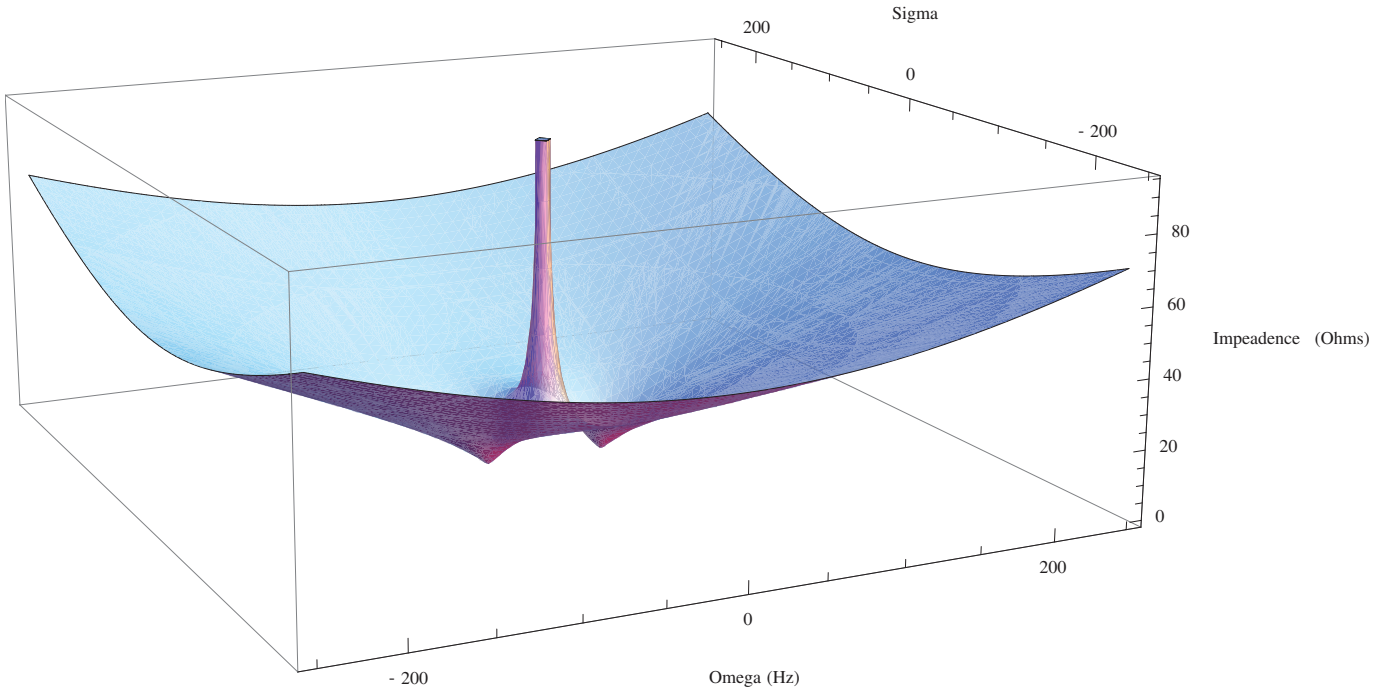

FIGURE 25. S-Domain Representation of the M8a's Mechanical Impedance

The zeros, for example, of the mechanical impedance kernel can now be found using the quadratic equation:

$$\begin{aligned}(\hat{j}\omega)\cdot\mathbb{Z}(\omega,0)_{mech} &= m\cdot(\hat{j}\omega)^2 + c\cdot(\hat{j}\omega) + k\\ 0 &= m\cdot(\hat{j}\omega)^2 + c\cdot(\hat{j}\omega) + k\\ \hat{j}\omega &= \frac{-c\pm\sqrt{4mk+c^2}}{2m}\end{aligned}$$

The plus / minus sign in the quadratic equation reflects the incompleteness of the information provided by the Fourier 'slice'. Because the slice is the projection of the poles and zeros, the side of the slice on which they occur cannot be determined mathematically. That is, a zero at $s = 1 + \hat{j}1$ gives the same Fourier projection of a zero at $s = -1 + \hat{j}1$.

A physical understanding of the system can determine the correct placement of these poles and zeros. Because the offset from $\sigma = 0$ is determined by the resistance or damping of the system, it can be reasonably

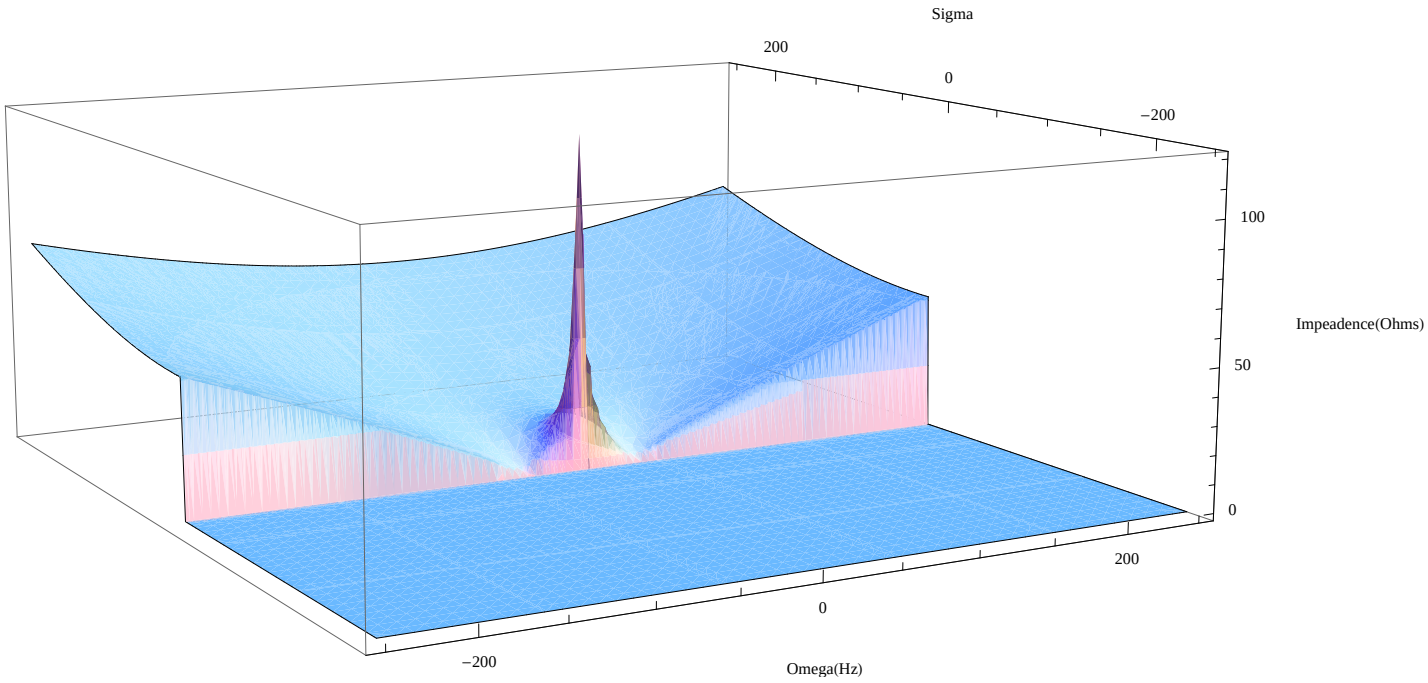

FIGURE 26. S-Domain Representation Sliced at $\sigma = 0$

concluded that negative resistances and damping do not occur. Therefore, the poles must occur on the negative side of the $\sigma = 0$ plane.

One way of estimating the parameters of the electrical and mechanical kernels might be to find the minimums and maximums of the Fourier projection, call these the zeros and poles, and write a series of equations that relate the ω placement of these points to the kernel parameters (e.g. L and R). However, this is not a preferred method. A more error tolerant way is to curve fit the system excitation data (e.g. $\frac{\hat{V}(\hat{j}\omega_n)}{\hat{I}(\hat{j}\omega_n)}\Big|_{Q=0} = X_n$) to the kernel model of the system (e.g. $\mathbb{Z}(\omega_n, 0)_{elec} = L \cdot (\hat{j}\omega_n) + R$). Using this technique, inducing the characterization parameters from the measured data becomes a function of solving an overdetermined linear system. In this system, an array is formed representing the discrete frequency response of the dynamics under investigation in the excitation bandwidth. A matrix is then formed in which the rows represent the unit frequency response of one linear parameter of the unknown kernel. For example, a row that would correspond to real resistance (R) would be be filled with ones – the resistive element adds the same impedance to the circuit regardless of excitation frequency. This is contrasted to a row that would correspond to the inductor term (L) where the row would filled with values that were equal to the frequency value of each cell (or radian value if working in a $\frac{rads}{sec}$ framework).

This array of discrete frequency response values and matrix of unit frequency response are related by an array of values that represent the unknown kernel parameters. Mathematically, this is written as:

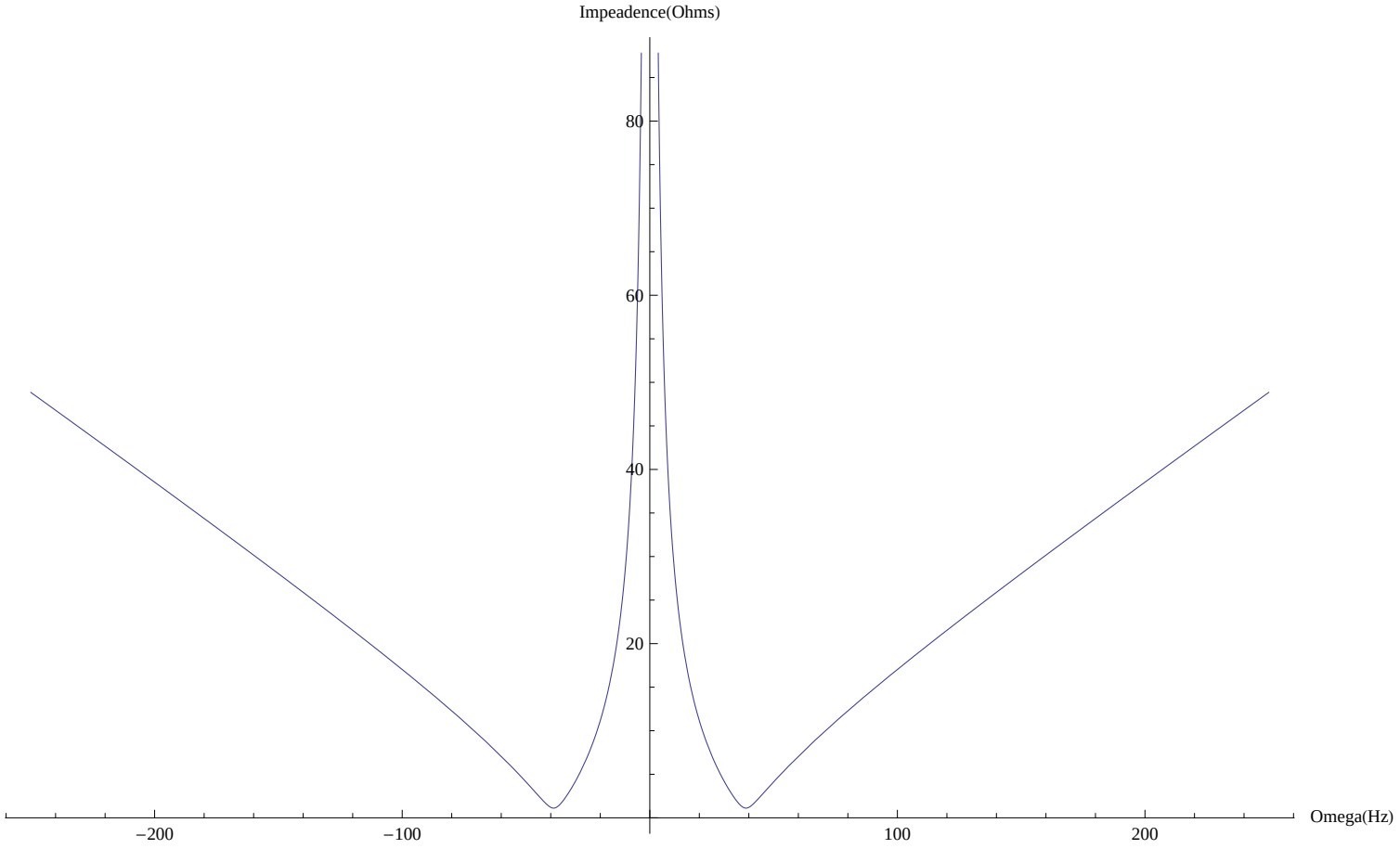

FIGURE 27. Fourier Representation of the M8a's Mechanical Impedance

$$\begin{bmatrix} \frac{\hat{V}(f_1)}{\hat{I}(f_1)}\big|_{Q=0} \\ \cdots \\ \frac{\hat{V}(f_n)}{\hat{I}(f_n)}\big|_{Q=0} \\ \cdots \\ \frac{\hat{V}(f_N)}{\hat{I}(f_N)}\big|_{Q=0} \end{bmatrix} = \begin{bmatrix} 1 & f_1 \\ \cdots & \cdots \\ 1 & f_n \\ \cdots & \cdots \\ 1 & f_N \end{bmatrix} \begin{bmatrix} R \\ L \end{bmatrix} \tag{H.2}$$

The system of equations displayed in Equation H.2 is experimentally over constrained. That is, there are more frequency bins for which information is obtained than is absolutely required, but this technique tends to reduce the effect of experimental error if one is to choose an error-prone bandwidth. As noted in body of this paper, the total bandwidth was $0.1Hz$ to $250Hz$ with bin widths of $0.1Hz$.

There are many methods for solving over constrained systems, each focusing on a different type of error reduction. However, for the characterization parameters given in this paper, a QR decomposition method

was used. This method is numerically stable and is designed to minimize the L2-norm of the error array (e.g. $|||[Ax - b]|||$). The results of this entire process are visually displayed in the following figures (28 - 33).

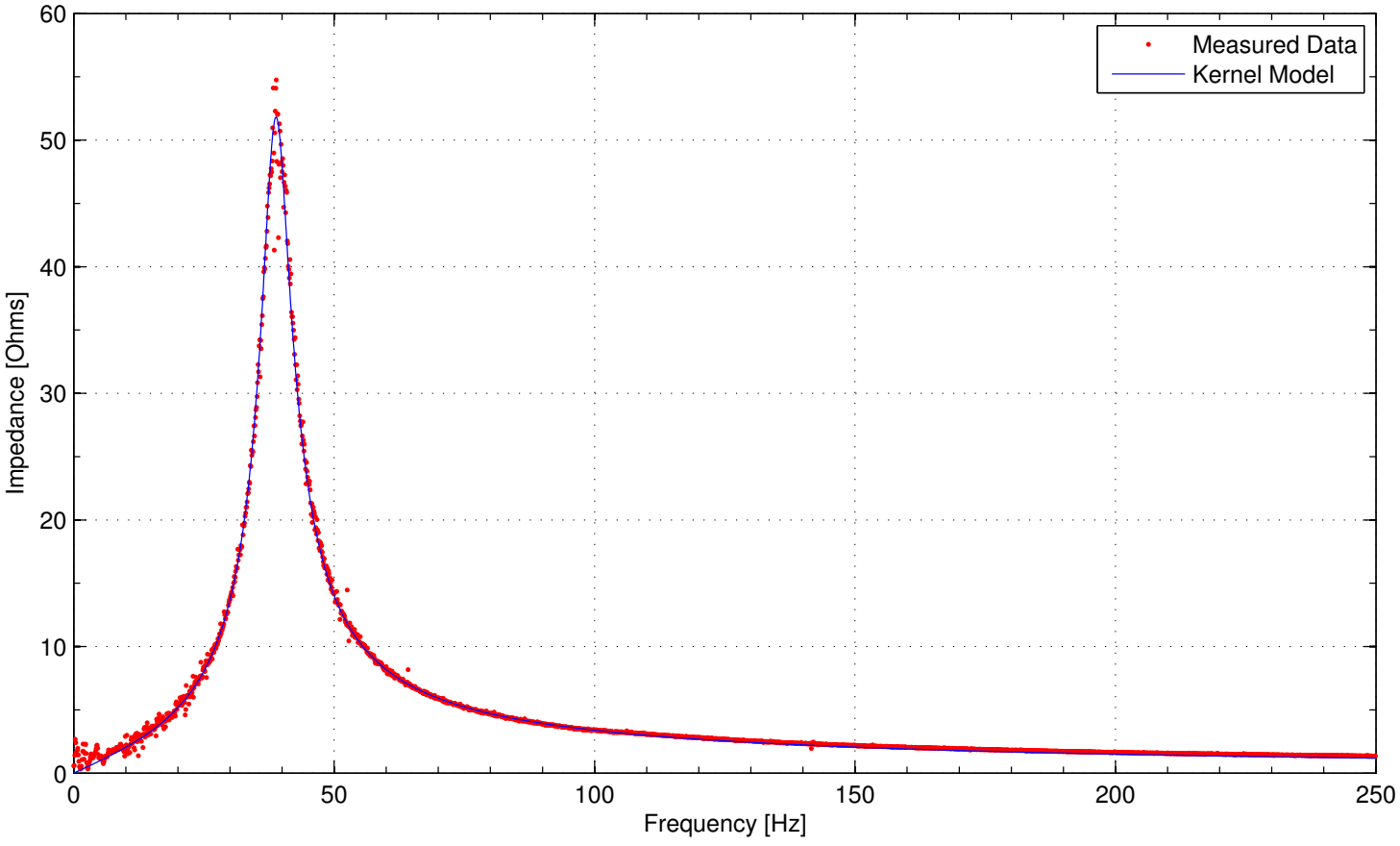

FIGURE 28. Absolute Value of $\frac{(Bl)^2}{\mathbb{Z}(s)_{mech}}$

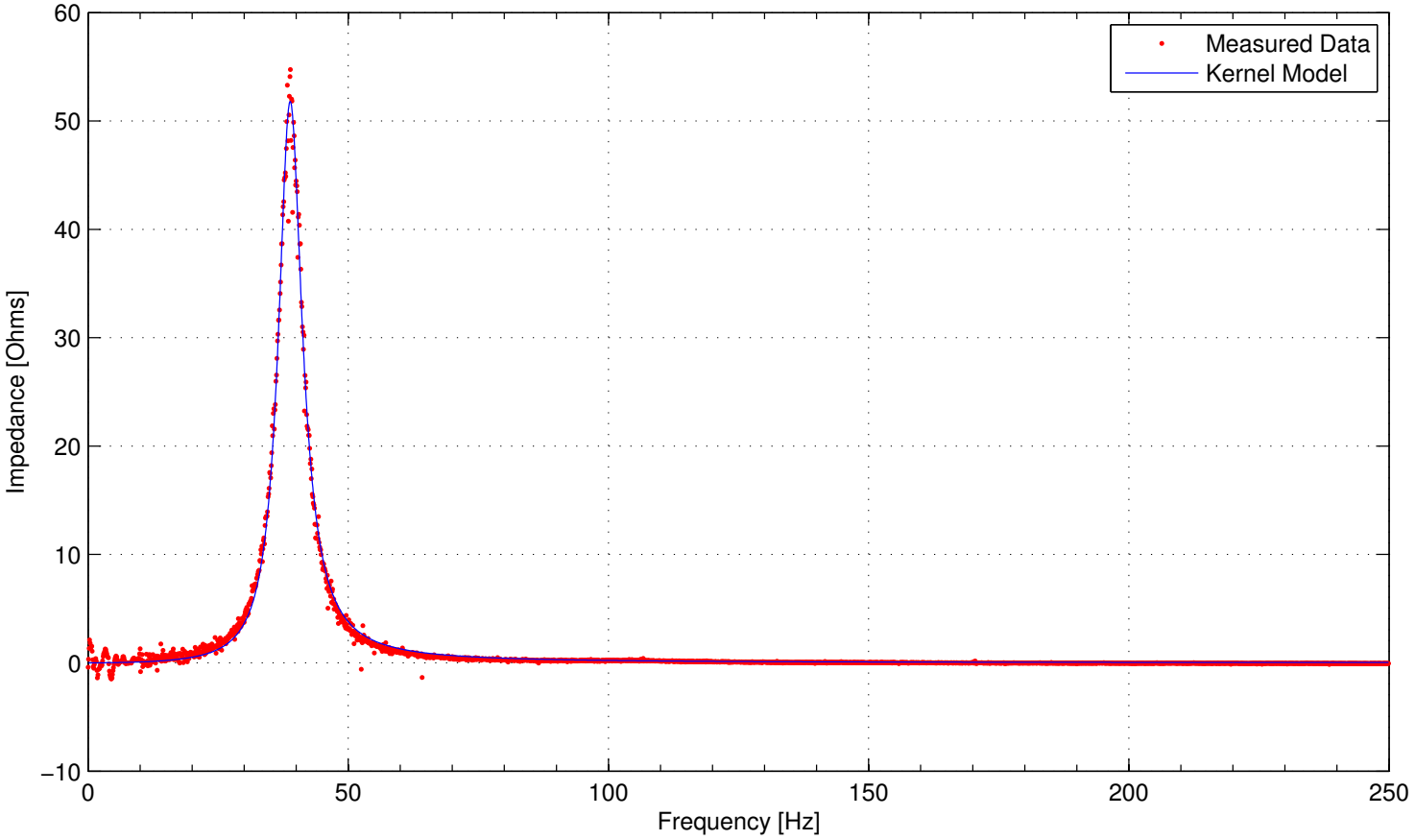

FIGURE 29. Real Part of $\frac{(Bl)^2}{\mathbb{Z}(s)_{mech}}$

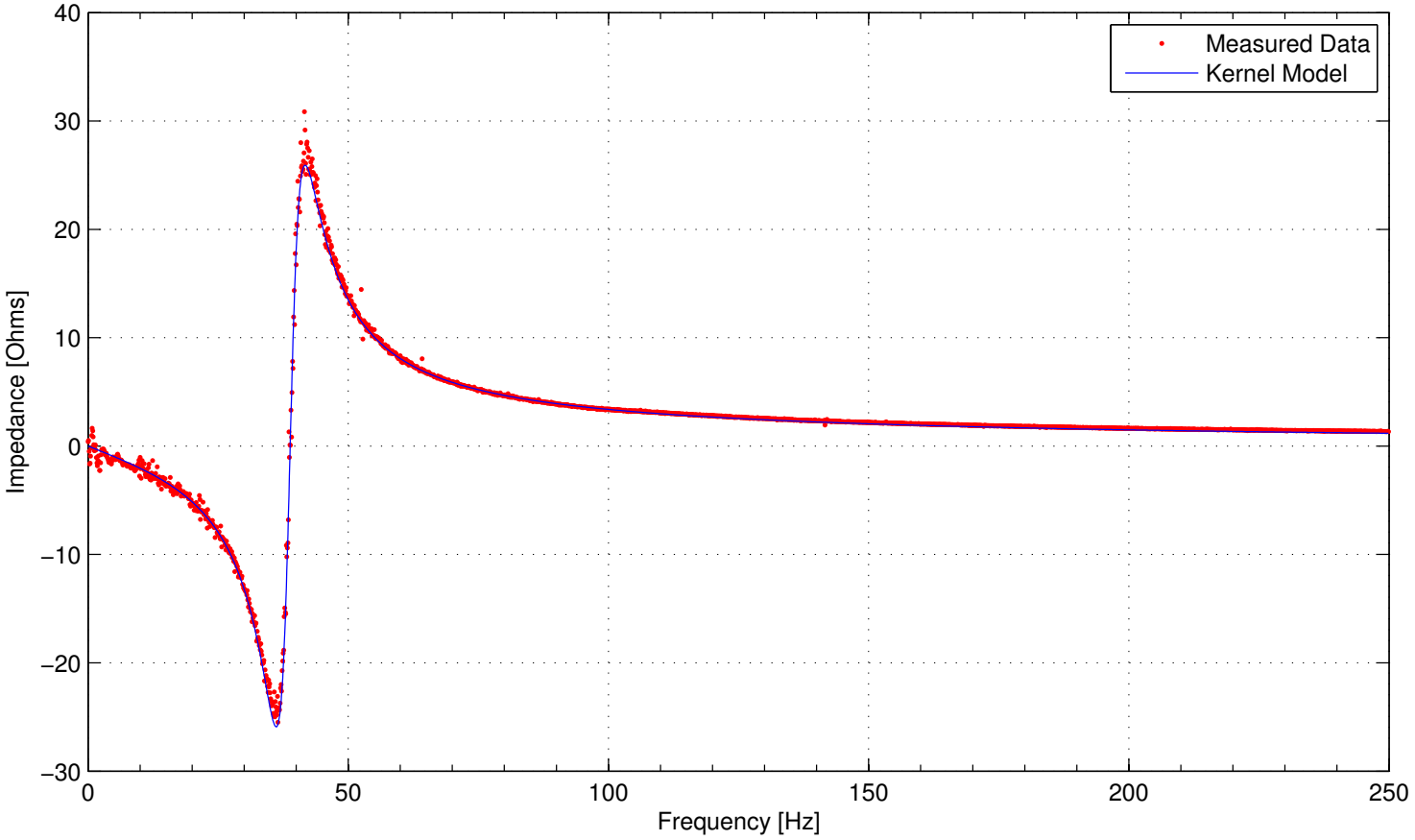

FIGURE 30. Imaginary Part of $\frac{(Bl)^2}{\mathbb{Z}(s)_{mech}}$

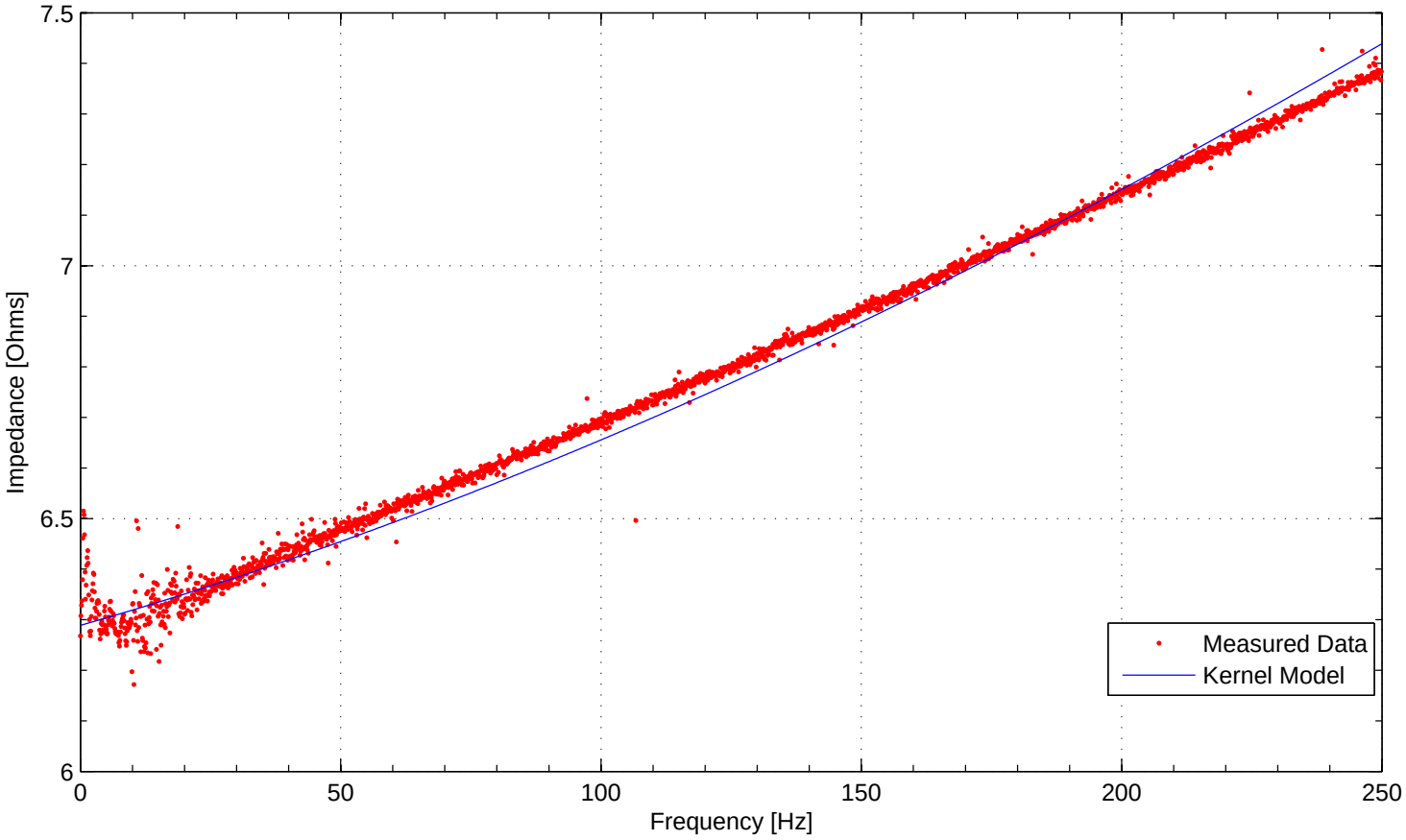

FIGURE 31. Absolute Value of $\mathbb{Z}(s)_{elec}$

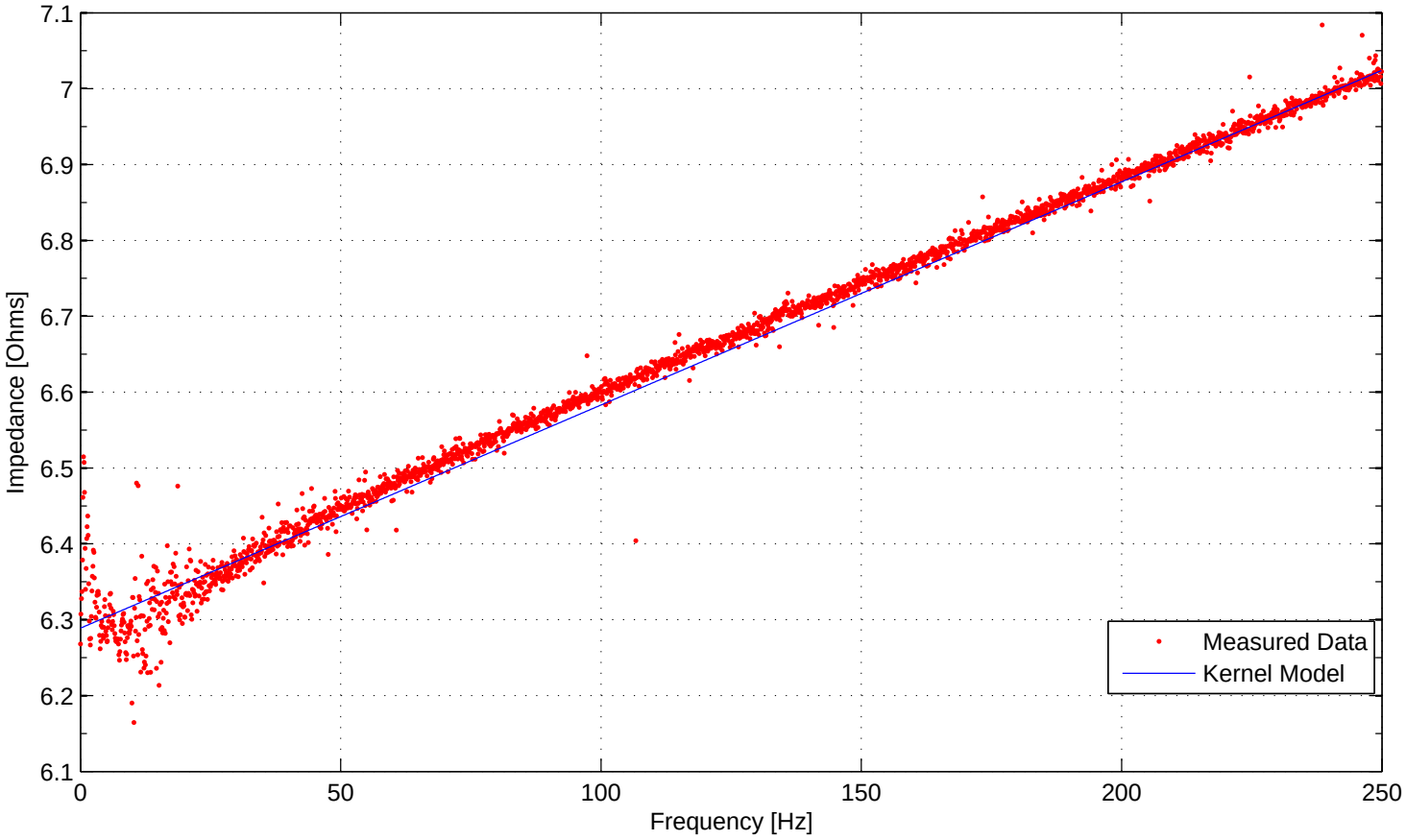

FIGURE 32. Real Part of $\mathbb{Z}(s)_{elec}$

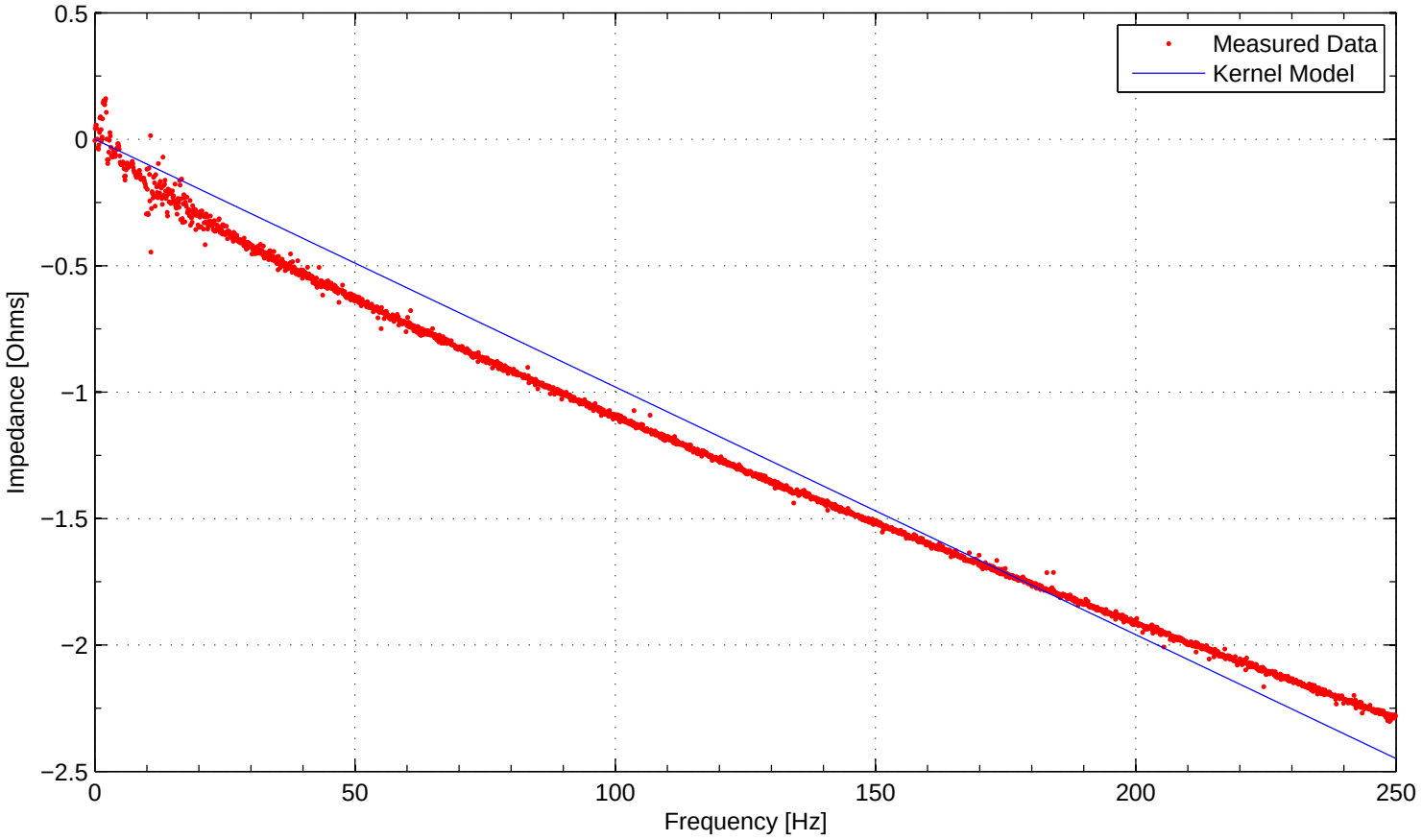

FIGURE 33. Imaginary Part of $\mathbb{Z}(s)_{elec}$

Appendix I. Photographs of the Device

This appendix section is provided to visually recount may of the fabrication details of the device that is described in this paper.

I.1. **Rough Fabrication.** The rough fabrication of the device's cavity relied on finding most of the components from scrap heaps. These parts were plasma cut, ground, cleaned, and finally welded to the final form. Electrical and instrumentation ports were also added during this stage.

Figure 34. Original 8 in Diameter ANSI B36 Steam Pipes

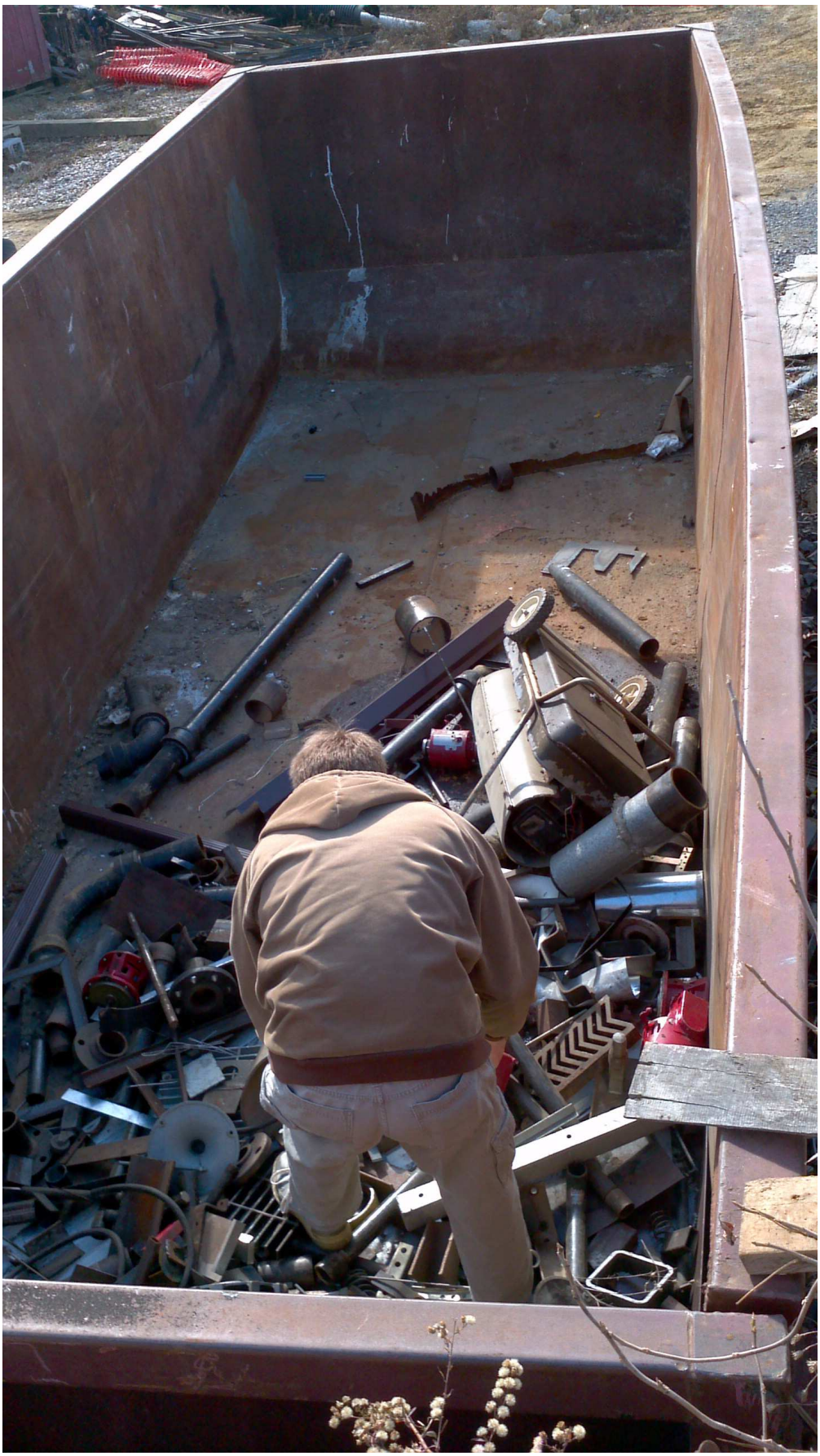

FIGURE 35. Collecting Parts

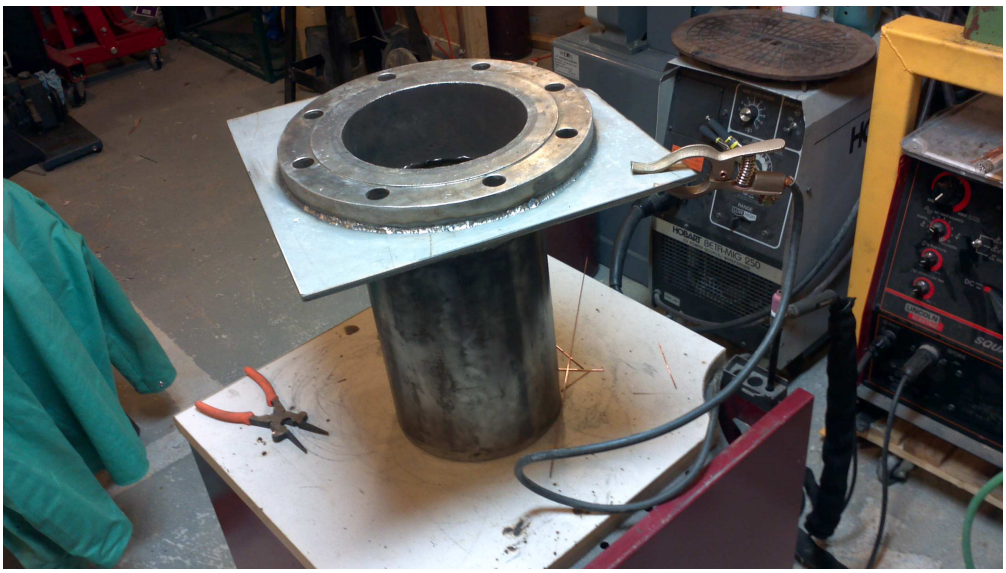

FIGURE 36. TIG Welding of Pipe Sections

FIGURE 37. Plumbing and Wiring of Bottom Pressure Cavity

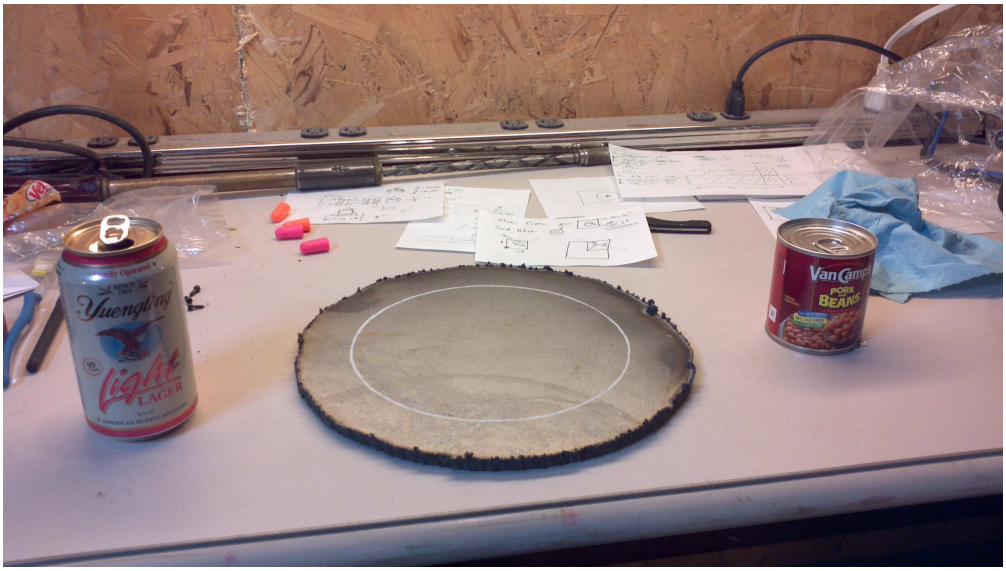

FIGURE 38. Layout and Plasma Cutting of the Paramagnetic Loudspeaker Flange

FIGURE 39. Pressure and Instrumentation Ports as Viewed from Inside the Cavity

FIGURE 40. Pressure and Instrumentation Ports as Wired

I.2. **Fine Fabrication.** The fine fabrication of the device relied on machining several components to add the inductive probe instrument to the loudspeaker.

FIGURE 41. Centering the M8a Loudspeaker on the Mill

FIGURE 42. Centering the M8a Loudspeaker on the Mill

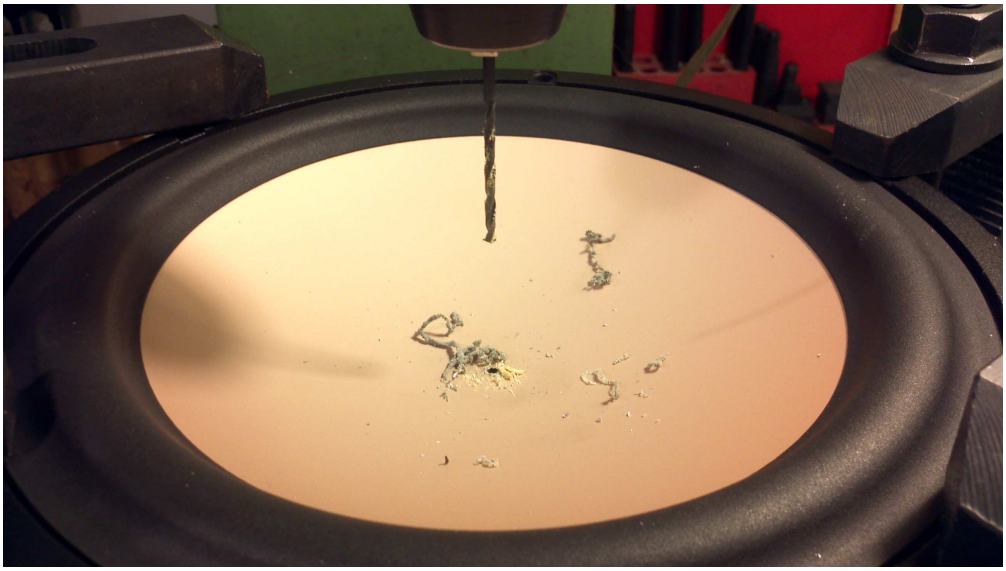

FIGURE 43. Drilling a Hole for the Inductive Probe Target

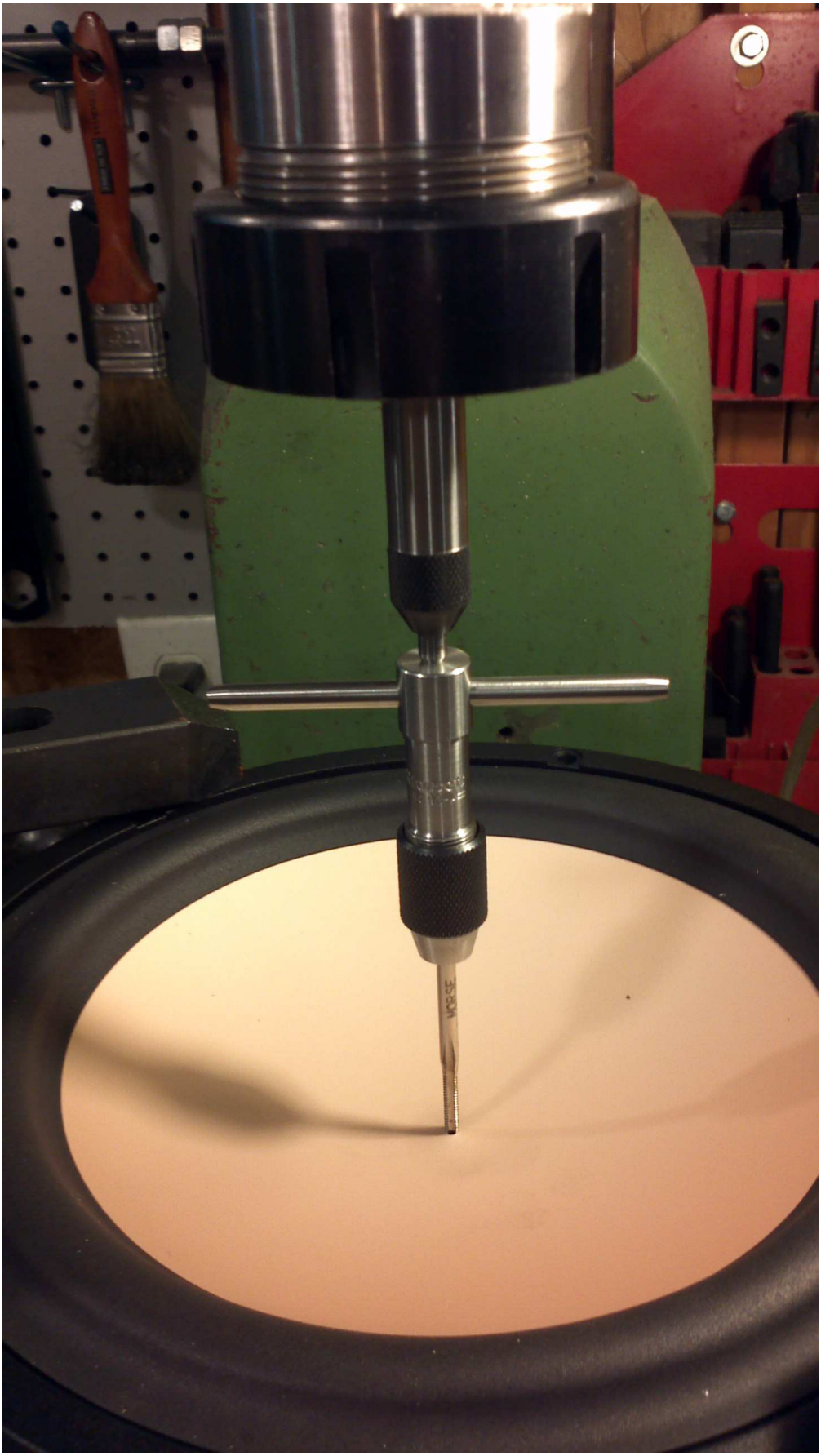

FIGURE 44. Tapping the Hole for the Inductive Probe Target

FIGURE 45. Close-Up View of the Inductive Probe Target

FIGURE 46. Inductive Probe Target as viewed from Loudspeaker Vent (Back)

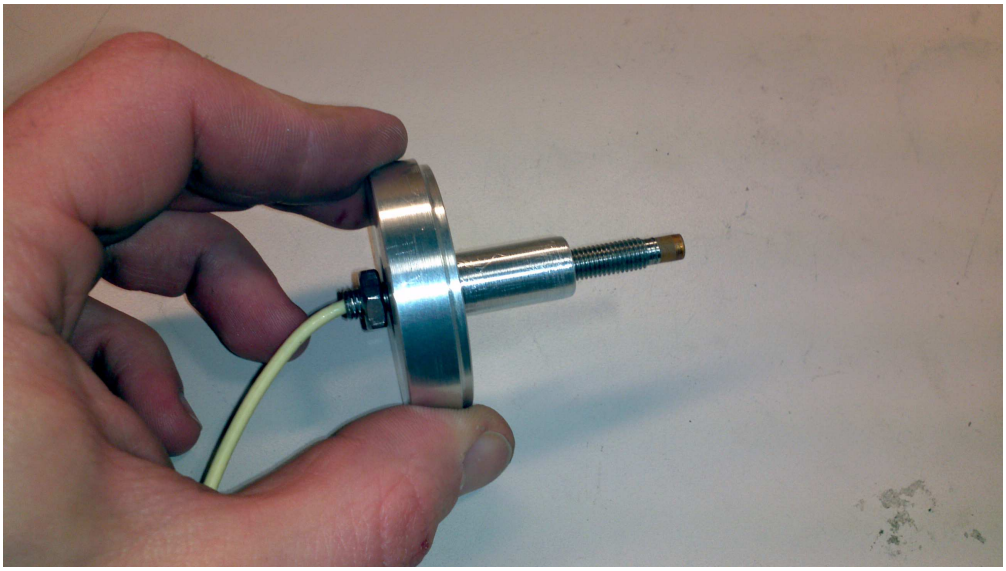

FIGURE 47. Inductive Probe and Press-Fit Fixture

FIGURE 48. Inductive Probe and Press-Fit Fixture

FIGURE 49. Inductive Probe and Press-Fit Fixture

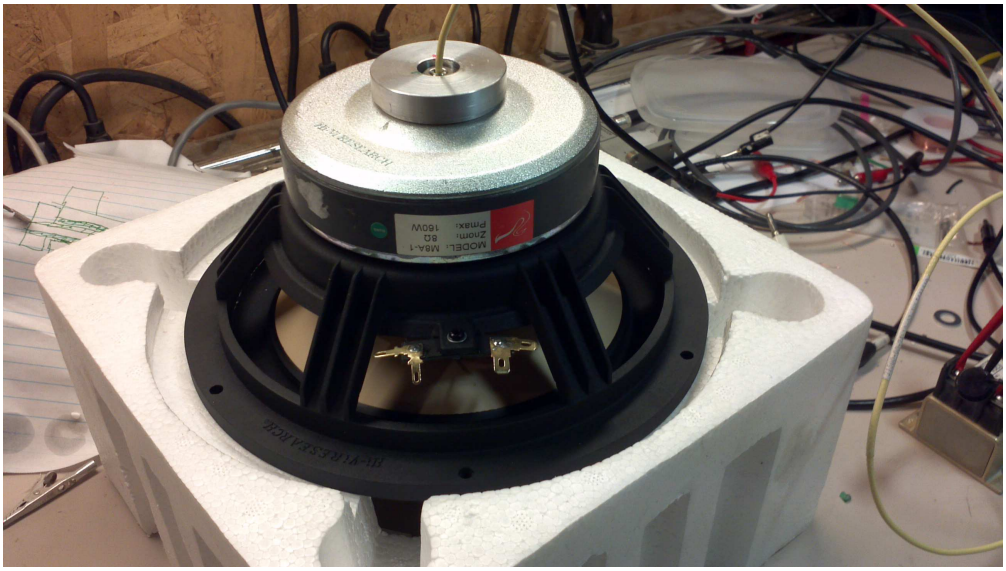

FIGURE 50. M8a Loudspeaker with Inductive Probe Installed

BAKER ENVIRONMENTAL HYDRAULICS LABORATORY,
DEPARTMENT OF CIVIL AND ENVIRONMENTAL ENGINEERING,
VIRGINIA TECH, BLACKSBURG, VA 24061, USA.

E-mail address: bdillon@vt.edu

URL: http://www.behl.cee.vt.edu